ART-99-578-001-TR

DEMONSTRATION AND EVALUATION OF THE STREAK TUBE IMAGING LIDAR FOR USE IN BYCATCH REDUCTION

Final Report

ANDREW J. GRIFFIS

31 August 1999

Distribution:

      1 original and 2 copies – U.S. Department of Commerce, NOAA
      1 copy – Southwest Fisheries Science Center

This document consists of 104 pages.

TABLE OF CONTENTS

LIST OF FIGURES

8

LIST OF TABLES

1.   Report title

Demonstration and Evaluation of the Streak Tube Imaging Lidar for Use in Bycatch Reduction

2.   Abstract

The Airborne Streak Tube Imaging LIDAR (ASTIL) was evaluated for use in detecting schools of tuna in the Eastern Tropical Pacific (ETP) waters in order to aid in reducing bycatch of dolphin associated with yellowfin tuna. Three airborne experiments were conducted and data were collected for southern bluefin tuna, yellowfin tuna, akule (trachiurops crumenophthalmus), giant bluefin tuna (GBFT) and dolphin[1]. The LIDAR signature of tuna was studied and extended to an evaluation of fish and fish school detection of GBFT using STIL experimental data. The utility of fish school detection was confirmed for GBFT in terms of detection statistics for binary hypothesis testing and also by direct implementation of a three-dimensional matched filter algorithm. Based on the GBFT observations, modeled performance estimates were made for yellowfin in the ETP for an upgraded ASTIL system.

3.   Executive summary

This report details the evaluation of the ASTIL for use in detecting schools of tuna in the ETP waters in order to aid in reducing bycatch of dolphin associated with yellowfin tuna. The discussion begins with a restatement of the problem at hand, followed by summary descriptions of the organizational means of accomplishing the work, and a statement of the work intended and the work achieved. The body of the report delineates the pre-experimental, experimental and post-experimental data collection and analyses, and features many graphical portrayals of data and concepts.

This research succeeded in establishing, for the first time known to the authors, a quantitative demonstration of the detection of tuna and tuna schools with airborne LIDAR. A school of more than 70 tuna was imaged and used to build a three dimensional detection algorithm that was demonstrated as part of the work presented here. The tuna species used for this work was the GBFT which was imaged in the waters of New England. GBFT with an apparent packing density of $0.04/m^3$ were detected at 2-6 meters water depth with a median signal to noise ratio of 7.7. The yellowfin tuna was not able to be evaluated this way, owing to the scarcity of data collected. Data collected for southern bluefin tuna (SBT) were used to initiate and further the understanding of the GBFT data that were collected.

The GBFT data were further used to produce a receiver operating curve (ROC). The ROC data indicated that the prototype ASTIL sensor could yield useful GBFT performance with a probability of detection in excess of 80 percent for single tuna detection scenarios. The GBFT data and sensor model were used to estimate yellowfin tuna (thunnus albacares) performance for

---

[1] Two of the airborne experiments were funded directly by this research. One (southern bluefin tuna) experiment was only provided with data analysis support by this research.

an upgraded ASTIL sensor and showed potential for performance at 18-45 meters water depth, depending on the sensor configuration and the precise nature of the collected data.

The work conducted spanned nearly two years, beginning with the data analysis in support of airborne experiments in Boston Bay, South Australia in April of 1997, extending to the Hawaiian Islands in September of 1997, and concluding in the Cape Cod, Massachusetts region in the Summer of 1998. Two separate aircraft installations were concluded in association with this research, as two intensive field experiments were fully supported[2]. Data are shown for 3D, 2D and 1D portrayals of the STIL data collected.

4. Purpose

The problem that is addressed by this research is that of dolphin bycatch in the ETP yellowfin tuna fishery. While there may be mechanical and technique innovations that can provide some relief to this problem by allowing caught dolphins to exit, this research approaches the problem early in the fishing operation by trying to direct fishing operations to tuna schools that are not associated with dolphin.

Specifically, this effort sought to demonstrate the basic feasibility of using an airborne LIDAR system to locate schools of yellowfin tuna that are not associated with dolphin. The LIDAR technology that was evaluated was a prototype Streak Tube Imaging LIDAR (STIL) developed by Areté Associates with support from the Office of Naval Research (ONR) for generating high-resolution imagery of the ocean floor from an underwater vehicle.

Broadly, the objective of this research has been to conduct experiments that would yield data from which an assessment could be made of the basic feasibility of locating (detecting) schools of yellowfin tuna in the ETP using ASTIL system. However, when this research was proposed, the laboratory sensor equipment that had been demonstrated was not suitable for conducting an airborne experiment. Consequently, one of the proposed objectives of this research was to modify the laboratory sensor for airborne experiments, with support from preliminary predictive models that might indicate how best to modify the sensor. Finally, given that suitable data could be obtained, the research was to culminate in a data-based assessment of performance, accompanied by some estimates of the overall performance of the sensor in detecting fish. This performance assessment, then, would be the basis for summary statements on the feasibility of using the ASTIL technology for dolphin bycatch reduction in the ETP yellowfin tuna fishery.

Delineated more in accord with a breakdown of work, the objectives were as follows:

- Identify, through modeling and simulation, the key sensor parameters and settings to modify in order to adapt the laboratory STIL sensor into an ASTIL sensor that would provide the data required for this assessment
- Modify the sensor and confirm its operation in simple terrestrial and (if possible) over-water targets

---

[2] The aircraft operations for the first experiment, in South Australia, were not supported by this research, though the two efforts did overlap.

- Conduct airborne experiments in southern California and Hawaii, per opportunity, to obtain yellowfin tuna imagery
- Analyze the airborne LIDAR data to quantify performance for yellowfin tuna detection
- Use the measured sensor performance to make the assessment of the ASTIL sensor utility to the bycatch problem

The research emphasis was on the collection and analysis of LIDAR data relevant to the dolphin bycatch problem. As will be made clear in the sections of this report that follow, this aspect of the research was carried through to completion with very gratifying results. However, owing to the timing of the grant award and the timing and nature of the opportunities that arose during the period of this grant, it was neither possible nor prudent to carry out the research precisely as proposed. The next several paragraphs elaborate some of the underlying differences between the proposed research and the research that was actually conducted. It is hoped that will help avoid some confusion for the reader when the research carried out is discussed in sections that follow.

The proposal for this effort was written in the spring of 1996, approximately half of the way into the ONR-sponsored research for the STIL sensor. The proposed research was to have been under contract, if awarded, by the end of 1996. This would have allowed for some calculations to be made and subsequent sensor modifications to be introduced in time to participate in National Marine Fisheries Service (NMFS) experiments during the spring of 1997. Furthermore, if adequate coordination could be made, an experiment was to have been conducted coincident with a billfish tournament in Hawaii later in the summer of 1997.

Thus, in a period of one year, the sensor modifications could have been made and the data collected, while still leaving enough time for some analysis and an assessment of performance. Fortunately, circumstances prevented the execution of the research as proposed. It was not possible then to predict that this was a fortunate turn of events, but it clearly worked out to be so in the end. As will be elaborated briefly, there were two aspects of the actual timing of the research that were of significant benefit to the overall objectives: 1) the delay in the grant award, combined with opportunities with other fisheries interests, allowed for an infusion of Areté IR&D that advanced the sensor well beyond the *anticipated* minimum needed (and therefore proposed) for the present research, and 2) the ensuing extension of the award to allow for additional experiment opportunities and also to accommodate non-interference with the ONR effort (from which this research needed to borrow significant technologies) allowed this research to benefit greatly from the data analysis tools and techniques that were developed under the ONR STIL program.

Late in the summer of 1996, interaction with researchers at the Commonwealth Scientific and Industrial Research Organization (CSIRO) gave rise to a request for STIL sensor modifications that would allow for imaging SBT in the waters of South Australia. As CSIRO was interested in distinguishing juvenile SBT from adult SBT for the purposes of stock maturity estimation, significant changes in data collection speed and laser pulse repetition rate were required to even consider doing the experiment, planned for March/April of 1997 (approximately the same time as the NMFS experiment with which Areté would collaborate if an award was made). As CSIRO could not fund sensor modifications, and since Areté had an ongoing interest in doing airborne research, but as yet had no indication of funding for such research, Areté chose to fund

the modifications to the laboratory STIL sensor in order to gather the SBT data needed for the CSIRO experiment. The IR&D funds were approved in December of 1996, as it appeared that the proposed bycatch research was either going to be delayed or not funded. The sensor design changes were made and implemented by late February of 1997 (though several were forced to delay, owing to the short time for testing) and experiments were conducted in South Australia between March 26 and April 10 of 1997.

The SBT experiments had the advantage of observing captive schools of SBT, which proved very advantageous for an airborne sensor that was very immature and still needing engineering support for ongoing operations. After optimizing the sensor in the field, good data for SBT were obtained that showed the importance of resolution and sensitivity in conducting experiments[3]. In addition to these observations, it was clear that the planned sensor improvements that could not be finished in time for the CSIRO trials still needed to be implemented prior to conducting further experiments.

The present grant award was approved for contractual expenses starting April 1, 1997. However, as most of the critical sensor changes had been made already, the early approach to the research needed to change from simulation and analysis to support engineering modifications, to that of analyzing relevant experimental data and tuning and upgrading an existing sensor for further experiments. Such analysis did proceed, and engineering upgrades were made, but conflicts with ongoing ONR research precluded participation in or planning for the billfish tournament in the summer of 1997. Instead, an experiment was planned and carried out in late September of 1997 in the Hawaiian Islands. These experiments did not yield any significant amount of data on yellowfin tuna (more will be mentioned on this later), but useful data were collected on other species, and some operational lessons were learned and expertise in analyzing data continued to grow[4].

Because no significant tuna opportunities were obtained in Hawaii, as confirmed by analysis of data in the fall of 1997, this effort was extended an additional 9 months, and an experiment was planned in New England for GBFT, as the associated fishery had a good history of opportunities for aerial observation. Furthermore, the GBFT allow for unambiguous association of a LIDAR signature with a known species. Also, owing to the size of the GBFT, it was hoped that the LIDAR signature of the tuna would be large enough to be fully resolved without flying so low as to alarm ("spook") the fish, and the shallow depth of the fish provided visual confirmation to the spotters, while facilitating good LIDAR imagery. All of these factors proved to be instrumental in obtaining a good set of tuna data, though aircraft logistics and the narrow field of view of the existing sensor prevented the collection of an exhaustive database of GBFT imagery.

The analysis of the data from these experiments was conducted in part on site, though the careful review of the data for detection performance was delayed, again owing to conflicts with the ONR development efforts and experiments, until late in 1998 and up to the present time. However, as before, this delay has proved very beneficial, as the significant improvements in data processing

---

[3] The findings section will show that this was true of both the school problem and the individual tuna detection problem – the requirements are the same for both where early, non-operational research is concerned.
[4] Of the 3 months that had high probability of spotting schools (July-September), the last was chosen (July-August were not possible due to interference with the STIL sponsoring program with ONR, which owned the equipment).

that have been made under ONR sponsorship have yielded much additional data and insights into performance that would not have been possible on a shorter time scale. The following sections of this report will detail all of the efforts expended in this research, and will provide the reader with a better grasp of not only the sensor operation, but also its utility for conducting airborne research in the fisheries. It is hoped that the above paragraphs have provided some historical context to clarify the distinctions between the proposed research and the research actually carried out.

5. Approach

5.1 Sensor development and test

The purpose of the sections that follow is to provide an account of the activities and accomplishments of this research. The discussions need to provide enough detail to give an accurate sense of the work performed, and yet be concise enough to be understood in the larger context. Thus, some details associated with the experiments may be discussed only superficially here, whereas some details on the sensor technology will be reiterated here in order to enable the reader to more readily grasp the technical issues surrounding the STIL prototype.

5.1.1 System design and modifications

This section of the final report will elaborate the hardware and software changes introduced into the STIL laboratory sensor[5] in order to ready it for use in field experiments. In order to help the reader understand the changes introduced, it will help to review the principles of operation for the STIL sensor. Then the changes introduced to the laboratory system can be presented more clearly.

5.1.2 STIL sensor operation

Figure 1 shows a conceptual view of the STIL and how it forms three dimensions by collecting 2D images of range and azimuth in a pushbroom fashion. Generally, the STIL sensor generates LIDAR data by projecting a fan-beam pulse of laser light and range resolving the backscattered light with a streak tube receiver, yielding a two dimensional range-azimuth image from objects in its field of view. Figure 2 shows the basic streak tube architecture that is the core element of the receiver optics. It is very similar to a standard image intensifier tube in that it has a photocathode that produces electrons which are accelerated to a phosphor screen (~300 phosphor photons are created for each electron). The major difference is that a streak tube has an extra pair of plates that deflect the beam much like the deflection plates in a standard cathode ray tube (CRT) tube used in oscilloscopes and TVs. In normal operation the input photons are limited to a single slit image plane. The deflection plates have a fast ramp voltage applied that deflects the beam from the top of the phosphor screen to the bottom very rapidly. The image on the phosphor screen has spatial information in the slit direction and time information in the streak direction. A CCD camera is attached to the streak tube to collect the image on the phosphor screen.

---

[5] Including changes introduced prior to the award of this grant, since some of those changes were proposed as part of this research.

15

In a typical streak-tube laser-radar configuration (Figure 3), a short-pulse-time high-pulse-energy laser is used as a transmitter. The transmitter beam is spread out into a single line, which is directed towards the area of interest, and the receiver optics image the line back onto the slit input to the streak tube. Coverage of the target in the dimension perpendicular to the line illumination is generally accomplished via motion of the vehicle carrying the sensor, which allows one to build up a complete image from a series of individual line images (i.e., a "pushbroom" system), although a 1-D scanner system could also be used from a fixed platform.

The sweep time of the streak tube represents the amount of time that it takes for the electron beam from the photocathode to be fully swept across the phosphor screen, which corresponds to the total range gate time (i.e., the total amount of time that the system digitizes range data). The starting point of the range gate is controlled by the trigger signal used to begin the sweep. Computer control of both the sweep time and the sweep start trigger allows the operator to have a very flexible laser radar system that can change its range gate size, range digitization starting point, and range sampling resolution very rapidly. This would allow for a system to search large areas of range with coarse resolution and then "zoom in" to get high resolution around a region of interest, for instance.

Each column of pixels in the CCD corresponds to one channel of digitized range data, such as would be collected from a single time-resolved detector, such as a photomultiplier tube (PMT). The size of the range bins is simply the sweep time divided by the number of pixels in the CCD columns.

The airborne STIL system that Areté uses for bathymetry and terrestrial mapping contains a diode-pumped solid-state Nd:YAG laser that is frequency doubled to 532 nm. This wavelength was chosen for maximum water penetration for the bathymetry task, as well as for being near the peak of the streak tube photocathode responsivity curve. Figure 4 shows the laboratory configuration of the STIL system prior to modifications, and Figure 5 shows the corresponding airborne system block diagram, with some of the system evolution to the present time indicated accordingly.

Figure 6 shows a set of images taken from STIL during terrestrial mapping data collection[6]. A photograph of the area imaged, a single shot from the data over the imaged buildings and also the reconstructed 3D image are shown here as an intuitive example of ASTIL data. As with the ASTIL ocean data, the sampling of the target plane is different in the along-track and cross-track directions (where "track" refers to the direction of motion of the aircraft, which is orthogonal the line-illumination direction). The along-track sampling[7] is simply the velocity of the aircraft divided by the pulse repetition frequency (PRF), in this case 65 m/s and 100 Hz, respectively, which yields a ground sampling of 65cm. The cross-track sampling is a function of the field of view of the receiver (15 degrees), the altitude (350m), and the number of pixels across the slit image (256), which yields a sampling of 32cm.

---

[6] These are included here not for their relevance to this problem, but because the imagery are more intuitive than the ocean data.

[7] Here, sampling is used as a descriptor instead of resolution; this is because the PRF and forward velocity for fixed wing operations often implies that the along track imagery are not continuously covered at the beam-driven resolution; rather the along track dimension is sampled at the laser PRF and corresponding projected beam size.

5.1.3 CSIRO experimental effort

During the fall of 1996 it was decided that Areté would begin considering conducting an airborne experiment with CSIRO for the purpose of studying the population dynamics of juvenile SBT. The experiment, if deemed feasible, was to be conducted in South Australia during March of 1997. The population dynamics issue of interest to the STIL experiment was the size distribution of SBT within a school. This experiment was not fully a part of this research, though the two efforts overlapped and have been mutually beneficial. More importantly, however, the experimental requirements for the CSIRO effort turned out to be directly applicable to the requirements of this research and enable the collection of data that may have otherwise been impossible to obtain.

Since the size of the fish is a LIDAR measurement that is tightly coupled to the resolution, this became a system parameter of primary concern while requirements were redefined for potential participation in the CSIRO experiment. And while it was not known at the time the Saltonstall-Kennedy (SK) grant work was proposed, the detection of any tuna in subsequent SK experiments would also require resolution performance on a par with that which was determined to be necessary for participation in the CSIRO experiments, as it later became evident that school imaging for the purposes of detection and single tuna detection with an imaging system carry the same resolution requirements. So it was serendipitous that the modifications to the laboratory system that were originally proposed were superseded by the requirements established in the CSIRO experiments[8].

The specific requirements for participation in CSIRO experiment were as follows: a) the LIDAR system must be able to detect SBT within a school with individual fish that varied in length from 60 to 120 cm and b) the deployed system must be operated from a light twin aircraft. A depth penetration of 10m was set as a goal, and it was hoped that the system would lend itself to operation at greater depths, but the goals set for the first experiment were mainly to provide proof of concept data that would encourage or remove from consideration further LIDAR experiments.

Operation from a light twin aircraft implied that the laboratory system would have to be compact, light and would have to be assembled in fairly rugged chassis – much more rugged than the laboratory system, which relied on a "portable" optical bench for its ruggedness. The modifications implied by operation in small aircraft were related mainly to mechanical and layout issues. However, it was soon to be discovered that more substantial design changes would be needed in order to achieve the performance implied by the altitude, depth and resolution requirements.

In open ocean flights, higher altitudes are generally preferred to lower, owing mainly to flight safety. However, many airborne experiments are conducted at between 150 and 300 meters altitude; thus, these made good starting points for lower and upper altitudes for making design rule calculations. A good number to use for light twin airspeed is 120 knots, which is about 60 m/s. So the flight parameters used for design calculations were 150 and 300 meters altitude and 60 m/s.

---

[8] Section 6.3 of this report will discuss these issues more at length.

The smallest SBT size to be resolved (along the long axis) was 60 cm, or 0.6m. In order to sample (collect image data) at twice the highest resolution needed (i.e., Nyquist rates), the samples would need to be 0.3m apart. Thus, at 60 m/s ground speed, this implied that the laser PRF would have to be 60 / 0.3 = 200 Hz in order to image an along-track oriented SBT. For sampling this axis of the SBT along the cross-track dimension, the 0.3m sampling merely implies 0.3m/300m = 0.001 radians angular resolution at 300 meters altitude; this angular resolution was already met with the laboratory system, though the proposed SK system modifications would not have met this requirement, thereby also precluding school imaging of yellowfin tuna in the same size class (1 meter length was the median length to be imaged).

There were also implied requirements for imaging an SBT along its narrow axis. Using a 5:1 aspect ratio[9] as an educated guess at the fish shape, the resolution requirements would be more stringent by a factor of five. The implications of these requirements and the aforementioned requirements are tabulated in Table 1 along with the associated parameters for the laboratory STIL system. A few observations follow directly from this table.

Table 1. Resolution and data rate requirements for CSIRO experiments as compared to the laboratory STIL configuration. The CSIRO requirement is shown for major and minor axes of SBT.

Parameter	Laboratory STIL	SK Proposed	CSIRO Requirement
Along-Track Res.	6m	2m	0.3m (0.06m)
Cross-Track Res.	0.001 rad	0.002 rad	0.001 rad (0.0002 rad)
Image Capture Rate	10 Hz	30 Hz	200 Hz (1000 Hz)

First, the CSIRO requirements (which turned out to be very close to the requirements for this research) could not be met with the proposed SK system configuration. Second, the increase in resolution for imaging the hypothetical 5:1 aspect ratio fish body required more than an order of magnitude improvement in resolution over the laboratory system if the minor axis of the fish were to be fully resolved. However, for the major axis of the fish the resolution requirements could be met for some situations, provided that the other system parameters were not forced to take on values that would be prohibitive (i.e., if the implied laser PRF were unavailable).

Thus, as the values shown in Table 1 indicated that an ideal sensor solution could not be found within the allowed time or cost, the issue for consideration became whether or not there was a scenario, or set of scenarios, that would still allow a successful experiment to be constructed. It was determined that, if adequate numbers of SBT were schooled with expected[10] [11] packing densities, it wouldn't be necessary to fully resolve the fish along both axes in order to gain information on the distribution of fish lengths within a school. Rather, it would be adequate to resolve the major axis and rely on the law of large numbers, or make multiple passes over the school being imaged in order to get statistically significant samples at orthogonal directions with

---

[9] This turned out to be a reasonable number for rough calculations, as an SBT was measured to have a tip-tail aspect ratio of 6.5:1 (39 inches long, 6 inches wide, 16kg), which implies that the body aspect ratio is just slightly less.
[10] Data Analysis of the Aerial Survey (1991-1996) for Juvenile Southern Bluefin Tuna in the Great Australian Bight, A. Cowling, T. Polachek, C. Miller, Draft CSIRO Report, Division of Fisheries Research.
[11] Conversations with Dr. Ann Cowling, Division of Fisheries Research, CSIRO.

respect to the fish. So while it was realized that this sort of operational scenario would not necessarily be adequate for an operational sensor, it would yield data suitable for assessing basic feasibility, provided that enough fish signature was present for gathering the data.

The LIDAR signature of an object is driven by its size relative to a resolution element of the sensor and also by its contrast with respect to the background media the object is immersed in (water, in the present case). The contrast, furthermore, is a function of how light reflects from the object. A common assumption is that the object have a Lambertian reflectivity character, meaning that it reflects light uniformly back toward the source of light (the laser). For example, flat paint is often a good Lambertian reflector. The opposite of a Lambertian reflector is a mirror – the light reflects in only one direction, depending on the angle of the mirror with respect to the light source.

The assumptions made for the proposed SK work, and also the CSIRO work, assumed that the fish would have an essentially Lambertian reflectivity profile. It was also assumed that the dorsal reflectivity, or the total amount of light reflected from the dorsal aspect of the fish, would be less than 10 percent, and perhaps even low single digits[12]. It will be shown later in this report that the reflectivity was consistent with this expectation. Thus, based on the single-digit reflectivity expectation, a Lambertian model was assumed for the SBT that yielded an effective reflectivity of 2%, which was regarded as conservative.

Given the aforementioned fish model assumptions, the remaining design issues to settle were the laser and the CCD camera that would capture the STIL images generated on the phosphor of the streak tube. It was clear from a review of the data in Table 1 that significant changes would need to be made to the laser and camera system (especially the CCD camera and associated data acquisition system) in order to accommodate the CSIRO experimental objectives. The situation was exacerbated by the fact that, as the laser PRF increases, the energy per pulse tends to decrease (holding the average power roughly the same), meaning that fewer photons would be available to image with, which tends to degrade overall performance. Furthermore, as the CCD frame rate increases, the noise also increases while sensitivity decreases, holding the choice of CCD technology constant. Fortunately, there were some solutions that became available at approximately the same time that the design modifications were moving forward that made it possible to put together a system that would provide the opportunity to conduct the proof of principle experiment desired for the CSIRO trials.

The system configuration that was settled upon for the CSIRO experiments is shown in Table 2. While it is not appropriate to elaborate herein the details that led to each point in the engineering tradeoff process, a few comments are in order to help motivate the changes. First, the desired laser PRF of 200 Hz was not met as per Table 1. This was driven mainly by the availability of a suitable laser; the 100 Hz laser used had to be rented, and even then was only available for a few months. This stressed the sampling conditions somewhat, but the 100 Hz data rate still allowed

---

[12] Fish Identification by Remote Sensing, B.R. Loya, TRW Technical Report 11435-6001-R0-00, 1968. This research produced a very careful measurement and analysis of the dorsal spectral response of several dozen live pelagic species, and indicated that a non-Lambertian reflectivity may be appropriate, though such a non-Lambertian model was not yet available at the time of this research.

for 0.6m along-track sampling, which if used with a cross-track sampling that met or exceeded the Nyquist rate, was still deemed acceptable for meeting the proof of principle criteria.

Second, the reduction in laser energy introduced by the higher PRF induced a need for better light collection efficiency. As a new CCD camera was to be needed anyway, the improved light collection (nearly the factor of 10 lost in laser energy) was chosen by changing to a CCD having nearly the same size as the laboratory system, but which could be coupled directly to the phosphor of the streak tube via a fiber optic taper. Lastly, in order to collect the data coming from the CCD camera at 10 times the rates of the laboratory system, the data acquisition system was replaced with a ruggedized PC chassis that was populated with digital signal processing (DSP) boards having the bandwidth and programmability needed to collect the image data and facilitate its storage on a removable disk drive.

Table 2. ASTIL configuration for the CSIRO experiments

Parameter	STIL Laboratory	SK Proposed	ASTIL/CSIRO
Laser PRF	10 Hz	30 Hz	100 Hz
Laser Energy/Pulse	200 mJ	120 mJ	12 mJ
Field of view	15 degrees	15 degrees	15 degrees
Camera Format	256x256	128x128	256x256
Digital Resolution	12 bits	12 bits	14 bits
CCD Camera	PI EFT512	PI EFT512	SMD 1M60
Angular Resolution	0.001 rad	0.002 rad	0.001 rad
CCD-Phosphor	Lens coupled	Lens coupled	2:1 fiber taper
Data Acquisition	PC via PI controller	PC via PI controller	PC via DSP
Raw Data Rate	1.3MB/sec	0.9MB/sec	13.1MB/sec

The system having been defined and specified as in Table 2 above, in December of 1996 Areté committed the internal research and development funds to procure components, integrate them into the ASTIL configuration, and flight test the sensor in Tucson prior to shipping the system to Australia in early March of 1997. Figure 7 shows the installation of the ASTIL transceiver section aboard the Partenavia Explorer used for Tucson flight testing. The associated system block diagram deployed at that time is shown in Figure 5.   The corresponding aircraft photograph with the Tucson test participants is shown in Figure 8. For reference, Figure 9 shows an example of sea surface energy densities for several different system configurations.

For the CSIRO experiment, CSIRO funded all of the aircraft and logistics support (directly, not through Areté) and also covered the expenses of one test engineer for Areté. Areté paid the expenses for an analyst up to April of 1997, after which time the SK grant was available to provide funding for on site and post-test analysis of the LIDAR data gathered for the tuna.

The experiments in South Australia lasted from March 26 through April 8. A more detailed description of the data collected was tabulated earlier, which showed the conditions for each data set collected. In excess of 30 flight hours were spent in the waters of South Australia, and observations of captive SBT, dolphin, and both bay and open ocean conditions were made with the ASTIL sensor.   An example of one of the captive SBT schools imaged is shown

photographically in Figure 10. A photograph of the CSIRO participants is shown in Figure 11. The aircraft installation used in the CSIRO experiments is shown in Figure 12.

5.1.4   Data analysis for CSIRO SBT data

A significant amount of time was spent during and after the CSIRO experiment analyzing data, and much of the first year of data analysis for this research leveraged the CSIRO SBT data (hence, the prevalence of these data in this report). As is typical, the data analysis emphasis varied throughout the experiment, beginning with a review of the inherent sensor performance from a radiometric point of view, followed by the optimization of in-flight settings, and finally to the assessment of the tuna signatures collected with the sensor.

The radiometric calculations made early in the experiment indicated that the sensor was operating within a factor of three of theoretically predicted values, which is an acceptable on site error, given the uncertainties in environment and in the new sensor components that had not yet been carefully reviewed in the laboratory for radiometric performance. These radiometric issues were revisited in more detail later in the overall ASTIL development effort, and in subsequent SK work, which is discussed in a subsequent section of this report.

The calculations and data analysis for optimizing the sensor centered around the focus settings, the installed pitch angle of the sensor, and the flight altitude required for adequately resolving the SBT. The focus settings had been accidentally left in the position needed for ground tests for the first two flights; review of the data, combined with some in flight experiments quickly made this clear and brought about a correction. The pitch angle of the sensor was initially 2 degrees, but was increased to 4 degrees in order to help reduce the ocean surface glint that was plaguing the data. When combined with a nose-up aircraft attitude of 4 degrees, this allowed for experiments to attain an off-nadir incidence angle of up to 8 degrees, which helped reduce the glint considerably.

Once the focus and glint issues had been addressed, the analysis of data could center more on the acquisition of good quality tuna signatures. To help this process, flights were made at 305, 150 and 75 meters altitude. As these flights were all conducted over buoyed nets containing captive SBT, the edges of the nets clearly marked the boundaries of the nets in the image data. Thus, one could unambiguously assess the performance of the sensor at the various altitudes as concerned the quality of the tuna signatures. The immediate and obvious result was that tuna signatures were not visible at all from 305 meters, were marginally visible at 150 meters and were very clearly present at 75 meters. The difference in these altitudes was partly energy at the surface, but most of the performance enhancement was due to the increased resolution that accompanied the decreased range. Consequently, subsequent experiments flew principally at 75 and 150 meters altitude, with the emphasis on the lower altitude.

An example image of an SBT signature in a single image of ASTIL data is shown in Figure 13, where the image has been processed to remove artifacts associated with surface reflection and exponential decay in the water. The SBT is the bright portion of the image in the lower half of the figure.

The early conclusions from analyzing the imagery like that shown in Figure 13 were that: 1) the SBT signature was slightly less reflective than the conservative estimates made in the preparatory design calculations, and 2) the water in Boston Bay (where the tuna nets were kept) was turbid enough to limit detection performance to the top ten meters or less[13]. Figure 14 and Figure 15 show photographs of a representative SBT from one of the fish schools that were imaged. The typical low dorsal reflectivity and corresponding high belly reflectivity is evident in these photographs.

These early conclusions will be explained more fully in the findings sections of this report. However, it is important to point out here that the findings from the on site CSIRO analysis did impact subsequent experiments and helped greatly in their planning, and the data continued to be invaluable in understanding the LIDAR/tuna issues relevant to school detection.

5.1.5 System enhancements

Many of the system enhancements incremental to the laboratory STIL configuration were implemented prior to the experiments with CSIRO, as shown in Table 3. Thus, most of the planned enhancements, as originally proposed for the SK, were not needed. In fact, based on the CSIRO data analysis, it was clear that they would have been prohibitive for gathering useful data on tuna. However, several items were added after the CSIRO experiments that had been planned but were not finished in time for the CSIRO tests, and some items were added over the course of time because it became clear that they were needed for proper use of the ASTIL sensor.

Table 3. ASTIL system enhancements prior to and subsequent to SK Grant effort

Item	Date Implemented
100 Hz data acquisition	Jan-Feb 1997
Fiber coupling for CCD camera	Jan-Feb 1997
High speed, high resolution CCD camera	Jan-Feb 1997
Ruggedized sensor and equipment racks	Jan-Feb 1997
100 Hz laser	Jan-Feb 1997
Realtime display	May 1997
GPS data collection	August 1997
Nadir-viewing video camera	August 1997
100 mm f/2 objective lens	August 1997
30 Hz laser	September 1997
Coarse attitude data collection	September 1997
GUI-driven sensor control	January 1998
Flat panel touchscreen display	May 1998
Realtime Kinetic GPS	October 1998
Cmigit INS system	October 1998
Polarizer	October 1998

---

[13] The apparent diffuse attenuation coefficient ranged from 0.12/m to 0.20/m in Boston Bay.

A quick review of the funding allocated for sensor improvements under the SK effort and the funds required to implement all of the above changes will lead one to the conclusion that these could not have been implemented under this effort. Only three were funded under the SK effort (GPS data collection, nadir video camera, coarse attitude data); the remaining items were funded under both ONR and Areté IR&D, as the ASTIL sensor is a derivative of an ONR STIL effort for underwater imaging, and Areté has an interest in the airborne technology for commercial uses.

While it is important to note that multiple sources of funding have made the SK experiments possible, it is perhaps more important to note that the ASTIL development started prior to the SK effort and continues to this day. Furthermore, the SK effort has motivated improvements to the sensor that help serve SK purposes and other applications as well. Lastly, the findings in this report will influence the ongoing developments with the ASTIL sensor, and will enable the technology to be evaluated further in this area experimentation, as opportunities arise.

5.2 Model calculations for fish detection and sensor radiometric performance

The engineering efforts to modify the laboratory sensor, the preparations made for airborne experiments, and the on site data analysis efforts involved model calculations that provide theoretical estimates of performance. While some model calculations were run as full image simulations, most of the model calculations were radiometric in nature, as these are more tightly coupled to assessing proper sensor behavior and the understanding of the physics of the tuna detection problem.

The research originally proposed was to rely on simulations of at-depth fish schools generated with an STIL simulator (developed under ONR sponsorship) that was to have been completed by early 1997. However, this simulator was not completed until early in 1998, and the development of the ASTIL prior to SK funding reduced the motivation to perform such simulations in support of design tradeoffs. Nonetheless, some simulations of at-depth tuna were run using the gated-LIDAR simulator (which was available) to gain a heuristic understanding of the effect of multiple scattering upon the images of tuna. So some use was made of simulated LIDAR imagery; however, this was minimal and extensive use of such simulation was not justified, given the objectives of this experiment (to gather data on tuna for assessing detection feasibility). Furthermore, the data collected in the CSIRO experiments indicated that the ASTIL design had the resolution performance required, and that further improvements could not be affordably made in order to advance the objectives of this research.

An example of a radiometry calculation for the ASTIL sensor is provided in Figure 16. Here, the number of CCD counts measured per pixel is plotted as a function of depth for both the water volume backscatter and a single pixel target having Lambertian backscatter characteristics and a reflectivity of 2%. This model calculation predicts a contrast (target-background/background) in excess of 20. This contrast was significantly in disagreement with the actual measured contrast of tuna.

5.3 Experiments

5.3.1 Hawaiian Islands experiment

The proposed SK effort featured a collaborative billfish experiment in Hawaii during August of 1997 (projected from a November 1996 start date). However, owing to sensor improvements in process and conflicts with the ONR effort (from which the ASTIL system borrows its components), this experiment could not be planned. However, the objective of conducting an experiment in Hawaii remained, as the waters near Hawaii were known to be frequented by schools of yellowfin tuna during the summer and early fall months.

The conduct of the experiment was very much like that of the CSIRO experiment, as it involved the inevitable shipping, uncrating, ground testing and test flights needed for any remote deployment of an airborne sensor. The principal difference that was a significant hindrance to the effort was the difficulty in obtaining a ready-to-fly aircraft for the experiments.

Much effort was expended in finding a fixed based operator (FBO) who could support the test, helping the FBO make modifications to his aircraft, and also cajoling he and the local FAA representative into enabling the experiment to proceed[14]. Nevertheless, the experiments were conducted throughout the islands, as portrayed graphically in Figure 17.

From Table 3 it can be seen that the 30 Hz laser was integrated in time for this experiment. The reason the 30 Hz laser was chosen was because it could provide a factor of ten times more laser energy per pulse than the 100 Hz laser could. This selection would seem to impede good data collection if the objectives were the same as for the CSIRO experiment. However, the objectives were not the same, as the SK effort is concerned much more with schools than individual fish behavior, so that one need only about sample throughout a school, and not across an individual fish. Thus, the along-track sampling was approximately 2m, and the cross-track sampling was unchanged with respect to prior ASTIL experiments.

The flights shown in Figure 17 represented 30 hours of flight time in the Piper Aztec operated by Commercial Flyer, Inc., of which 28 were spent in search of schools or ferrying to areas of interest. Following the last day of flying, the sensor was uninstalled, re-crated and shipped back to Tucson.

5.3.2 Data analysis for Hawaiian experiment

The data collected in Hawaii had only a few probable tuna signatures – there were no schools of tuna detected, and only a few times during which a school of possible tuna were suspected, based on the proximity of birds at the surface. Thus, the data analysis effort consisted of reviewing data from other species and checking the radiometry of the data for consistency with theoretical calculations.

---

[14] The technical monitor for this effort within NMFS was significantly instrumental in helping make this test a reality, as the hurdles presented by the FAA process were many, and the number of eligible FBOs in the Islands is small.

The non-tuna species imaged was a school of akule imaged on September 17. Some probable tuna were also imaged on September 24, and these were reviewed for consistency with other data sets. The radiometric calculations were made to assure proper sensor operation, and these yielded no significant discrepancies between theory and experiment.

5.3.3 New England Aquarium experiment

Ideally, the experiment in Hawaii would have yielded enough imagery of ETP tuna to use in assessing the performance of the ASTIL sensor for the bycatch reduction problem. However, as noted above, only a few potential tuna signatures were obtained, precluding any meaningful analysis regarding the optical characteristics of tuna in the context of a school. Thus, an additional experiment was planned, after consulting with NMFS and NOAA scientists doing research on tuna-related issues.

The objective of the experiment was to find a tuna schooling event or migratory pattern that was reliable and had been studied adequately to allow an experiment to be planned and executed within a period of 3-4 weeks, so that costs could be minimized. Also, it was desired to image schools of fish that could be unambiguously identified from the air, and which could be readily spotted from the aircraft, if possible[15].

The first possible opportunity was an experiment with NMFS in collaboration with Dr. Barbara Block (Monterrey Aquarium), who was studying GBFT near Cape Hatteras. These tuna have the features mentioned above that aid in conducting airborne LIDAR experiments. However, the experiment was in the spring (March/April) and the notoriously poor weather in that region during that time of year motivated the consideration of a subsequent opportunity.

That opportunity was an experiment conducted with Dr. Molly Lutcavage (New England Aquarium), who has been conducting aerial surveys of GBFT for several years, and who has an ongoing interest in using LIDAR for estimating stocks. This experiment could be conducted anytime during the summer and early fall months; thus, as the weather in the waters near Cape Cod is amenable to airborne experiments, a period in July was selected for the experiment, based on previous observations of tuna, aircraft availability and sensor availability with respect to ongoing ONR STIL efforts[16].

The experiment was conducted jointly with the New England Aquarium, as Dr. Lutcavage set up coordination with the local spotter pilot's association (Mr. Jonathon Mayhew), and a few local fishermen. The cooperation amongst these fishery players were exceptional, and made it possible to obtain the data that was gathered. Table 4 shows the support team that made the GBFT experiments possible.

---

[15] This was not a new issue, of course, but prior experiments had been planned a bit naively, it having been assumed that nearby fishermen would be able to assist in the identification process.

[16] This was less of a concern in this experiment than previous ones, as the ASTIL sensor hardware was a backup to the newly developed EOID sensor hardware, and not the principal means of experimentation.

Table 4. Support for New England GBFT experiment

Support Role	Name and Organization
Local support coordinator	Dr. Molly Lutcavage, New England Aquarium
Pilot and aircraft provider	Mr. Tim Flynn, AeroMarine Survey, Inc.
Spotter	Mr. Wayne Davis
Spotter Pilot's Assn. Liaison	Mr. Jonathon Mayhew, President of NESPA
Boat support for aircraft overflight	NESPA volunteer spotter pilot
Aircraft support for aircraft overflight	NESPA volunteer spotter pilot
Hangar support and FAA clearance	Columbia Air Services (New London, CT)

Aircraft installation and integration began on July 20 and was completed on July 24, when the first check flight was over the waters near New London, CT. The data flights were all made in the vicinity of the southwest end of Cape Code. These flights began July 25 and were completed July 29. Originally, 30 flight hours had been planned for this experiment. However, because of the difficulties experienced with aircraft logistics[17] and the anticipated onset of storms, the experiment was ended after 19 hours of flight time had been expended, which was very soon after the first (and only confirmed, to date) GBFT school data were observed (approximately 14 of the 19 hours were spent directly on tuna spotting efforts). So while only a small portion of data was collected with respect to what had been hoped, the data that was collected proved to be adequate, as will be shown later in this report.

The sensor was uninstalled, crated, and shipped back to Tucson on July 31, concluding the effort after 11 days.

5.3.4 Data analysis for GBFT data

The data analysis for the GBFT data was begun immediately after the experiment ended, in order to obtain some indication of the adequacy of the data set for use in making the assessment that was the goal of this research. Some image processing and 3D reconstruction work soon yielded a set of fish signatures, 2D images and 3D images that led to the conclusion that data of adequate statistical significance and of sufficient quality had been obtained in the GBFT experiment alone to finish the research. Summary notes and data files were generated for the GBFT experiment in preparation for the final report effort, which would have to wait until December to resume, as there were personnel conflicts with the STIL effort for ONR, the primary sponsor of the STIL research.

The analysis conducted for the GBFT data, once resumed, began with a hand-tabulation of individual signatures and associated data, which formed a database representing "ground truth" for the subsequent analysis of the detection of the GBFT. Signal processing tools from the ONR effort proved invaluable in reducing the data and extracting the relevant fish LIDAR signatures needed to assess the optical properties of the fish and for comparing the reference database to subsequent automatic detection computations.

---

[17] For instance, installation was plagued by FAA regulatory hindrances, and aircraft positioning greatly impeded the imaging of schools. The lessons learned section has some general comments in this regard.

5.4 Development of a performance model based on experimental outcomes

With a database of fish LIDAR signatures and associated image and school statistics in hand, the analysis proceeded to develop a performance model based on a probability density function for the LIDAR signals associated with both the fish in water and the water without fish, representing the target and background for subsequent signal analyses. The formulation of the performance model was developed, in keeping with binary hypothesis testing, with an eye on predicting probabilities of detection and false alarm. The purposed of the model was to allow performance calculations to be made as a function of new sensor configurations, so that some estimates could be made for operational ASTIL sensors (the present experiments being conducted with a sub-optimal prototype), without building new hardware and having to conduct airborne experiments for each sensor parameter variation.

As part of the performance model development, a target detection algorithm was built to measure the actual performance using the data collected on GBFT. Such a measurement would serve as a baseline from which modeled performance estimates could be made[18]. This was based on a matched filter detection routine that computed the ratio of signal (fish) to noise (water without fish), or the signal to noise ratio (SNR). The results of this performance measurement were then used to generate histograms of signal and noise, in addition to a ROC, which illustrates the tradeoff between probability of detection and the associated probability of false alarm.

Having developed a performance model accompanied by measured performance on GBFT, the performance model was exercised jointly with a radiometric sensor model (developed over the course of the sensor development) to explore the sensor design parameter variations for an optimum operation point for detecting tuna.

5.5 Generation of LIDAR fish image database

In the proposed research, it was hoped that enough observations of schools would be obtained to compile a LIDAR database of school and/or fish signatures. As such a plethora of data were not obtained, there was little need to make the effort to formalize a database. Rather, select portions of data have been isolated and processed, in the hope that these can be made available on the world wide web to those researchers that are actively engaged in airborne LIDAR experiments.

5.6 Project management

1. Areté Associates
   a. Andrew Griffis: Principal investigator, R&D engineer, director of flight tests, data analyst for field experiments. Planned and coordinated the activities of the engineers and scientists prior to and during field tests, and also during post-test data analysis. Principal author of the final report.
   b. Elisabeth Bryan: Data analyst and scientific programmer. Developed high level language routines for analysis of image data, including the generation of graphical output.

---

[18] So the measured performance can be viewed as the tie-point from which performance is extrapolated using the analytical performance model.

Provided quick-look assessment following experiments and performed the analysis of fish LIDAR signatures needed for performance modeling.

   c. Jeffrey Plath: System software and sensor engineer. Developed real-time software for high speed data acquisition and supported field tests as a sensor operator and field engineer for CSIRO and Hawaii trials.

   d. William Ryder: Sensor operator and field engineer. Provided logistics support for sensor assembly, disassembly, shipping and aircraft operation for New England experiment, including system modifications after and during testing.

   e. Glen Redford: System software support for upgrades to software for real-time display and GPS data logging. Added GUI functions to C/C++ routines running on host computer. Supported pre-flight laboratory test support.

   f. Brian Redman: Systems analyst. Developed performance model based on observed tuna signatures and ocean ambient data, which served as a basis for both the predictive statistical model and the observed detection measurements. Provided graphical performance estimates for final report.

2. Commercial Flyer
   a. Clyde Kawasaki: Co-owner. Provided a Piper Aztec for experiments and hangar space for equipment storage and install/uninstall operations. Assisted with obtaining FAA flight authorizations.
   b. Wally Suenaga: Co-owner and spotter pilot. Flew aircraft and aided in flight planning for finding schools of fish.

3. Aero-Marine Surveys
   a. Tim Flynn: Owner and pilot. Provided a Piper Aztec for experiments and hangar space for equipment storage and install/uninstall operations. Assisted with obtaining FAA flight clearances. Flew aircraft with input from co-pilot spotter.
   b. Columbia Air Services: hangar, FAA and aircraft logistics. Provided aircraft services and engineering support for obtaining FAA clearances.

4. NMFS: Chuck Oliver. Provided research support for early tuna pre-test investigations (i.e., literature searches), aircraft and aircraft provider research and coordination; provided liaison support for FAA clearance in Hawaii; provided points of contact for experiments conducted in the United States. (US Gov't funding)

5. New England Aquarium: Molly Lutcavage (New England Aquarium funding). Aided in experiment planning, coordination with fisheries owners, and review/analysis support prior to and following the trials. Coordinated interaction with spotters and boat owners.

6. New England Spotter Pilot's Association: Jonathon Mayhew (volunteer). Provided support for test planning and spotter coordination/planning prior to and during the experiments.

7. CSIRO: Dr. Ann Cowling. Provided aircraft logistics, experiment planning, coordination with fisheries owners, and review/analysis support prior to and following the trials. (CSIRO funding)

8. Tasmanian Air: Supplied (under contract with CSIRO) pilot for Aerocommander 550. Provided aviation with support from spotter. (CSIRO funding)

9. Derek Hayman: spotter pilot for SBT fisheries in South Australia. Provided aviation and spotter services. (CSIRO funding)

6.   Findings

The purpose of this part of the final report is to communicate the "bottom line" results and to present the rationale and/or data that led to those results. Consequently, the following discussion will begin with what amounts to raw data and proceed to develop that raw data into meaningful performance predictions based on robust physical and mathematical analyses. The raw data will be presented briefly as the experimental effort is delineated, and elaborated further in the context of the data analysis.

The raw data for the ASTIL sensor are two dimensional (2D) data formed by imaging and range resolving the backscattered light from a single fan beam pulse from the ASTIL laser. Most of the analysis presented here will deal directly with the 2D data and transects of these data, which are typically one-dimensional (1D) range-slices. The reason for this is that the performance of the ASTIL system that can be addressed through sensor improvements is driven largely by the performance associated with a single image. The single image performance, in turn, is best measured in terms of the depth-dependent performance of a single region in the cross-track direction, or a 1D image slice in depth.

The 3D image data presented here are mainly a tool for understanding the school shape and packing density, and also for aiding in the understanding of how the ASTIL sensor can be used to studying and quantify fish school behavior in general.

The emphasis in the data presented here will be the GBFT data collected in New England, as this is the highest quality tuna data collected during this effort. The LIDAR signatures are prominent enough to study, measure and draw conclusions from, and they are of sufficient quantity to provide statistical significance. For these reasons, the GBFT data form the backbone of this report. Data from the other experiments will also be shown, but will not be as prominent as the GBFT data.

Where necessary, the discussion of issues concerning other LIDAR sensors is included, for the sake of clarity in understanding the issues relevant to the present investigation, and also any research that may follow.

The presentation of results will conclude with what amounts to a "lessons learned" discussion, as some noteworthy insights have been gained from the conduct and analysis of these airborne LIDAR trials.

6.1   Understanding ASTIL image data

The purpose of this section is to provide a brief tutorial or introduction to the data that is generated with the ASTIL sensor. Earlier in this report, the basic principles of operation were expounded. This section will extend that discussion so as to enable the reader to more fully understand the material presented in subsequent sections.

As shown in Figure 18, an image that has both surface and bottom backscatter in it, the ASTIL sensor has raw data that are two-dimensional images having range along one dimension and

azimuth or cross-track as the other dimension. These are usually shown as the vertical and horizontal dimensions, respectfully. The image shown in Figure 18 has several features to note. First, the surface return[19] has several bright spots in it corresponding to regions across the ocean surface that tend to collect and focus the backscattered light with high intensity back towards the ASTIL receiver. This can be mitigated through the use of a polarizer on the receiver objective lens that rejects the co-polarized return from the air-sea interface, thereby yielding near-surface images that are dominated by water volume backscatter instead of the (sometimes) excessive enhanced backscatter that can be obtained from surface wave focusing and smooth water surfaces that are perfectly perpendicular to the sensor optical axis. Such a polarizer was not implemented at the time these data were collected but has been demonstrated since then with gratifying results.

Second, the image shows return from the bottom (of Boston Bay), that is less intense and removed in range from the surface return. The return is less intense because the water introduces exponential attenuation that increases with increasing depth. The return is also less intense at the bottom due to the fact that LIDAR return signals generally decrease as the square of the range from the LIDAR; however, this range dependence is not nearly as pronounced as the exponential decay.

Third, the surface return appears to be wider in the range direction than the bottom return. This is easier to see if a slice along the range direction is taken through the image in Figure 18. Such a slice, or range-transect, is shown in Figure 19. It can be seen in this figure that the return signal from the surface region extends in depth and appears to be slightly wider than the return from the bottom. This is due to the fact that the backscattered light from the surface-only portion is actually a combination of the surface return with the volume backscatter from the water molecular and particulate constituents, leading to a return that is peaked at the air-sea interface, and decays exponentially in depth. The bottom return is simpler, as it is just a replica of the transmitted laser pulse, scaled in intensity by the exponential attenuation of the water and the square of the distance from the transmitter[20]. This distinction between surface, water volume backscatter, and solid objects as pertains to the LIDAR return, is important for the reader to bear in mind as other images are studied. This is because the return signal from a fish in the water will be distinct from the water volume and surface signals in the same way that the bottom return is distinct from these signals. The main exception will be the magnitude of the fish return (smaller than the bottom, for tuna) and the size (less cross-track extent), as the imagery to be shown soon will show.

Now while the ASTIL raw data are fundamentally two dimensional in nature, the sensor does provide three-dimensional information by stacking images in a pushbroom fashion, so that the third dimension is formed through repetitive acquisition of 2D images. A sequence of images that is intuitive to view is from the data collected in Hawaii.

Figure 20 shows a sequence of eight 2D images collected during the Hawaii experiment of September 1997. These images are of the same format as the images shown in Figure 18, except

---

[19] By "return" is meant the light that backscatters, or returns, to the receiver from an object that was illuminated with the sensor laser.

[20] This is a paraphrase of the LIDAR range equation.

that the cross-track extent and bottom depth are greater in Figure 20, as noted. The school of fish is absent in the first image, begins to appear in the upper left hand side near the surface in the second image, is very obvious by the fourth and fifth images, and is fading out by the eighth and last frame. It may not be immediately obvious from the 2D images, but the way the cross-track extent of the akule school changes as the sensor samples along it is indicative of a nearly circular disc of fish in the water.

The disc-like shape of the school is much easier to see when the image sequence of Figure 20 is stacked together into a 3D volume data set, and rendered as a 3D perspective image shown in Figure 21. This typifies the objective of the ASTIL sensor – resolving objects at high resolution in three dimensions. The size of the school is approximately 13 x 14 meters across and on the order of 1m in depth, for about 182 cubic meters of fish. The school was not very deep, measuring about 3.5 meters average depth. The ocean bottom was at 25m depth, and is faintly visible in the 2D images, whereas in the 3D images one can readily discern not only the bottom, but also the shadow of the ASTIL-illuminated disc of akule. Hence the ability to combine 2D images into 3D images greatly enhances the understanding of the submerged object(s) being studied.

Obviously, given a 3D data set, one can also study features within that data set with 1D and 2D sections made along arbitrary axes. For the data being evaluated in this research, the sections tend to be in the along-track, cross-track and depth dimensions. These sections are used most often to aid in the understanding of the optical properties and sizes of the fish being imaged, and for assessing the sensor radiometric accuracy. These techniques, and the 2D and 3D images from which they're drawn, will be elaborated further in the balance of this report.

6.2   ASTIL observations of tuna

The purpose of this section of the report is to display and discuss the data gathered with the ASTIL sensor for the three species of tuna imaged in this investigation. The data displayed here will be primarily 2D in nature, with discussion focusing on both the 2D and 1D nature of the LIDAR signature of the tuna data. Only one tuna species will be shown in three dimensions, as only this set is of sufficient signal quality to readily lend itself to 3D imaging without extensive signal processing and fine-tuning of image data.

The three species imaged, their locale, and the general nature of the respective LIDAR data are tabulated in Table 5 below. From this table it can be seen that the SBT imaged were in water that was twice as turbid as the open ocean water, as indicated by the diffuse attenuation coefficient (K) that non-captive tuna would inhabit, and they were smaller than the GBFT by more than a factor of two.

Table 5. Tuna species imaged with ASTIL sensor

Species	Location of Experiment	Water Quality	Size (kg, WxL)	Quantity Imaged	Depth
Southern bluefin tuna (SBT)	Port Lincoln, South Australia	Bay/moderate K=0.15/m	10-40kg 0.1x 0.6m	500+	3-8m
yellowfin Tuna	Oahu, Hawaii	Clear/ocean K=0.07/m	Unknown	2-3	3-4m
Giant bluefin Tuna	Cape Code, Massachusetts	Clear/ocean K=0.08/m	150-300kg 0.3 x 2m	70+	2-6m

These factors caused the analysis of data to rely more on the GBFT data than on the SBT data, though both were important to the overall experimental effort. The SBT were captive, so that the association between LIDAR data and tuna in the water was unambiguous. The GBFT were not captive, but they were identified visually by multiple spotters and surface craft during the airborne experiments, so these are also high confidence data as concerns the identification of the fish species. The yellowfin data were clearly too sparse to work with, and they were not as confidently identified with tuna as were the SBT and the GBFT. However, the fact that the yellowfin data were not the prime focus of the data analysis does not negate the applicability of the analysis to the yellowfin species. Fishermen and those associated with the fishing industry will confirm the visual (optical color/reflectivity) similarity of the species[21], and common placement in the food chain with similar predators would tend to lead one to the conclusion that the optical properties of the tuna species would be similar[22]. As will be shown, the yellowfin data collected in this research are not abundant enough to draw statistically significant conclusions with. However, they do serve to support the other observations indicating that the species are optically similar, and therefore can be studied as such.

The following discussion will review data for GBFT, SBT and yellowfin. The GBFT data will be used to derive representative optical properties of tuna, and so will be reviewed more at length. The SBT data will be shown for comparison and contrast with the GBFT data, and the yellowfin data will be shown mainly as a single point of comparison with the other two species.

6.2.1   Giant bluefin tuna (thunnus thynnus) data

Approximately 14 hours (of 19 total flight hours) were spent in airborne experiments targeting the GBFT fishery in New England waters near Cape Cod, Massachusetts. Of these hours, only less than one minute of real time data was gathered over a school of tuna, though many opportunities were available; the difficulty, as was pointed out earlier, lay in the type of aircraft used and the associated logistics of the sensor installation. Nonetheless, the small amount of

---

[21] Discussions with Derek Hayman in April 1997 (spotter pilot from Port Lincoln, S. Australia), Wally Suenaga in September 1997 (spotter pilot from Oahu, HI), and fishermen in both S. Australia and Hawaii. Video footage of yellowfin provided by NMFS and comparison with photographs of SBT also indicate optical similar from the dorsal viewing angle, in addition to the evident direction-dependent reflectivity, and perhaps color, of the tuna.

[22] Fish Identification by Remote Sensing, B.R. Loya, TRW Technical Report 11435-6001-R0-00, 1968. The measurements presented in this report indicate very clearly that the dorsal reflectivity that is evident with the naked eye is confined to a fairly small range of single digit reflectivities, meaning that within factors of 2, the problem will quite likely be driven by the physical size of the tuna, and not the factors that cause marketplace differentiation.

time for which the tuna were imaged was adequate to draw meaningful conclusions about LIDAR and tuna, owing mainly to the quality of the LIDAR tuna signatures gathered.

A map showing the proximity of the GBFT school to Cape Cod is shown in Figure 22. The southwestern locations are near New London, CT, from which the experiments were based. Examples of unprocessed GBFT data collected with ASTIL were shown in Figure 23 and Figure 24, and several processed images are also shown in accompanying figures.

6.2.2   Southern bluefin tuna (thunnus maccoyii) (SBT) data

Approximately 30 flight hours were spent in South Australia (this research supported only the analysis of data for those experiments). Image data of SBT were collected for captive schools of fish in Boston Bay, which is the harbor region for Port Lincoln, South Australia. An example of ASTIL data for SBT is shown in Figure 13.

6.2.3   Eastern tropical pacific (ETP) yellowfin data

Only one or two instances of yellowfin tuna were imaged during the Hawaii experiment in 1997. These were collected near a buoy slightly to the north of Pearl Harbor. An example of ASTIL data for these is shown in Figure 25 and the corresponding contrast estimate is shown in Figure 26. Approximately 20 hours of flights were committed to searching for yellowfin both near and around the Hawaiian Islands, without a single spotted school of fish for which image data could be collected. The imagery collected were obtained incidentally while spotting near a buoy.

6.3   Tuna contrast and resolution considerations

Unlike the schools of akule or other pelagics like sardine or krill, schools of tuna do not pack closely together so as to form an optically continuous amorphous mass of fish that can be detected by a LIDAR with resolutions close to those of the ASTIL sensor[23]. Thus, detection of single tuna becomes an issue of concern for a LIDAR. Also, the tuna do not have as high a reflectivity as some of these high-packing-density pelagics. Both of these issues have a direct impact upon LIDAR performance, as the LIDAR depends upon the difference between water backscatter and fish backscatter to determine the presence of a fish. The quantity that one can measure in an image that describes this difference is known as the contrast.

Image contrast for a LIDAR viewing submerged objects in the water is determined by the water reflectivity, the reflectivity of the object being imaged, and the resolution of the LIDAR. For an imaging LIDAR, the resolution is determined by a pixel and range bin size; for a non-imaging LIDAR (i.e., flying spot) the resolution is determined by the spot size and the range bin resolution.

---

[23] It is recognized that, if fine enough resolution were applied to the problem, even the high packing density fish such as sardine could be distinguished, though not necessarily from an airborne platform. For instance, Figure 28 shows imagery for small fish in which the sensor is providing cm-level resolution at an underwater standoff range of 8 meters.

33

Consequently, the ideal non-imaging LIDAR would be designed so that its beam would be either fully occupied by the tuna, or fully occupied by water. Thus, if the fish reflectivity were sufficiently bright with respect to water, the optical distinction between fish and water would be maximum – the contrast would be maximized. Likewise, an ideal imaging LIDAR (streak-tube or gated ICCD) would be designed so that the tuna fully occupied at least one pixel in an image so that adjacent water-only pixels would be readily observed in contrast to the (brighter) tuna-related pixel.

The water reflectivity is a well-studied parameter that can be treated as a constant once the water type is known, for the purpose of first-order calculations. The calculations presented here will use a clear ocean water type that has a volume backscatter coefficient of $\beta(\pi) = 0.0007$/m. Estimates of tuna reflectivity vary from 1% to 13% depending on what source was consulted[24][25]. For the purposes of this discussion, values of 1.5% and 10% will be used for bracketing the reflectivity at low and high boundaries; the former value is the correct one, though the latter value was used in some of the calculations made early in this endeavor.

For a target viewed against a background, the contrast is determined by the difference between the target and the background, normalized to the background. For the present case, the fish is represented optically by the target effective reflectivity and the background is determined by the water volume backscatter. Mathematically, this is given by

$$C = (T - B) / B \qquad\qquad (Eq.\ 1)$$

Where C is the contrast, T is the target and B is background. From this equation, it is clear that in order to obtain high contrast (good image quality), one must maximize the difference between the target and the background. Some substitutions will allow the target and background quantities to be expressed in terms that relate more closely to the sensor and water parameters of interest. Let

$$T = \rho_e \qquad\qquad (Eq.\ 2)$$

and

$$B = \beta(\pi) \cdot \Delta z \qquad\qquad (Eq.\ 3)$$

Here Δz is the range resolution (depth bin size) for the LIDAR and ρ_e is the effective reflectivity, or the reflectivity apparent to the LIDAR, while $\beta(\pi)$ is the aforementioned volume backscatter reflectivity associated with the water column being illuminated with the LIDAR transmitter (the laser). Substituting into the expression for contrast, we now have fish contrast given by

$$C = (\rho_e - \beta(\pi)\cdot\Delta z) / \beta(\pi)\cdot\Delta z \qquad\qquad (Eq.\ 4)$$

---

[24] Oftentimes, the tuna are assumed to be similar to other pelagics, leveraging work such as that presented by B.R. Loya referenced earlier.

[25] Evaluation of the Capability of the Experimental Oceanographic Fisheries LIDAR (FLOE) for Tuna Detection in the Eastern Tropical Pacific, J.H. Churnside, et. al, NOAA Technical Memorandum ERL ETL-287, March 1998.

In the above it is assumed that the fish fills the entire resolution element of the LIDAR, or in the language of imaging systems, it completely fills the pixel(s) in which it is observed. In such a case, assessing the optimality of the LIDAR for observing individual fish becomes a matter of setting the resolution to resolve the fish and then examining the impact of fish reflectivity and sensor optical efficiency. However, it is not always the case that a LIDAR can achieve arbitrarily high resolutions. In fact, high resolution in any remote sensing system comes at a price and will have attendant performance tradeoffs with respect to lower resolution systems having comparable optical efficiencies. Thus, there is strong motivation to build only enough resolution into a LIDAR to provide the data that are needed. As a result, it is important to treat the case for which the fish to be imaged are under-resolved.

In order to represent the cases for which the fish does not fill the entire pixel, we need to add scale factors to account for the part of the pixel occupied by the target and that part which is just water. This can be achieved by introducing a fish-area parameter, A_f, that represents the LIDAR cross-section of the fish. The LIDAR cross-section for the fish will be assumed to be the same as the physical cross section of the fish in a plane normal to the LIDAR angle of viewing. For a nadir-viewing airborne sensor that is directed toward laterally swimming fish, this cross section is the same as the profile of the fish viewed from the dorsal region. The expression for contrast can now be written as

$$C = [\rho_e\, A_f\, /\, R_{xy} + (1 - A_f\, /\, R_{xy})\, \beta(\pi)\cdot\Delta z - \beta(\pi)\cdot\Delta z]\ /\ [\beta(\pi)\cdot\Delta z] \qquad \text{(Eq. 5)}$$

Which readily simplifies to

$$C = (A_f\, /\, R_{xy})\, [\rho_e - \beta(\pi)\cdot\Delta z\,]\ /\ [\beta(\pi)\cdot\Delta z\,] \qquad \text{(Eq. 6)}$$

where R_{xy} is the area at the water surface for a sensor resolution element[26] and the ratio $A_f\, /\, R_{xy}$ is the fractional area inside the resolution element occupied by the fish.

In its simplest application this expression provides the LIDAR contrast for a single fish in the water. In order to represent multiple fish in the water, or a given water column, it is necessary to include the number of fish per volume resolution element. Letting the number of fish be represented by N, and making this modification, the contrast equation yields

$$C = N(A_f\, /\, R_{xy})\ \cdot [\rho_e\ - \beta(\pi)\cdot\Delta z\,]\ /\ [\beta(\pi)\cdot\Delta z\,] \qquad \text{(Eq. 7)}$$

This expression can be directly evaluated for the dependence of contrast upon the parameters in the right hand side and a sense of the optimal point gained graphically. Such a plot is provided in Figure 27. The selection of parameters was made to be consistent with realistic conditions as much as possible. The figure shows three plots, each for a different packing density, D.   The fish area used was 0.05 m^2, which follows from a similar argument to that posed by Hunter[27],

---

[26] So the volume resolution element, or voxel, is $R_{xy}\Delta z$.
[27] Evaluation of the Capability of the Experimental Oceanographic Fisheries LIDAR (FLOE) for Tuna Detection in the Eastern Tropical Pacific, J.H. Churnside, et al, NOAA Technical Memorandum ERL ETL-287, March 1998.

where a box-shaped 20kg tuna is used for a case study, and for which the box dimensions were 10 x 20 x 100cm. The corresponding dorsal-view area for the present research would then be 10 x 100cm. However, the calculations presented here will use half the area, as the actual shape of a fish bears little resemblance to a rectangle and can safely be approximated by an inscribed parallelogram filling half the circumscribed rectangle. Hence the fish area used is $0.05m^2$. The depth resolution used is 1m. The ASTIL system and some flying spot systems can provide sub-meter depth resolutions. However, the equivalent range of a typical commercial laser is much closer to one meter (corresponding to approximately 9ns in water), so that in order to capture all of the photons and enhance the contrast, the laser-driven range resolution is a better choice. Finally, the water volume backscatter used in these calculations is 0.001/m, which is closer to a coastal condition than that of the ETP, but as most of the data gathered in this research was gathered in coastal regions, such a parameter selection will allow for a more direct comparison when necessary.

If the contrast in Equation 7 is plotted as a function of pixel area, the data in Figure 29 result. It is evident in this graph that, even when the fish reflectivity is 10% (as opposed to the observed value of 1.5%), the resolution element must have less than $1m^2$ of area in order to obtain contrast adequate for generating detectable signatures[28]. And when the reflectivity is 1.5%, the required resolution is a few tenths of a square meter, which leads to pixels having dimensions of 20-30cm on a side.

As the minimum requirements for contrast are met when the numerator is nonzero, it is worth the effort to look briefly at the numerator expression in order to determine the conditions necessary to make the numerator nonzero. Specifically, one can examine

$$\rho_e - \beta(\pi) \cdot \Delta z = 0 \qquad \text{(Eq. 8)}$$

From this we see that contrast is maximized on the positive extreme by making ρ_e as large as possible. On the negative contrast extreme, contrast is maximized by letting ρ_e approach zero. Knowing in advance that ρ_e is indeed small, one is tempted to conclude that Δz can be made very large (low range resolution), thereby providing relatively high contrast images in shadow (negative contrast). However, this decrease in range resolution will reduce the contrast per Equation 7. Also, the shadow signature of the fish, or its negative contrast image, will be preferable to the positive contrast signature only near the water surface, as multiply scattered photons diffuse away negative contrast images as fish depth increases. But the near surface region is precisely where the fish are least likely to be found, statistically speaking[29]. Thus, the objective in maximizing contrast will be to make ρ_e (fish backscatter per pixel) as much larger than $\beta(\pi) \cdot \Delta z$ (volume backscatter per pixel) as possible.

Returning to Equation 8, one can manipulate the parameters a bit in order to separate the sensor-dependent parameters of interest from the fish parameters. The sensor parameters of interest are embodied in the resolution terms, R_{xy} and Δz. The fish parameter of greatest interest for this

---

[28] The finding of this research is that fish detection is possible for contrasts approaching 4, but becomes marginal below that value.

[29] Study of tuna behavior by the use of sonic tags, Newsletter Enyo (Far Seas) Fisheries Research Laboratory, Shimizu 44:1-5 (this source from Hunter and Churnside, NOAA Report LJ-95-02).

analysis is N, the number of fish in the resolution element. The packing density for a single sensor resolution element (a voxel), in fish per unit volume, is given by

$$D = N / (\Delta z \, R_{xy}) \qquad\qquad (Eq. 9)$$

If we solve for N and substitute, a new expression can be obtained for contrast

$$C = D \, A_f \; \cdot [\rho_e \; - \beta(\pi) \cdot \Delta z \,] \; / \; \beta(\pi) \qquad\qquad (Eq. 10)$$

In this expression, the sensor resolution is buried in the packing density. However, this form for contrast allows for some understanding of the limiting contrast without immediate regard to a sensor resolution. For example, if a packing density is assumed, contrast can be plotted as a function of the effective reflectivity, as shown in Figure 27 where a reflectivity value of 1.0 is the maximum (100%). In this case, it is implicit that either the size of the resolution element or the number of fish per resolution element will be changed to produce the contrast plotted.

The calculations shown in Figure 27 and Figure 30 emphasize the same point: sub-meter resolution is required in order to use a LIDAR for directly studying tuna that are observed in schooled formations. Otherwise the data collected will not have enough contrast to indicate the presence of fish when indeed fish are present in the sensor field of view. The way this was applied in the sensor development was to create a requirement to maximize resolution. Since the streak tube already provided very good depth resolution, this led to a focus on improving the cross-track and along-track resolutions over that of the laboratory system.

This finding regarding the resolution requirements can be extended beyond that which was known prior to the experiments if we take advantage of the knowledge gained from this experiment and calculate resolution requirements based on observed conditions. The SBT and GBFT schools observed with the ASTIL sensor had LIDAR-derived apparent packing densities of $0.16/m^3$ and $0.04/m^3$, respectively[30]. As the SBT observed were in keeping with the hypothetical 20kg tuna being examined in this analysis, the $0.25/m^3$ packing density used in the calculations above can safely be used as a representative number (especially as there may be undetected tuna in the school). The median LIDAR contrasts that were observed for the SBT and GBFT were 2.7 and 4.4, respectively. However, the SBT were observed in more turbid water[31], and once this is accounted for, the GBFT data and SBT data come into close agreement for more typical expected open ocean water conditions. Thus, a contrast value of 4.4 can be used as value representative of the problem.

Figure 30 shows the relationship between tuna reflectivity and lateral resolution for parameters suitable for a 20kg tuna, based on the data collected in this experiment. Both JWT IB and JWT

---

[30] The data from which these numbers were derived will be shown in a subsequent section of this report.

[31] The assumption here is that the turbidity increased the scattering so as to reduce contrast by spreading the backscattered light, and the increase in water volume backscatter decreased the contrast by increasing the background contribution with respect to the direct backscatter from the tuna. The SBT were observed in water measured close to JWT Coastal-1 ($\beta(\pi)$ = 2.7e-3) and the GBFT were observed in water measured close to JWT II-III ($\beta(\pi)$ = 1e-3 to 1.8e-3), so that a 2.7X-1.5X contrast difference would be expected, all other things being the same. This implies that the contrast of 4.4 would have been reduced to the range of 0.6 to 2.9, which spans the observed value of 1.5 for the SBT.

II waters are shown, the former being representative of ETP conditions, and the latter case representing the waters typical for the GBFT data shown in this report.

Given that the effective reflectivity of tuna has been estimated to be between 1% and 2%, the required resolution is a few tenths of a square meter. Specifically, the second plotted point in the lower left hand corner of that figure corresponds to 1.5% and 0.16 m^2, indicating that the LIDAR with the 1m depth resolution would need to have pixels with an area of 0.16 m^2, or 0.4m (40cm) on a side, if square. As a point of comparison, the SBT data collected in South Australia and mentioned above (packing density calculation) were collected with the ASTIL sensor having a cross-track resolution of 9cm and an along-track resolution of 30cm, so that the equivalent R_{xy} was $0.9*0.3 = 0.27m^2$, which is reasonably close to the theoretical value presented above[32].

6.4   Calculation of expected LIDAR returns for tuna

In order to have a sense of what to expect from a given experiment, it is advantageous to compute, in advance, the theoretical values for the data that are sought. For a LIDAR experiment, a parameter that related well to the observed image data is the SNR. The SNR is a ratio of the signal excess power to the background power, and has its foundations in RADAR signal theory, but is equally useful in LIDAR signal treatments as well.

For the airborne LIDAR viewing fish in water, the signal excess is the LIDAR return from the fish, and the background is the water volume backscatter from a volume set by the lateral resolution and the limiting depth resolution associated with the laser pulsewidth. The noise is determined by the receiver photonics and electronics. As a photocathode is involved early in the receiver signal chain, the quantum efficiency of this element, scaled by the noise figure of the receiver, sets the noise for the LIDAR, independent of the water environment. The noise figure of the receiver, in the case of the prototype streak tube, is driven by a microchannel plate (MCP) that provides photoelectron gain within the streak tube. The radiometric quantities and sensor parameters needed to complete the calculations for SNR are tabulated in Table 6.

---

[32] This is not to be taken as a claim that the theoretical model has been validated, *per se*, since there are many factors unaccounted for here that would possibly move the results by 20 or 30 percent. Rather, the value is in demonstrating that it was for good reason that the SBT experiments led to the conclusion that sensor resolution had to be maximized in order for the prototype ASTIL sensor to lead to SBT observations.

Table 6. LIDAR parameters used in experimental SNR calculations

LIDAR Parameter	Value
Laser energy per pulse	0.012 J
Laser pulsewidth	9 ns
Laser wavelength	532 nm
Streak tube quantum efficiency at 532 nm	10%
Streak tube MCP gain	1-1100
MCP noise figure	5
Receiver field of view	15 degrees
CCD format	256 x 256 (binned 4x4)
Receiver resolution/pixel	0.001 radians
Water volume backscatter coefficient	0.0007/m
Water total scattering coefficient	0.2/m
Water diffuse attenuation coefficient	0.08/m

Figure 31 shows the calculated SNR performance using the sensor parameters from Table 6 for two cases: with and without in-water scattering, which induces spreading or blurring in the image. Also shown is the theoretical upper limit on measured SNR for the sensor. This is essentially a description of the dynamic range of the digitizer, which is a digital CCD camera. The most obvious feature of the plot is the discrepancy between the SNR with scattering and the SNR without scattering.

The term, spreading refers to the blur introduced by water molecules and particulates when imaging through water, as is the case with the airborne LIDAR. This blur, induced by photon scattering, acts to reduce the contrast. Since contrast, which describes the difference between the target and the background, decreases as blur increases, the SNR will likewise drop off with increasing blur. As the amount of spreading incurred depends on the amount of water the light has to travel through, loss of contrast increases as the depth increases. These trends are borne out in the model calculations shown in the figure.

The pre-experiment conclusion drawn from the SNR data as plotted above was that the GBFT would have to be near the surface in order to detect them unambiguously and open ocean water conditions would be required. As will be shown, these conditions were met, making it possible to obtain the GBFT data that has been alluded to. Such calculations were also made for earlier experiments, though the results were not as useful as for the GBFT, as the conditions needed for success were not as fully met, and the problem was not as fully understood. But this is characteristic of any research endeavor, and if the problem were fully understood at the outset, there would have been little motivation to pursue the experiments.

6.5 Experimental observations

The purpose of this section of the report is to show experimental results and make comments as needed to help explain what is being shown. Thus, this section will begin with 2D and derived 1D imagery in order to acquaint the reader with ASTIL data for tuna and other species that were observed. 3D and the associated 2D (projections) will also be shown, but only for the GBFT

data that were gathered in the last experiment conducted as part of this effort. This section will conclude with some schooling statistics derived from this project, after making some observations about the nature of tuna LIDAR signatures.

6.5.1 Observed images: 2D, 2D w/ 1D slices

Earlier in this report, images of akule were shown in order to illustrate the 3D nature of the ASTIL sensor. In this section of the report the reader will also see that the akule are fundamentally different from tuna in terms of their LIDAR signature, owing mainly to their packing density and reflectivity. However, before presenting tuna data for direct comparison with akule, LIDAR data for one additional type of animal will be shown.

This additional animal is dolphin[33], imaged in Boston Bay, South Australia during the joint experiments with CSIRO in 1997. An unprocessed dolphin image is shown in Figure 32. This shows the obvious signature of the dolphin and its relatively smooth optical profile. Since this dolphin was imaged on three consecutive shots, it is known that this represents a mid-body LIDAR signature of dolphin, and it is also known that the dolphin was approximately 2m in length[34].

When the dolphin image is processed to remove the exponential and range-squared trends, the dolphin signature and its associated shadow are more obvious, as shown in Figure 33. As the discrete nature of the pixels is apparent, one can easily count the number of pixels across the dolphin as being around 6 pixels. Using the fact that the cross-track resolution (again, the horizontal axis as shown) was 8cm per pixel for this image, an apparent dolphin body width of 48cm can be derived. If in-water spreading is accounted for, this number reduces to roughly 30cm (depending on the water type, which was not directly measured). This is a reasonable result for a mature dolphin.

The point of this discussion of the dolphin LIDAR signature is interesting in its own right, but has a particular application to the purpose of this research, which is that of dolphin bycatch reduction. As there is a known association between dolphin and tuna in the ETP, and as LIDAR may be useful in helping to reduce dolphin bycatch through more targeted fishing, it is important to know that there are measurable differences between dolphin and tuna. The differences that will be seen here have to do with size and also reflectance properties, or LIDAR signature. Such differences can be used to help identify schools of tuna not associated with dolphin, or at least to characterize the nature of the association more fully, so that risk of bycatch can potentially be mitigated.

An example of some GBFT data for comparison with the dolphin data are provided in Figure 23 and Figure 24. The corresponding processed images are shown in Figure 34 and Figure 35, respectively. An example of two different 1D profiles are provided in Figure 36 that show both the overall context of the LIDAR return in Figure 34, in addition to a transect that highlights the LIDAR return from the GBFT. While there are not statistically significant observations of

---

[33] The spotter was not certain as to the precise species.
[34] The airspeed was 60m/s and the laser PRF was 100 Hz, meaning that images were spaced 0.6m apart. Three images implies at least 1.8m of travel.

dolphin with which to compare signatures of tuna, the initial reviews of the image and transect data indicate that the reflectivity profile and the physical size could play a discrimination role in comparing yellowfin and dolphin signatures.[35]

6.5.2 Observed images: 3D, 3D w/ 2D projections

One of the principal features of the ASTIL sensor is its ability to image submerged objects in three dimensions. This section will present an example of 3D imaging that is specific to tuna. Both GBFT and SBT data were reduced and prepared for 3D imaging, but the GBFT data are of better quality for viewing via 3D rendering.

The data were prepared much the same way as for the akule school shown in Figure 21, except that the akule school did not require a shape sensitive threshold for selecting multiple objects for viewing within the volume. The akule was a single entity that could be separated from its water volume directly. The tuna presented here required a detection process that separated individual tuna from water in 2D images, which were then stacked to form a 3D volume that could be rendered.

The 3D image of the GBFT school imaged in New England is shown in Figure 37. There were over 60 GBFT detected in this school when automatic detection algorithms were run. If the 3D image is projected up onto the water surface, a topographical map of the school can be seen, as shown in Figure 38. Other projections can be made, as needed for studying the school. This projection serves to illustrate the utility of the 3D data obtained with the ASTIL sensor.

6.5.3 LIDAR signature observations (shape, reflectivity)

From the data gathered on the GBFT, the LIDAR response to the GBFT, or its signature, can be gleaned. Since the ASTIL sensor is a 3D sensor, information on all three dimensions can be reviewed. This section presents some analysis of the signature data for the GBFT. The purpose is mainly to illustrate the use of the sensor data, but also serves to indicate some areas where care must be exercised in handling LIDAR data.

Figure 39 shows an average range profile for GBFT. The full-width at half-maximum (fwhm) of the laser pulse, as represented by the range profile, is slightly more than 1m. The average is formed by collecting 1D range-slices of GBFT signatures by extracting a fixed number of pixels either side of the peak value location that is provided from the matched filtered image. The matched filtered image peak location represents a signal maximum location that is akin to a centroid. So it may have some skew or offset with respect to the peak signal for a particular 1D transect through the signature (e.g., range). This graph is essentially a replication of the laser pulse profile, akin to the LIDAR return signal from a diffuse surface.

The profile shown in the above mentioned figure was formed by averaging vectors after aligning them by the location of the matched filter peak pixel, which is dependent upon the 2D response of the LIDAR to the GBFT. If the profiles are first aligned by the raw-data peak-value and then

---

[35] This issue will be addressed in more detail, if possible, in a subsequent technical publication.

averaged, the result changes. This change is most pronounced in the range direction, as shown in Figure 40. Here both the matched-filter (MF) aligned and raw-aligned averages are shown. The same exercise is repeated for the cross-track and along-track directions in Figure 41 and Figure 42, respectively. In these images, as with Figure 40, there is a marked increase in the measured contrast for the GBFT when the average profiles are aligned by the maximum in the raw image data. Part of this is due to the fact that any asymmetric object will likely have maxima along individual axes that are not identically equal to the global maximum representing an integrated response over many dimensions. It is possible that such a distinction is adequate to explain all of the difference observed in each of the three plots.

Figure 41 shows the average cross-track profile for the GBFT. The apparent width of the tuna (fwhm[36]) is approximately 0.5m. This is not the same as the physical width of the tuna, as the in-water spreading is not accounted for and the orientation of the tuna is neither uniform nor known with certainty for this experiment. Thus, for present purposes, it can only be said that the *apparent* cross-track signature has been measured. Likewise, the along-track profile is shown in Figure 42. The fwhm along-track profile measures 0.6m, which is only slightly more than the cross-track profile.

Though the along-track and cross-track profiles remain ambiguous as to the true orientation of each tuna, the values measured are consistent with expected results. The GBFT are on the order of 30cm physically in width, and 5m of water can readily introduce several centimeters of apparent width. Thus, when combined with the likelihood that both the along-track and cross-track measurements contain parallel, perpendicular and diagonal transects of tuna bodies that are 2m in length, the 50cm average is reasonable.

The issue of whether or not the pronounced peak (for raw peak aligned data) in these graphs is merely an artifact of handling noisy data can be explored some using computed images. If we first form an image of a symmetric 2D signature using a Gaussian, and then add noise to it, we can approximate the LIDAR signature to a symmetric target with a Gaussian laser pulse. If an ensemble of these is generated using a variable noise field, then the signature selection process that led to the prior three figures can be emulated and examined in a more controlled fashion.

Figure 43 and Figure 44 show examples of this type of calculation for target SNRs of 9 and 36, respectively. In Figure 43 the effect is very close to that shown in the Figure 40, and the SNR of 9 used is comparable to the signatures of the more visible GBFT. Figure 44 shows what happens when the SNR is much higher; the effect of averaging 1D transects diminishes when the noise decreases. The noisiness of the data can be easily seen in the 2D images that are shown inside the plot region for these figures.

Thus, it would indeed appear that aligning noisy data according to peak value will tend to enhance the peak by (artificially) adding coherence to the resultant data. However, there are still many issues that remain uncertain that are tied to the LIDAR signature of the tuna, and more data are needed to obtain reliable answers. For instance, the apparent high reflectivity of tuna when viewed from beneath the surface of the water (while illuminating from the surface via sunlight) remains a puzzle when the low reflectivity of the tuna is measured with the LIDAR. Also, the

---

[36] Full Width at Half Maximum

suspicion formed by the authors that the tuna may have specular reflectivity properties that enhance viewing off-axis from the light source but diminish the direct backscatter (as for a LIDAR) term, remains unaddressed by this research.

So there are many open issues regarding the tuna LIDAR signature. This section has shown some of the utility of the ASTIL data to address these issues, and has shown some specific tuna observations to illustrate the progress that has begun to be made in this research.

In addition to graphical studies of the LIDAR signature as shown above, the LIDAR data can be used to derive observed fish contrasts, which can be used to estimate reflectivity if the water optical properties are known or can be estimated. An example of such a contrast analysis is shown in Figure 45. Here it is seen that the contrast is variable, but not depth dependent. This is reassuring, since the contrast should not change with depth if the school contains the same type of fish throughout.

6.5.4   GBFT schooling statistics (distribution, density)

The data shown in this report contain information about the tuna within a school that can be used to calculate *in situ* packing densities and distributions. They can also be used to graphically study the imaged fish school. This section will illustrate this by showing the statistics measured for the GBFT school[37].

Several graphs follow (Figure 45, Figure 46, Figure 47, Figure 48, Figure 49, Figure 50). These will simply serve as illustrations of the use of the ASTIL sensor to study fish schools. Each graph is described by a caption that is adequate to describe the information presented.

6.6   Measured detection performance

6.6.1   Introduction to detection (target vs background, filtering)

The performance of greatest concern in this effort is the ability to detect fish schools. Clearly, from the prior discussion on resolution, in order to detect schools of tuna one must first be able to detect the individual tuna within a school unless packing densities turn out to be much greater than is currently assumed. Thus, the problem of fish school detection is really an issue of detecting individual tuna.

An objective in nearly any sensor-related detection problem is to isolate the target of interest (tuna) from anything else that might be observed with the sensor that is known to be other than the target (water, noise, debris, etc.). A robust and time-honored approach to separating targets from non-targets, or more generally, in separating signal from noise, is that of filtering.

The filtering approach posits that there exists a mathematical operation (filter) which, when applied to the an image collected with a sensor, will yield an image with more visible targets and less visible noise or background. A test metric that allows for such an evaluation of "more visible" in an image is the SNR. A well-known filter that optimizes an image for SNR is the

---

[37] The statistics are derived from the so-called ground truth data set used in the detection analysis.

matched filter[38]. The matched filter will robustly deliver filtered outputs that have optimal SNR when the filter matches the image of the target of interest, and when the input image has a noise field that has zero mean and Gaussian statistics. When a matched filter is generated and targets are present, one need only apply a threshold to the filter image data and detect peaks, the highest of which will be targets.

Typically, one cannot obtain images with means that are identically zero or having statistics that are purely Gaussian. The usual approach is to prepare the images (pre-process) to enforce the zero-mean, Gaussian assumptions, and then proceed with matched filter processing. Such was the approach taken in this research. The exponential decay introduced by the water, the range-squared dependence inherent to LIDAR data, and the electronic and environmental artifacts introduced into the data all must be handled correctly and in the correct order in order to arrive at a matched filter image that is useful for detection.

The general approach taken in processing imagery for this research were as follows:

1. Use information on altitude and streak tube settings (sweep timing) to remove the range-squared dependence from the images collected.
2. Estimate the exponential decay for the ensemble of images that contain the particular images having targets.
3. Remove the exponential decay from the image ensemble.
4. Normalize the variance so that the variance for the image is a scalar.
5. Apply the matched filter by convolving the pre-processed image(s) with a filter that matches the shape of the target (tuna).

Once these image processing steps have been performed, the detection of targets can begin. Target detection is a simple matter of 1) applying a threshold (SNR, in this case) to the matched filtered imaged data, and 2) recording the position of targets that are higher than the threshold. Obviously, once the position of a target is known, other items associated with the target can be deduced. However, the declaration of a target at a specific point in an image is the "bottom line" for the detection problem.

6.6.2   Formation of "ground truth"

In any airborne remote sensing experiment it is important to have some reference points or known targets on the ground that can be included in the data analysis for experimental control. For instance, when the ASTIL sensor is being evaluated for terrestrial mapping applications, there are carefully surveyed ground control points that serve as "ground truth" data against which the outputs of the mapping algorithm can be compared, resulting in a measure of accuracy for the map data.

Unfortunately, it is not possible to provide such "ground truth" for an airborne experiment that seeks to image schools of fish in the open ocean. It is possible to identify that "a school of GBFT is present" with input from a spotter and the expertise of marine scientists participating in the experiment, but it isn't possible to provide positional data on size or depth to aid in

---

[38] Merrill Skolnick, "Introduction to Radar Systems", 2nd Edition, McGraw-Hill, 1982.

evaluating the outputs of a detection algorithm. The approach to this dilemma for this effort was to use known sensor and environmental physics and an experienced team of analysts to manually identify individual fish signatures for those instances when it was known that a school of known species had been traversed.

Thus, one of the principal tasks of data analysis was to carefully review images and sections of images in order to find and tabulate instances of fish from the ASTIL sensor data. These were then used to process images automatically in order optimize the detection algorithm used to find tuna and to generate statistically significant matched filter background/noise data. These background data formed the basis for the analysis of detection that followed. The processes used and the results arrived at are delineated in the next section of this report.

6.6.3   Formation/calculation of detection statistics

The purpose of this section is to show the mathematical approach taken for the detection problem. This section is not intended to provide an exhaustive discussion on the detection problem as it relates to tuna. Rather, it's intended to provide a sense of the general approach taken in implementing a solution, as there are many approaches that could have been taken. Thus, the process is reiterated, the equations used are described symbolically, and then some comments are made regarding the specific implementation of the detection scheme.

The process used to detect tuna followed the same approach as delineated earlier in this section. First the range-dependence of the data and the exponential decay caused by the water and its constituents were removed. Then the surface was detected and removed from consideration. Next, the sequence of 2D images containing the school was stacked to form a 3D data set. This 3D data set, or image, was then matched filtered for the 3D tuna signature.

For this research, the matched filter was implemented in the frequency domain, as this has computational advantages over equivalent spatial domain processing (i.e., convolutions). In order to jointly localize and detect the tuna, both a matched filter and its derivative were used. Thus, once a threshold had been applied to the matched filtered image, the zero-crossing of the derivative-filtered image was used to identify the location of the maximum.

6.6.4   Equations used to implement 3D matched filtering:

Gaussian Filter Equation:

$$g(x,y,z) * contrast(x,y,z) = \Im^{-1}\left\{\Im\{g(x,y,z)\}(f_x,f_y,f_z) \cdot \Im\{contrast(x,y,z)\}(f_x,f_y,f_z)\right\}(x,y,z)$$

where

$$g(x,y,z) = \frac{1.632236873}{fwhm_x \cdot fwhm_y \cdot fwhm_z \cdot \sqrt{(2\cdot\pi)^3}} \cdot \exp\left[-0.69314718 \cdot \left(\left(\frac{x}{fwhm_x}\right)^2 + \left(\frac{y}{fwhm_y}\right)^2 + \left(\frac{z}{fwhm_z}\right)^2\right)\right]$$

45

Gaussian Derivative Filter Equations:

$$\frac{\partial g(x,y,z)}{\partial x} = \Im^{-1}\left\{\frac{-i\cdot 2\cdot \pi \cdot f_x}{N_x}\cdot \Im\{g(x,y,z)\}(f_x,f_y,f_z)\cdot \Im\{contrast(x,y,z)\}(f_x,f_y,f_z)\right\}(x,y,z)$$

$$\frac{\partial g(x,y,z)}{\partial y} = \Im^{-1}\left\{\frac{-i\cdot 2\cdot \pi \cdot f_y}{N_y}\cdot \Im\{g(x,y,z)\}(f_x,f_y,f_z)\cdot \Im\{contrast(x,y,z)\}(f_x,f_y,f_z)\right\}(x,y,z)$$

$$\frac{\partial g(x,y,z)}{\partial z} = \Im^{-1}\left\{\frac{-i\cdot 2\cdot \pi \cdot f_z}{N_z}\cdot \Im\{g(x,y,z)\}(f_x,f_y,f_z)\cdot \Im\{contrast(x,y,z)\}(f_x,f_y,f_z)\right\}(x,y,z)$$

where

$contrast(x,y,z) =$ contrast for each data point defined as: $\dfrac{pixel\_counts(x,y,z) - ambient\_counts}{ambient\_counts}$

$fwhm_{coordinate}$ = full width of the average fish along the direction of a coordinate (x,y, or z), which is the half width at half maximum of the Gaussian filter

$f_{coordinate}$ = spatial frequency corresponding to a coordinate (x,y, or z)

$N_{coordinate}$ = Number of points used in the FFT along the direction of a coordinate (x,y, z)

$i = \sqrt{-1}$

$\Im\{\cdot\}$ = Complex Three-Dimensional Fourier Transform

$\Im^{-1}\{\cdot\}$ = Complex Inverse-Three Dimensional Fourier Transform

6.6.5   Comments on the implementation

The local peaks in the Gaussian filter output are determined by the points for which the outputs of the Gaussian derivative filter all cross zero from positive to negative along increasing x, y, and z directions, respectively.   The filtering (convolution) is performed using a complex Three-Dimensional Fast Fourier Transform and a complex Three-Dimensional Inverse Fast Fourier Transform.   Several filter widths smaller and larger than the value listed above were tried on the New England data set, and this choice of filter width seemed to give the best results in terms of minimizing false alarms while maximizing correct detections.

6.6.6   Generation of target and background probability density functions

Signal-plus-noise data points are the maximum filter outputs in a "fish sized" region around each of the fish signature points detected manually for which the contrast of a pixel is greater than 0.33, divided by the standard deviation of the filter outputs for all points in the data set. Noise data points are the filter outputs for each data point in two sub-regions of the data set where there were no fish detected manually, divided by the standard deviation of the filter outputs for all

points in the data set. The histogram and cumulative distribution data were generated and plotted in Figure 51. There were 104 signal-plus-noise data points and 451,009 noise data points. The signal-plus-noise mean was 7.709 and the standard deviation was 2.722. The noise only mean was -.069 and the standard deviation was 0.819.

6.6.7   Generation of a receiver operating curve

Based on the detection statistics discussed earlier, the tradeoff between the probabilities of detection and false alarm can be characterized graphically for the GBFT. The graphical portrayal of this tradeoff is known as a ROC. Using knowledge of where the tuna are and where they are not, one can adjust the SNR threshold upward from zero and downward from the maximum SNR achieve and simply record the number of detections corresponding to tuna and the number of detections that are not tuna. Then, treating the ground truth information on the school as representing all the possible tuna in that school (the universe for the calculation), percentages and probabilities can be formed from detection data just gathered.

Two ROC examples are shown in Figure 52 and Figure 53. These are actually the same data, but plotted on linear and logarithmic scales, respectively. The vertical axis in both curves is the probability of detection and the horizontal axis is the probability of false alarm. The linear curve is shown for a point of comparison, as such data are sometimes shown in this format. However, the easiest format for studying is the logarithmic plot, as the detail is more pronounced.

In Figure 53, for instance, if it was desired to achieve a false alarm rate of one in 10,000 tuna-like objects, a probability of detection of 80% could be achieved. Likewise, if one false alarm in 100,000 were required, the probability of detection would drop to 70%, and so on. Given the early nature of this research, such numbers are encouraging. However, one must not be deceived by the seeming improbability of encountering a false alarm.

First, the use of the term, tuna-like, is intentional. The noise statistics of the LIDAR and the clutter introduced by the environment will conspire to produce events that, from time to time, will look like tuna to the LIDAR. As will be discussed later, there are improvements that can be made in the prototype ASTIL sensor to help mitigate this problem. However, it will always be an issue of greater or lesser concern, depending on the fish and sensor parameters.

Second, the amount of time required to produce 10,000 or 100,000 events for the LIDAR to consider is made smaller by the high resolution and high data rate for the ASTIL sensor. The highest PRF tested with the ASTIL sensor[39] has been 100 Hz. At this rate, and given a 256x256 image format, the ASTIL sensor generates 6,553,600 pixel events every second. Not every pixel counts as a candidate fish event (multiple pixels were generated for each GBFT, for instance) and noise events don't naturally form tuna-like data. However, the rate of data collection must always be considered when reviewing numerical rates of false alarm.

---

[39] PRFs of 200 and 400Hz have been successfully tested on the more advanced sensor being developed for the ONR; this technology will eventually be available for airborne tests.

The data presented in the next section will apply these concepts to the GBFT data and show that, while the ROC implications are indeed encouraging, there are improvements that can and should be made in order to detect schools of tuna.

6.6.8   Application of the ROC to the GBFT data

Having generated the ROC performance data and the data set containing GBFT and non-GBFT events, the ROC was applied to the data by setting a detection threshold and then detecting tuna-like objects. These objects were then localized and plotted.

Figure 54 shows a plot of both the ground truth (analyst detections) and automatically detected tuna using nearly optimal[40] threshold settings for SNR. Here it can be seen that both detections and false alarms were registered. However, there are few false alarms outside the nominal school region, indicating that a school has been successfully detected. Figure 55 shows the results for the automatic detection only. Here it is quite clear that a school has been detected. It is in this sense that the authors find this result very encouraging: even with the shortcomings of the prototype ASTIL sensor, this result demonstrates that schools of tuna can be detected with airborne LIDAR.

6.6.9   Comments on the processing

Automatically detected tuna are defined as those peaks of the output of the matched filter for which the output value is above a user determined threshold and for which the contrast from the original data is greater than a user determined threshold. For the New England data set, the filter output threshold is 0.097 and the contrast threshold is 0.33.

The plotted values for detected tuna are the SNRs for the peaks remaining after thresholding. The SNRs are the thresholded filter outputs divided by the standard deviation of all filter outputs. The standard deviation of all filter outputs for the New England data set is 0.021. Therefore, the SNR threshold used in processing the New England data set to produce the graphs shown is 4.62 (0.097/0.021).

6.7   Performance summary of the prototype ASTIL for GBFT

This analysis has demonstrated the basic feasibility of detecting schools of GBFT with the prototype ASTIL sensor. While it has not been tested over diverse enough conditions to have confidence in near-term operational use, the data presented here indicate that even the prototype ASTIL sensor has significant utility in furthering our understanding of the tuna detection problem for GBFT, and may well provide a usable stock assessment data product, given some time for optimization.

---

[40] For this analysis, the analyst set a threshold that provided graphical results that were optimal – it was obvious that a school had been detected and only a few false detections occurred.

6.8   Discussion of performance requirements for yellowfin tuna detection

This section of the report will describe the performance requirements as implied by the experimental observations to date. The emphasis will be upon the performance requirements for conducting additional scientific experiments, as opposed to the performance required for operational survey scenarios. Some comments will be directed toward operational scenarios, and these will also be considered more in the discussion of projected performance. However, given the early state of this research, the present emphasis will be upon scientific objectives and on existing sensor technology.

6.8.1   Cross-track resolution requirements based on experimental results

The purpose this section is to use the GBFT results to estimate the resolution requirements for a similar experiment conducted in the ETP for yellowfin tuna. The purpose is not to articulate a design; rather it's to indicate the type of system that should have been attempted, had we had the benefit of knowing the outcome of the GBFT experiment in advance.

The performance measured for the GBFT was obtained with 0.001 radians angular resolution cross-track and approximately 30cm along-track[41], yielding a 20x30cm pixel size at the water surface from 200m altitude. For the GBFT, this resolution was demonstrably adequate for detecting schools. The measured LIDAR signature was 50cm; thus, 2.5 pixels per apparent target cross-track dimension yielded the GBFT data shown in this report. If the physical size of the fish is assumed to be 30cm, then the experimentally-based requirement becomes 1.5 pixels per target cross-track dimension. Conservatively, the experimentally-derived cross-track resolution requirement should be 2-2.5 pixels across the smallest tuna dimension to be imaged; this dimension is assumed to be the mid-body width (the head or fin sections would drive the design in the right direction, but would likely over-specify the design). The purpose of having multiple pixels per cross-track dimension is for the validation of fish signatures during data analysis. One of the features that distinguishes fish from photon noise in the imagery is the fact that photon noise tends to be a single pixel event, whereas a fish signature has multiple pixels (provided such resolution is designed into the system). This is a requirement that would not necessarily remain for a mature, operational system, but is vital for a prototype, investigative system.

For the ASTIL sensor, the along track resolution is also important, but is less variable than the cross-track resolution, as it is set by the transmitter optics and the laser beam divergence. For instance, the cross-track resolution can be varied by adjusting the amount of binning done on and off the CCD integrated circuit, but has its lower limit set by the CCD pixel size and the laser PRF that ultimately sets the imaging data rate. The ASTIL work conducted to date has set the along-track resolution at 0.0015 radians typically, thus coming close to the minimum ASTIL cross-track resolution used to date.

Assuming that the resolution obtained for the GBFT can be scaled to successfully detect other smaller tuna such as the ETP yellowfin, the resolution required to detect schools of yellowfin can

---

[41] The along-track resolution here is the optical resolution driven by the along-track size of the laser beam; the along-track sampling was 60cm, for 60m/s velocity and 100 Hz PRF.

be calculated directly. For the purposes of this estimate, a physical fish size of 15 cm mid-body width will be used. This corresponds roughly to a 100 cm body length[42].

Given the 15 cm mid-body width, and assuming that at 5m in ETP water (JWT-IB[43] at worst) the spreading is 30cm, the signature at 5m depth would have a Gaussian full width of 33cm. This follows from the convolution of two Gaussians, in which the resultant Gaussian will have a width that is the square root of the summed squares of the kernel and data Gaussian widths. Using the GBFT data, a spreading estimate in the JWT-II waters near Cape Code back-calculates to 40cm. If this is used as a reference point for setting the mean scattering angle in those waters, spreading calculations can be made for other waters. Such calculations are shown graphically in Figure 56. These spreading estimates are derived from Lutomirski[44].

For the ETP tuna problem, at 2.5 pixels per width, the required resolution is then 33/2.5 = 13cm, for imaging a 20kg yellowfin at 5m depth. Clearly, from Figure 56, a 13cm pixel size would yield more than enough resolution at depths beyond 5m, using the 2.5 pixel rule of thumb suggested above.

Thus, continuing with the exercise of scaling the GBFT work to the tuna detection problem in the ETP, if the flight altitude were again 200m, the 13cm resolution would require a cross-track angular resolution of 0.00065. This is nearly twice that of the prototype ASTIL sensor, but a resolution of which the ASTIL technology is capable, if system modifications are made. As the inherent resolution of the sensor CCD is 0.00025 radians cross-track, this is within reach, and requires software adjustments and laser PRF adjustments.

6.8.2   SNR needed for detection of fish and fish schools

The SNRs calculated for the GBFT are arguably adequate for detecting schools, assuming that the data collected (for instance, Figure 55) are representative of the general nature of the problem. This is an issue that can only be fully addressed through further experimentation in which data are collected on a large number of schools. However, given the assumptions about the similarity of the GBFT problem to other tuna species, if the resolution is increased in keeping with the estimated required resolution from above, the required SNR may be obtained for yellowfin tuna school detection.

The main caveat to this argument is the requirement that the clutter not change with the change in sensor resolution, and that the assumptions about the optical similarity between the GBFT and the yellowfin hold true. As has been argued already, these are not unreasonable assumptions. However, the paucity of data on the yellowfin precludes high confidence in the comparison.

---

[42] These numbers are from physical SBT measurements made during the CSIRO experiment, and are also close to the numbers used by other researchers, Churnside et. al, for instance, in NOAA Technical Memorandum ERL ETL-287.

[43] JWT is the Jerlov Water Type; these have been studied and tabulated for all the world's major bodies of water. For JWT-IB water, the total scattering coefficient is 0.077/m.

[44] Richard F. Lutomirski, et. al, "Moments of Multiple Scattering", Applied Optics, Vol. 34, No. 30, 20 October 1995, pp. 7125-7136.

6.8.3　Required laser energy

The remaining caveat to the argument that the GBFT results can be extended to the yellowfin pertains to the laser energy. Continuing with the prior argument, if the resolution is increased and the same SNR is required, additional photons per pixel will be required. For a doubling of resolution, a doubling of the laser energy is required. There are systems available that provide this, and there is an ASTIL configuration that can provide it presently.

However, the general rule of thumb for existing laser systems is that, without significantly increasing the cost, the PRF must decrease as the laser energy increases per pulse. This means that along-track sampling resolution must be degraded if the laser energy is increased, without adding system cost or allowing time for emerging technologies to mature and find markets[45].

6.8.4　Laser PRF (along-track resolution) requirements

There are two general classes of problems to consider where laser PRF is concerned. One is the problem of direct concern to this research: school detection. The other class of problem is that which was of greater interest to the CSIRO experiment: population dynamics.

The detection of schools of tuna does not require the detection of every tuna in a school. Another way to state this is to observe that discerning the presence of a school depends more on observing that a high number of tuna are detected per unit volume, rather than observing precisely how many tuna are in a given region. The latter datum will provide the former, to be sure, but only the former is needed if one is only concerned with the presence or absence of a school.

Consequently, while adequate sampling (high resolution) per image is still required in order to detect tuna within an image, one can under-sample the school in terms of the number of images gathered per school without losing the ability to detect that school. For example, in Figure 57, which shows the number of tuna detected per (laser) shot for the GBFT school rendered in Figure 37, not every shot is required to observe that a school is probably present.

To illustrate what would happen if a lower PRF were used, the GBFT data in Figure 57 were plotted along with data extracted from the original (100 Hz) data and resampled at ½ and ¼ the PRF, or 50 and 25 Hz, respectively. These resampled data are plotted alongside the 100 Hz data in Figure 58. Note that the data have been placed in a larger vector to provide context indicative of what a real school detection event might look like.

Figure 59 shows a smoothed version of Figure 58, where a boxcar average of adjacent shots is used to provide a better visual sense of the presence of a single school of fish. In this case it is perhaps easier to see how such data might be used in a deployed system to integrate a fish density statistic akin to the area under the curves just plotted, and declare a school if the density statistic passed a predetermined threshold.

---

[45] Current diode-pumped solid state laser systems can deliver both the PRF and energy needed for this problem. Market trends in laser utilization will bring these systems into line with existing flashlamp systems, but they have yet to merge, as the diode-pumped systems are still quite new.

6.9 Performance projections

6.9.1 Comparison of existing model with observations

Figure 31 showed an example of an SNR calculation akin to those performed prior to the GBFT experiments. The calculations presented there provided some indication of the sensor performance and environmental conditions required in order to successfully obtain LIDAR images of GBFT.

If the same calculations are made, but with the addition of measured performance and improved target information, a comparison can be made between the theoretical SNR model and the actual ASTIL performance. Figure 60 shows a plot of SNR versus GBFT depth for the waters near Cape Cod (JWT-II water, with b=0.2/m). As before both the scattered and unscattered cases are shown, in order to provide a visual measure of the effect of scattering upon SNR. The measured SNR for GBFT are also plotted as a single data point with an error bar representing the standard deviation of the SNR about the median. The median and standard deviation for the measured SNR were 7.7 and 2.7, respectively, for a median GBFT depth of 3.4m.

The model calculations shown in Figure 60 show good agreement with the measured data. However, this should not be mistaken for a statement that the model can be relied upon to predict GBFT SNRs as closely as shown in the plot. Some of the closeness is due simply to circumstance; part of the closeness is caused by the use of a measured contrast, instead of a derived reflectivity. The contrast used for the model calculations was 4.4, the median contrast measured for the GBFT.

Figure 61 shows a theoretical SNR plot for which a derived reflectivity of 1.5% is used, and the environmental parameters presumed typical for the anticipated waters of Cape Cod are used. The difference between using a measured contrast and deriving one from the reflectivity and environmental parameters lies in the number of assumptions that one has to make. In order to derive a contrast from a reflectivity, the water volume backscatter coefficient and specific bidirectional reflectivity properties of the tuna must be well known. As the tuna are not well enough characterized to know this and the environmental parameters were not measured *in situ* for these experiments, these parameters must be assumed. Figure 61 is not greatly in error with respect to the measurements, but it was generated with assumed fish and environmental parameters, leading to an error larger than when using a data-derived parameter that circumvents such speculation.

6.9.2 Extension of the existing model to deployable sensor configuration

If the sensor model used to predict the (single) GBFT SNR is modified to reflect a more operational tuna school detection system, some understanding of the utility of the ASTIL sensor to the bycatch reduction problem can be gained. The changes to the prototype ASTIL sensor that are needed have been implied in the preceding sections: 1) increased resolution, 2) increased laser energy, 3) larger swath, and 4) real-time tuna detection and school statistics accumulation. The first two improvements are self-explanatory. The last two improvements have not been

discussed in detail, so a few comments will be made here prior to recalculating the system performance for a more operational ASTIL sensor.

The need for a larger swath is driven by the need for efficient aircraft operations and area coverage rates that do not induce excessive cost (by having to fly many hours per square area surveyed). The prototype ASTIL sensor has a 15 degree swath. For a single-sensor system, a 30 degree swath is near the maximum obtainable without losing light to vignetting in the receiver collection optics or decreasing the size of the entrance aperture, which reduces light collection efficiency. As will be explained later, the 15 degree swath made for difficult survey operations, especially at altitudes above 100 meters. So increasing the swath towards the practical maximum of 30 degrees helps both the area coverage performance and the experimental logistics.

Since an operational system for bycatch reduction will be primarily a school-detection system, and since it will be impractical to involve an analyst in the review of every image collected, some automatic processing of data will be needed during operations in order to help locate and size the schools of tuna. Thus, a measure of real-time detection of tuna will be needed. The implication upon a system design is that this requires some minimum amount of SNR per tuna. A good design point to start with is the SNR achieved for the GBFT (median = 7.7), as this appears to allow for real-time detection with the prototype ASTIL sensor, providing a proven baseline to work from. The analysis in this report will begin with single-tuna detection statistics, as these form the basis for any school detection approach that does not treat the school as a lumped aggregate. Once the single-tuna statistics have been presented, possible aggregate approaches will be examined for operational system use.

6.9.3 Single-tuna detection statistics

Using the observed GBFT data as a point of departure, two ASTIL scenarios will be examined. First, the existing prototype ASTIL system will be applied to the ETP yellowfin problem, but with those modifications that can be readily made to the existing system (i.e., without major system redesign and subsequent development), and constrained by requiring scientific-grade data. Second, the ASTIL system will be applied to the ETP yellowfin problem, but after optimizing system electro-optics for currently available components, and with the constraint that the system be deployed primarily for operational survey, as opposed to scientific investigation. This constraint will allow the design parameters to be pushed a bit further toward optimal detection, but at the expense of losing some of the analytical value of the resultant data, as concerns LIDAR tuna signatures.

Figure 62, Figure 63, and Figure 64 show three ASTIL performance scenarios for studying yellowfin tuna in the ETP. All three figures assume a 100cm yellowfin in JWT-IB waters, using the existing ASTIL electro-optics and data collection system. The main difference is that these plots assume that the ASTIL firmware has been modified to allow for higher resolution (1024 cross-track pixels instead of 256) and that a higher energy laser has been used (130 mJ instead of 10 mJ). The change in water type from JWT-II increases the contrast to 6.4 from 4.4[46], and the order of magnitude increase in laser energy per shot enables higher resolution without sacrificing

---

[46] Based on Oishi-derived estimates of water volume backscatter coefficients. See also, Marine Light Field Statistics, R. Walker, John Wiley and Sons, 1994 (Table 5-4.4).

the energy density per fish (relative to the prototype ASTIL configuration used for most of the tuna data shown in this report). The solid line at SNR=7.7 in each figure represents the mean GBFT SNR observed in this research, and thus serves as a point of comparison.

Figure 62 shows that SNR values comparable to the mean GBFT results can be obtained down to 6-7m below the surface when flying at 500m altitude. Unit SNR occurs at 10m water depth. This SNR value is the point at which fish are indistinguishable from noise, taken one fish at a time[47]. These SNR values indicate that this configuration and altitude would be acceptable for examining surface schooling behavior as occurs during feeding events.

Figure 63 indicates that SNR values comparable to the mean GBFT results can be obtained down to 15m below the surface when flying at 200m altitude. This performance begins to provide data that are useful for night time operations[48], and would certainly allow for daytime observations of spotted schools.

Figure 64 indicates that SNR values comparable to the mean GBFT results can be obtained below 20m when flying at 100m altitude. This would definitely provide good performance during night time operations and would also be useful for daytime, spotted schools, probably even allowing for some "spooking" behavior in the school, as the dive velocity of the tuna would quite likely be overcome by the aircraft velocity in many instances.

These figures indicate that, even with some modifications this enhanced prototype ASTIL configuration would not necessarily provide an operational capability for both day and night operations. However, it would allow for robust night time operations at 200m altitude, and would at combinations of 100m and 200m altitudes would allow for useful daytime data to be collected, under the right schooling conditions.

Figure 65, Figure 66, and Figure 67 show estimated detection performance for an ASTIL sensor upgraded using current off the shelf technology. The improvements are: 200 mm f/1 front aperture, 25 degree field of view (swath = altitude), upgraded CCD camera (40+ percent quantum efficiency), and upgraded streak tube electronics (current Areté in-house design). Generally, there are significant improvements at 200m, and the value of the improvements drop off with altitude, as at 500m the tuna becomes under-resolved using the wider field of view.

The 200m altitude performance is arguably acceptable for night time survey operation, since the tuna will often be in the top 20m of water (again relying on existing published data on this subject). The 500m and 1000m altitudes are still useful, and may allow for some fisheries statistics to be gathered during both day and night operations.

What is clear from the SNR plots for single-tuna detection is that the anticipated maximum depths for tuna[49] (50m) cannot be imaged, and do not allow for direct detection for measuring school size or determining its presence. However, if the top 20m of water can be used to detect

---

[47] Aggregate fish detection scenarios are discussed briefly in the next section.
[48] Study of tuna behavior by the use of sonic tags, Newsletter Enyo (Far Seas) Fisheries Research Laboratory, Shimizu 44:1-5 (this source from Hunter and Churnside, NOAA Report LJ-95-02).
[49] Ibid.

and study schools of tuna, then there is significant applicability for the ASTIL system, even when limited by single-tuna detection. Detection of tuna at the deepest anticipated depths, while not allowing for imaging of individual tuna, may still be feasible if aggregate detection statistics are used to determine the presence of a school.

6.9.4 Aggregate tuna school detection statistics

An issue left open in the analysis of single-tuna statistics is that of 1) how one might leverage the single-detection statistics to generated composite school statistics and 2) how one could use other sensor-derived data to indicate the presence of a school. The first issue has been addressed conceptually, as it was shown that a plausible detection scenario could be demonstrated using the GBFT single tuna detection data. However, estimates of depth-dependent performance were not made for the case where multiple detections are used to accumulate detection statistics over a region, as opposed to detecting individual tuna. The second issue has not been directly addressed in this research, though some observations have been made that indicate it's a topic worth looking at briefly.

6.9.4.1 Aggregate tuna school direct detection performance

Using the system performance model for the updated ASTIL sensor discussed in Section 6.9.2, the single tuna detection performance can be used to estimate the detection performance when the detection event is an ensemble of detections, as opposed to a single detection event. The simplest way to extend the single tuna results is to assume that multiple detections can be combined independently and optimally so that the SNR will increase as the square root of the number of individual detections used to form an aggregate detection statistic.

Figure 68 and Figure 69 show such an estimate of SNR performance for the case where an updated ASTIL sensor is used to detect and optimally combine multiple instances of fish detections from one image (corresponding to one laser pulse). The packing density used for these calculations, expressed in body lengths between fish within the school, is one body length (BL). This unit BL packing density converts readily to a unit packing density for the number of fish per unit volume, if the relation $V = N (cL)^3$ is used[50] in conjunction with the 20kg, 100cm yellowfin tuna that has been assumed for the calculations presented in this report. Table 7 shows several body lengths and corresponding packing densities calculated using this same formulation. Figure 70 and Figure 71 repeat these calculations and illustrate how the performance changes as a function of body length.

Table 7. Packing density vs. body length for 20kg, 100cm yellowfin tuna

Packing Density (fish/m^3)	Body Lengths (spacing between tuna)
1.0	1
0.04	3
0.001	10

---

[50] Model Estimates of Acoustic Scattering from Schools of Large Yellowfin Tuna, Redwood Nero, Naval Research Laboratory Report NRL/MR/7174—95-7708, 1996.

Figure 68 and Figure 69 indicate clearly that detection performance can be improved by combining multiple detections, but care must be exercised in interpreting this result. As it is assumed that single detection have been combined to yield the aggregate performance, it is necessary that the single detection event have enough SNR to distinguish it from the background. Consequently, the data shown in Figure 68 must be compared to the data in Figure 65, where it can be seen that single tuna detection at 200m altitude and 20m water depth yields an SNR of only 4, which is probably adequate, but only marginally so. Likewise, the aggregate performance for 500m altitude suggests performance down to 20m, whereas the single shot performance becomes marginal at less than 10m water depth.

The conclusion that one can readily draw is that detection of schools is improved by combining the detections of individual tuna; however, not all of the available signal processing gain is realized in this approach: only those events that exceed a threshold will be considered. In order to recover this lost gain, one must use the detection events that are below the threshold (i.e., less than SNR=4, to use the numbers cited above).

One method of using these sub-threshold events is to use a detection statistic that includes all detection events, such as the mean SNR and its associated SNR variance. For instance, the GBFT data presented earlier had an SNR mean and variance of 7.7 and 2.7, whereas the background data had an SNR mean and variance of –0.07 and 0.8, respectively. So a school detection approach that used such statistics would involve measuring and tracking the statistical properties of the SNR detections as a function of time, and would declare a school detection when the mean SNR shifted appreciably from the background level. In this way, a greater percentage of the signal processing gain offered by aggregate detection could be recovered and used.

6.9.4.2   School detection based on apparent water optical properties

One measurement of the presence of a school that can be used to detect with is the measured diffuse attenuation coefficient. This approach treats the school as an additional scatterer in the water that degrades the light penetration, and can therefore be observed in the (indirect) measurement of attenuation. Such a range-return slope detector was tried successfully during the analysis of SBT data collected and has been considered by other researchers[51].

Figure 72 shows the ASTIL-derived in-water attenuation coefficient data[52] for two captive schools of SBT and some open water between the schools. While this graph does not represent proof of the efficacy of this technique for detecting schools, but it does suggest feasibility. Table 8 shows the change in the observed attenuation coefficient statistics when comparing the school data to the open water data. The shift in attenuation coefficient was about 0.07, or 17%; the

---

[51] Numerical Evaluation of the Possibilities of Remote Laser Sensing of Fish Schools, M. Krekoval et. al, Applied Optics, Vol. 33, No. 24, 20 August 1994.

[52] It should be pointed out that this is not an actual diffuse attenuation coefficient measurement, as a slit was in place that serves to reject multiple scattered light, meaning that the apparent attenuation coefficient will be higher than the actual. Companion data collected in these waters without the slit confirmed that the waters had K values of between 0.10 and 0.17/m typically.

corresponding variances changed by a factor 2 or greater. In combination, these shifts would indicate that indirect detection of schools, via the water optical properties, is possible.

Table 8. Attenuation coefficient statistics from data in Figure 72.

Data Segment	Mean	Standard Deviation	Mean/Std.Dev.
School 1	0.51	0.058	8.7
Between Schools	0.44	0.018	25
School 2	0.52	0.038	14

The depth penetration for such indirect detection approaches depends only on the water backscatter efficiency and the sensor radiometric performance. The tuna optical properties matter only insomuch as they affect the apparent water optical properties.

Figure 73 shows the SNR for the upgraded ASTIL sensor as concerns the measurement of water volume backscatter in order to measure the attenuation coefficient of the water column being imaged. Cases for averaging 1, 10, 100 and 1000 cross-track pixels are shown and labeled accordingly, all for JWT-II water and 500 meters aircraft altitude. As the assumed CCD for the system is only 1024 pixels in the cross-track direction, the 1000 pixel average represents an average across the entire fan beam. In practice, one would probably use either the 10 or 100 pixel average, as these would allow some measure of both the along-track and cross-track extent of a school, presuming that its attenuation signature was detectable.

The SNR shown in Figure 73 is not indicative of the maximum attainable SNR for measuring the water attenuation, as it only indicates the per-range-pixel SNR for direct measurement of the LIDAR return from the water volume being imaged. In practice, the entire water column away from the surface specular return would be used to estimate the attenuation for a particular cross-track pixel, so that the SNR per cross-track pixel would potentially increase by more than an order of magnitude. Consequently, the data shown in Figure 73 are conservative as a theoretical estimate.

The model data plotted in Figure 73, when combined with Figure 72, indicate the potential of a school detection scheme that is relatively simple and allows for depth penetration suitable for schools of ETP yellowfin tuna. However, these results are new and have not been studied extensively enough to allow for confidence in applying such a detection scheme broadly. A thorough study of the expected impact of the actual non-fish-related variation of water optical properties, combined with further experimentation to gather actual ETP school data would enable a direct assessment of the efficacy of this detection scheme.

6.9.5   Summary of detection performance

Based on the measured and modeled data presented in this report, some summary estimates of detection performance can be made. In order to maintain a modicum of simplicity and clarity in presentation, only the maximum anticipated depth for a selected tuna in nominal ETP waters will be tabulated for the several detection schemes presented.

Table 9 shows the estimated performance for an upgraded ASTIL sensor using the detection techniques discussed in this report. All of the detection approaches based on single tuna statistics were tabulated based on a 200m flight altitude. The reason for this is that the performance at 500m was shown to be only marginally adequate for realistic operations. Furthermore, as the probable interest in detecting tuna using matched filter single-tuna statistics is for understanding school behavior and gathering school population statistics, the sacrifice of swath for the decreased altitude and improved detection performance is likely to be a good tradeoff. The detection depth for these first two single-tuna matched filter approaches is limited fundamentally by the single tuna statistics; the detection event has to surpass a threshold in order to be counted in an aggregate detection scheme, so that the initial detection event still limits the performance.

The performance for single tuna events within a school can be extended substantially if the single shot statistics are observed without a threshold, meaning that no single tuna events are detected. This approach simply generates the matched filter events for each shot and extracts statistics from the histogram (or equivalent) of the matched filter image data. For this method, the single tuna detection data could be saved once a school had been found, but it's not clear at the time of this writing whether or not this detection approach would cater more to school studies or merely fish school detection. The 30m maximum depth shown here is for a 200m altitude, as it is assumed that the image data of the school would still be of interest.

The maximum performance to be obtained with the system occurs when the school is indirectly detected by measuring apparent water optical properties. This approach treats the tuna as additional scatterers in the water that increase the sensor-derived diffuse attenuation coefficient for the water column being imaged. Since it seems unlikely that such a scenario would be used for imaging schools, the 500m altitude was used for this estimate in an attempt to represent a realistic operational scenario. The maximum depth estimate is given as below 45m, as there is, theoretically, signal processing gain to be realized that was not included in the calculations made as part of this research.

Table 9. Estimated maximum detection depth for ASTIL detection of 20kg, 100cm yellowfin tuna in the ETP. Variable altitudes are used depending on configuration, so as to maximize utility.

Sensor Configuration	Detection Technique	Reference	Maximum Depth (m)
Upgraded ASTIL, H=200m	Single tuna matched filter	Figure 65	18
Upgraded ASTIL, H=200m	Single-shot multi-tuna matched filter w/ threshold	Figure 68	20
Upgraded ASTIL, H=200m	Single-shot multi-tuna matched filter w/o threshold	Figure 70	30
Upgraded ASTIL, H=500m	Single-shot water optical property detection	Figure 73	45+

Note: Table 9 does not reference packing density or body length, mainly because the packing density does not significantly impact performance when an entire school is considered, since multiple shots then contribute to the overall school SNR. The data shown here are derived from single-shot performance estimates when the packing density was unity, corresponding to BL=1. For the upgraded ASTIL sensor used for these calculations, this would be equivalent to an arbitrary packing density detection scheme but with the school size fixed at 150 tuna. Consequently, the estimates made here are again conservative if a school of 150 tuna is in some sense considered to be small.

6.10 Utility of ASTIL for school imaging

6.10.1 Government oversight and stock assessment

The data products presented in this report are supportive of the use of LIDAR for stock assessment and related measurements that are primarily concerned with aggregate fish school quantities. Schools of tuna probably represent the most difficult pelagic species to image with LIDAR, owing to the lower packing density and low apparent reflectivity. Even so, the ASTIL sensor indicates that there is probably a useful role for LIDAR in studying and monitoring fish stocks in the ETP. When packing densities are higher, the utility of LIDAR is greatly enhanced, as implied by both the data shown and the contrast analysis performed in this report.

6.10.2 Commercial fishing operations

Commercial concerns require cost justification that cannot be spread across an entire industry, as is the case with a government monitoring and oversight role. This means that there must be a positive cash flow generated by the use of the sensor, either through improved efficiency, or through improved marketability of so-called "green" products.

Any realistic assessment of profit and loss associated with airborne LIDAR operations in support of ETP tuna operations is well beyond the scope of this report. The reason is that operational scenarios must be explored thoroughly, with good quality input from representative industry players. Then the value added from LIDAR must be carefully quantified so as to determine the cost function for incremental fleet improvements with LIDAR. If these data could be determined, then a robust analysis of profitability and feasibility could be conducted.

The most that can be said at the present time is the LIDAR does yield useful information on schools of fish, and has increasing utility as packing density or single fish size increases for the species of interest. The results presented in this report substantiate this claim, and it is anticipated that future research will continue to enhance the utility of LIDAR for fish school observation.

6.11 Discussion of problems encountered

6.11.1 Aircraft logistics and alignment

Because of the relatively narrow swath of the sensor, it was difficult to align the sensor precisely over the schools when present, especially in the open ocean where there are no local references. This difficulty is compounded if the aircraft does not have at least a high wing design and/or a wide peripheral view for the pilot/spotter. The Piper Aztec used in both the Hawaii tests and the New England tests was quite difficult to operate in because of its lack of a high wing and because of its limited view from the cockpit. By contrast, the Partenavia Explorer used in the first ASTIL experiment is nearly ideal and has allowed for easy experimentation by comparison with the Aztec. The Aerocommander provided by CSIRO was also quite useful, having a high wing design.

6.11.2 Proximity to fish schools and size of available schools

The experiments conducted in Hawaii had the advantage of good weather, good water conditions and a good spotter pilot. However, the schools of tuna that were large enough to find and image as a school were too far out to sea to be reached with the Aztec aircraft. The experiment was planned based on reports and commentary from both fishermen and pilots that there were often tuna in close proximity to the islands. However, this information was somewhat anecdotal and may have been skewed toward the sport-fishing type of tuna sighting. Schools with many hundreds of fish, which is the type of school really needed for an airborne LIDAR demonstration, did not frequent the waters near the islands during our experiments, and some fishermen have indicated that these are more common to waters more distant from the islands.

6.11.3 Optimality of available sensor technology

On a developing technology, the list of items to improve often outpaces the opportunities to make the improvements. The ASTIL sensor development is no exception to this rule. Early experiments lacked a real-time display, which was implemented by the time the Hawaii tests were conducted. Data collection was clumsy and required operator finesse in the first experiments; by the end of the testing in New England, an operator graphical user interface (GUI) had been implemented on a touch-screen display. Also, navigational data and attitude information were added to the collected data, so that data registration was possible. These and many similar improvements were made during this effort, all of which have helped to produce better ASTIL data.

The one sensor parameter that did not change over the course of the experiments was the cross-track resolution and the swath. As was mentioned earlier, the resolution was set to the maximum that could be had at the time this development was begun; and only recently has a higher resolution mode been implemented on a separate (but similar) system. The swath also remained constant, as this was set by the availability of commercially available collection optics.

As this report has shown, additional resolution and swath would have helped improve the quality of the data. It is not clear that such changes would have yielded data on yellowfin, as the

difficulties with proximity to schools and their sizes would still have been present. However, the quantity of GBFT data may have improved with swath, and the quality would certainly have improved with higher resolution.

6.12 Description of need, if any, for additional work

This research has established proof of principal for LIDAR imaging of tuna under several conditions. However, the database that has been collected is still quite small, and additional experiments will help the understanding of the detection of tuna with LIDAR.

First, an experiment that specifically addresses the bidirectional reflectivity of tuna would be very valuable for gaining closure on the LIDAR signature of tuna. Many things have been established in this regard during this effort, but some of the issues not covered include 1) diffuse component reflectance of tuna, 2) specular component reflectance of tuna, 3) angular dependence of the reflectance of tuna, and 4) spectral behavior of the reflectance of tuna. All of this points to the need for a good physical model of tuna, and other species if possible, so that this work can be extended meaningfully with both analyses and experiments.

Second, additional experiments with tuna will only help to strengthen the understanding of the tuna detection problem. The experiment in Hawaii did not succeed for a number of reasons, perhaps the greatest of which was the simple lack of opportunities over bona fide schools of tuna.

Last, additional experiments with other pelagic species will help address questions of viability of LIDAR to commercial fishermen and for biomass and stock assessment as well. This was not a point of emphasis in this effort because of the dissimilarity between tuna and sardine, for instance – there was a fundamental lack of relevance. However, the data that was collected (i.e., akule) indicated that there are meaningful experiments that could yet be conducted for non-tuna pelagics.

7.   Evaluation

The goal of demonstrating the utility of the ASTIL sensor for dolphin bycatch reduction in the ETP was achieved generally, but not with the specificity that was desired. Ideally, the experiments would have yielded images of schools in the open ocean, perhaps even with and without dolphin. Instead, images were collected for captive schools of SBT, dolphin, and GBFT, which allowed for an equivalent analysis to be conducted that used analytical tools and physical reasoning to bridge the gap between the data collected and the desired ETP yellowfin data.

The utility of the ASTIL sensor for tuna detection was most clearly demonstrated by the SNR separation measured between the tuna and the background, and the subsequent automatic detection of the GBFT school in New England. Because of the similarity established between the GBFT and the SBT, and because the SBT are physically similar (not identical, but similar) to the yellowfin, the detection results presented here are conclusive in regard to detectability of tuna, as known scaling laws allow the GBFT results to be extended to smaller species of optically similar tuna.

The research goal that could not be addressed in this work was that of determining how well one could use the ASTIL sensor to reduce bycatch. This was a reasonable goal to desire, but one that still requires more data than has been collected to date. The general reasons for the paucity of yellowfin data have already been delineated.

Modifications were made to the goals and objectives in only one notable case: sensor hardware development. Because of the timing of the award, some of the hardware development had already begun under Areté funding. The proposed effort was much less ambitious than that which was undertaken with Areté internal research and development funds. This was fortunate, as the proposed system configuration would not have led to experimental success (the resolution was too low – a fact that was discovered experimentally and confirmed later analytically), and the funds needed for analyzing and understanding the tuna detection problem would have been spent on hardware instead.

To the extent that goals and objectives were associated with schedules, modifications were made here as well. A combination of the timing of the award, the need for non-interference with the ONR effort that owned and needed much of the STIL equipment, and windows of opportunity for collaboration with other researchers (i.e., the New England Aquarium) precluded a pre-planned experimental execution. It was serendipitous that many of the analytical tools used in the detection assessment of the GBFT were available only because of having occurred after much of the "heavy lifting" had been done on a separate ONR STIL effort.

7.1 Dissemination of project results

This report will serve as the first and principal means of disseminating the project results and for interested researchers, data will be made available on the Internet for independent research. Select data products will be made available on the World Wide Web as well, and many collaborators and researchers have accessed and reviewed the data presented already. Finally, the authors will prepare a publication that summarizes this work so that others will be aware of the progress made and will be enabled to extend the work as possible.
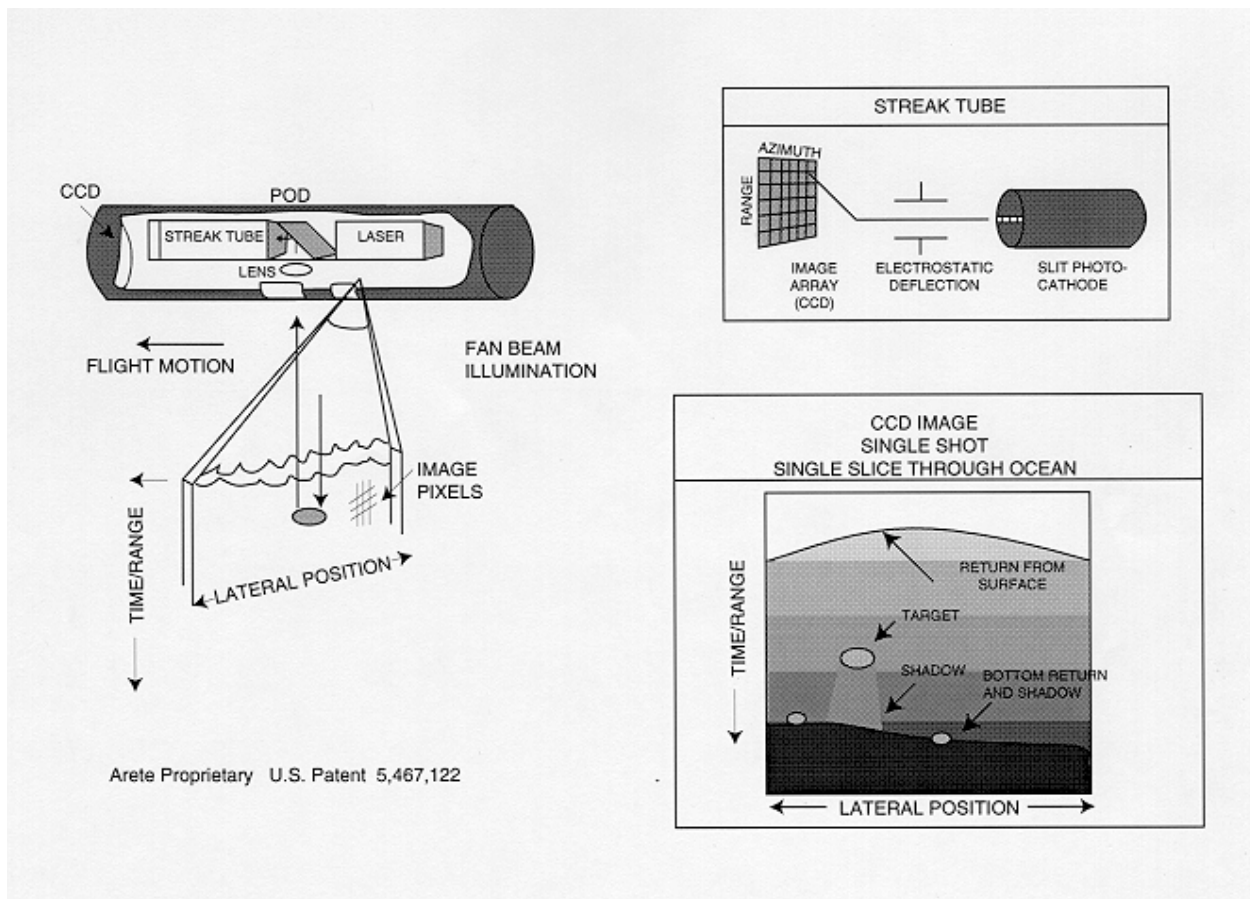
Figure 1.   Conceptual view of STIL as a 3D sensor for subsurface viewing.
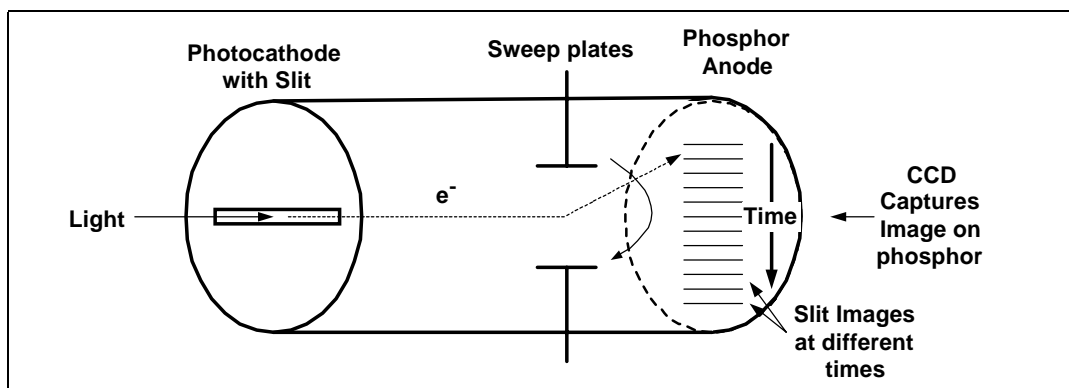
Figure 2.   Streak tube architecture from a photonics point of view.
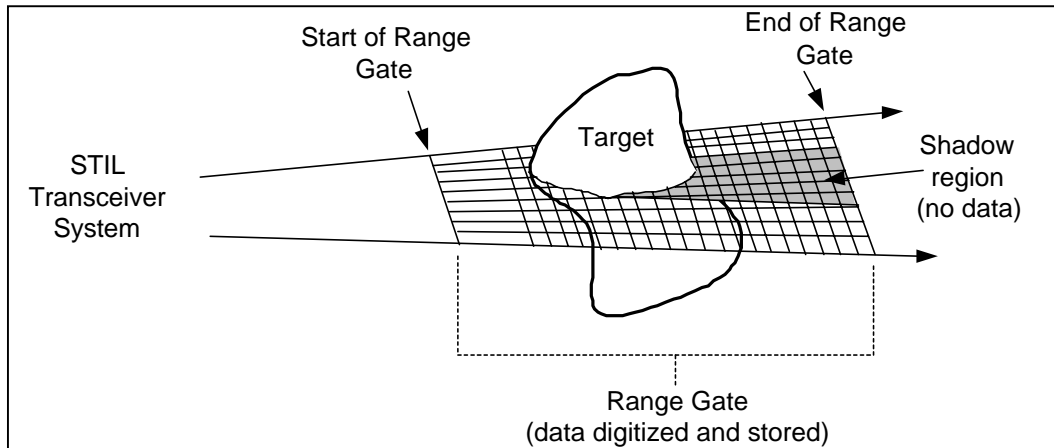
Figure 3. Typical streak tube lidar data collection illustration. Coverage of the dimension perpendicular to the plane of data collection is achieved by either motion of the sensor or a 1-D scanning system. A method to collect volume data with one laser pulse, rather than the single slice shown here, is described in Section 2.2.3.

STIL Laboratory System Configuration
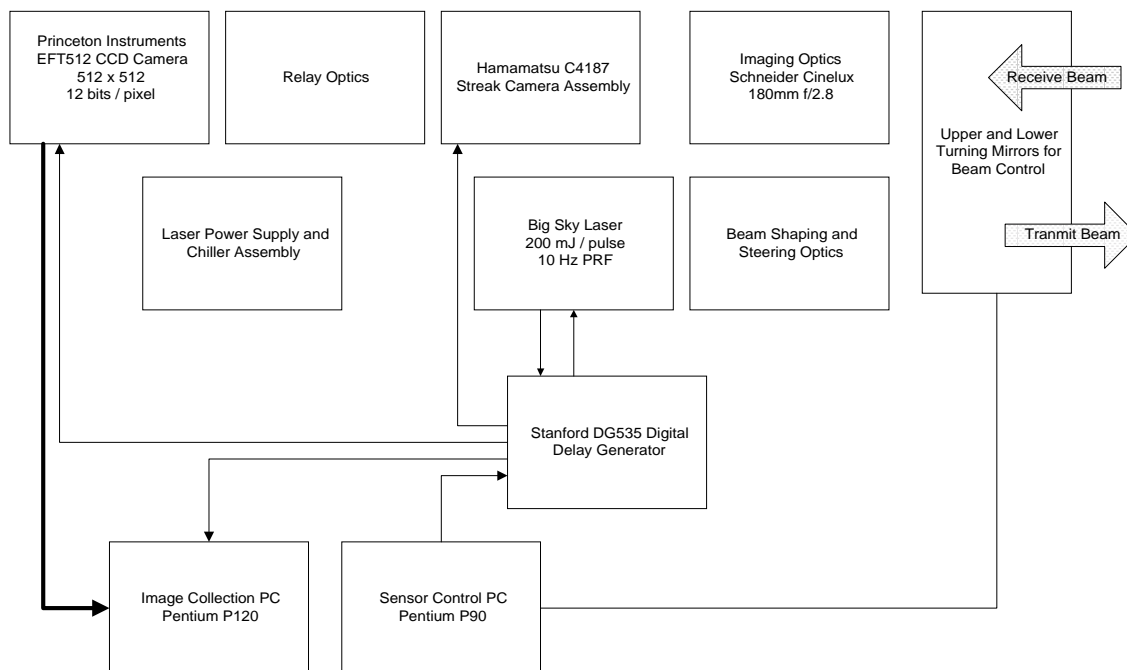
Figure 4. Block diagram of STIL laboratory system prior to ASTIL development efforts.
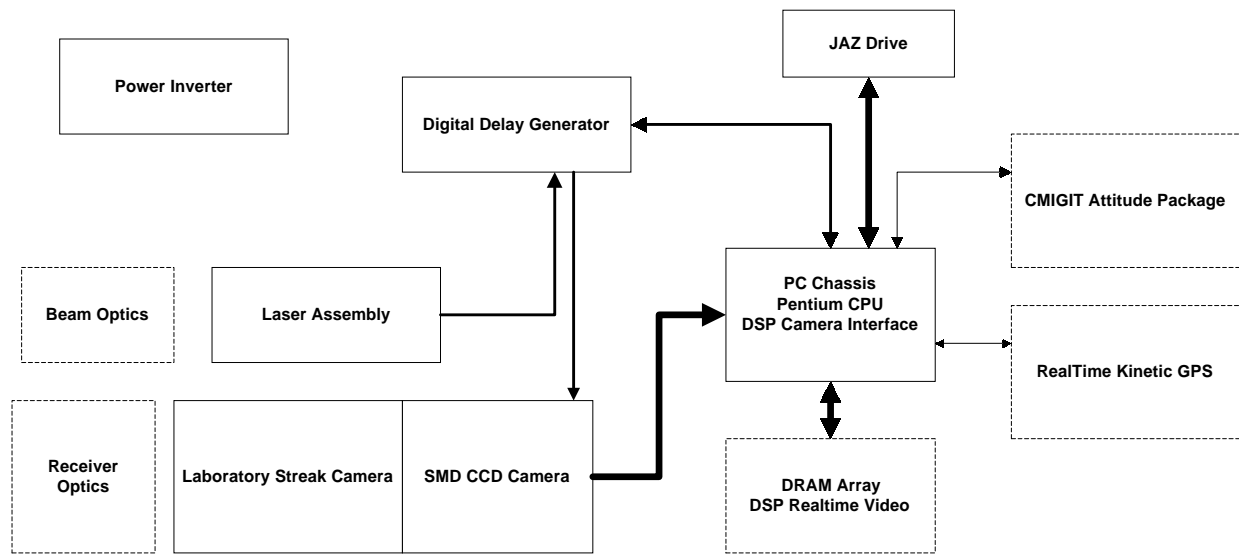
Figure 5. ASTIL system configuration. Dashed blocks indicate components added or upgraded after the initial CSIRO experiments.

(a)

(b)

(c)
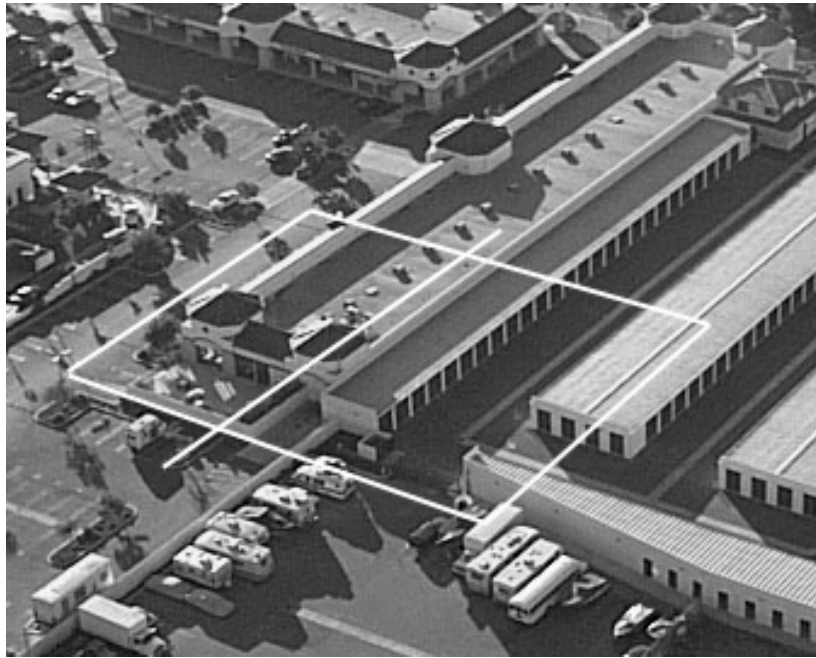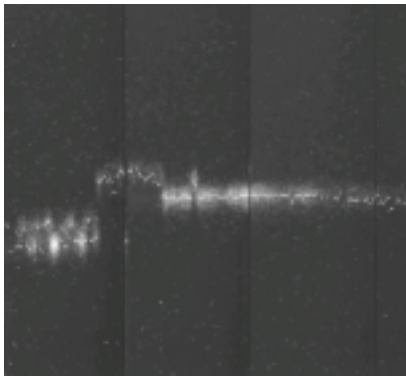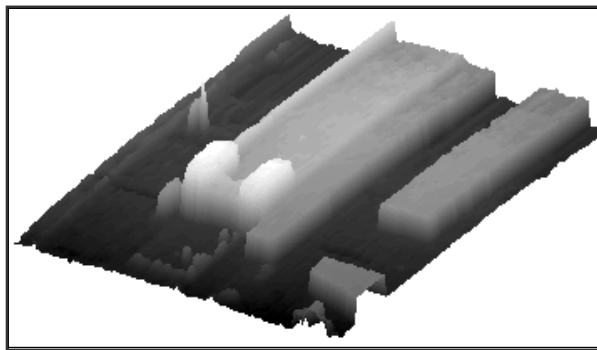
Figure 6. Terrestrial mapping data. (a) Aerial photo of the buildings being surveyed. (b) Single laser shot showing raw data for one line image, indicated by single white line in (a). (c) Range image of area outlined in square in (a) generated by reconstructing from the individual line images.

Figure 7. ASTIL installation in the Partenavia Explorer for the first airborne tests
in February of 1997.

Figure 8. Jeff Plath, Andy Griffis and Pat O'Brien with the Partenavia Explorer in February of
1997 for Tucson flight tests.
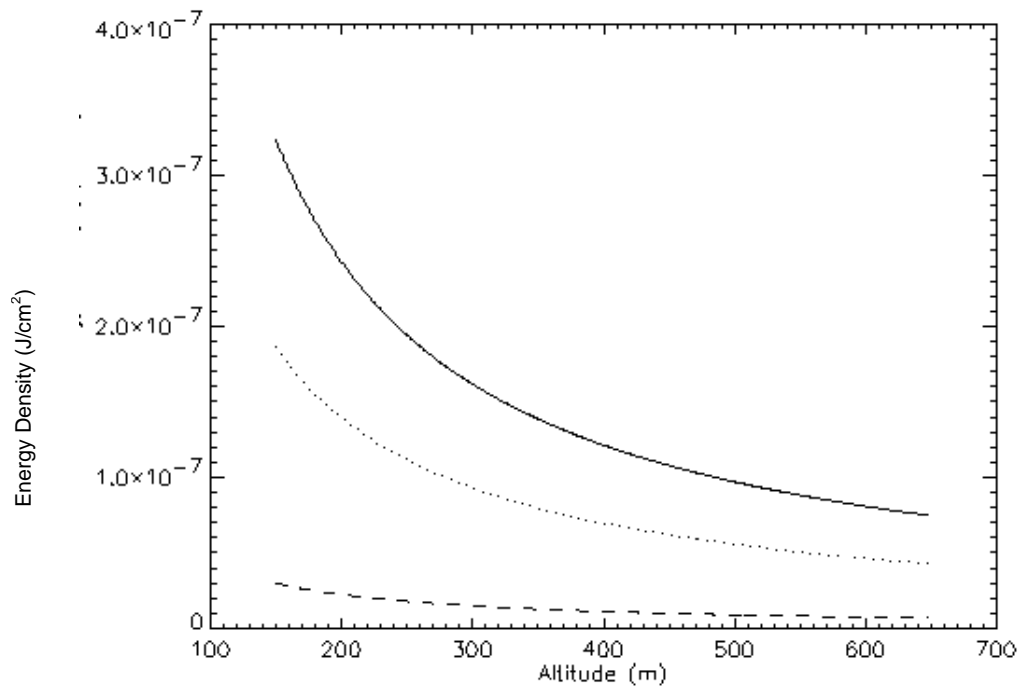
Figure 9. Energy density as a function of altitude for 3 ASTIL sensor configurations. Solid is for 130mJ and 15 degree swath (prototype ASTIL at 30Hz); dotted is 130mJ and 25 degree swath (upgraded ASTIL); dashed is 12mJ and 15 degree swath (prototype ASTIL at 100Hz)

Figure 10. One of the SBT fish nets in Boston Bay, South Australia.

68

Figure 11. Andrew, Tasmanian Air Pilot, Dr. Ann Cowling, and Derek Hayman, who provided aircraft and logistics support for the CSIRO experiments.
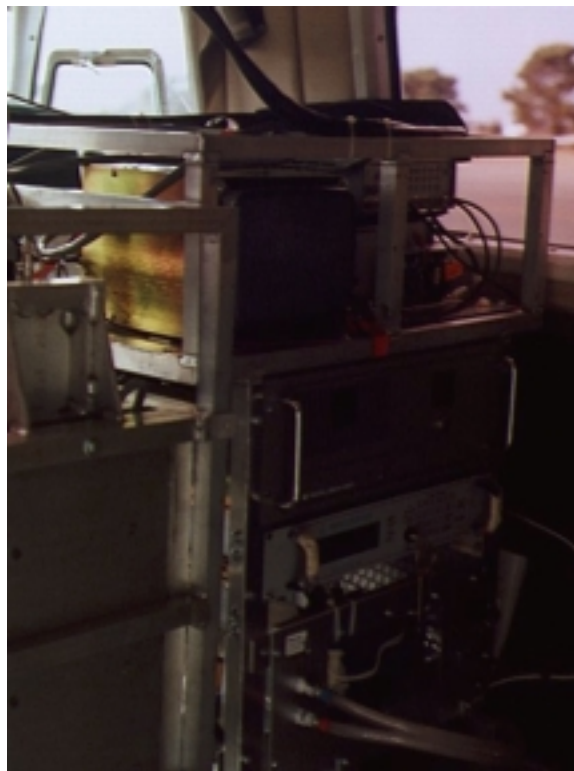
Figure 12. ASTIL installation aboard the Aerocommander 500 provided by CSIRO and Tasmanian Air. Both racks were installed across the width of the aircraft body – the only installation to date to allow for this.
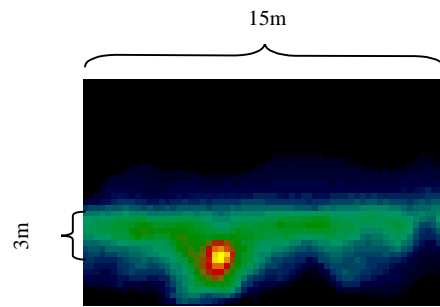
Figure 13. Example of a single SBT signature at 3m depth.

Figure 14. Top view of a 16kg SBT.

Figure 15. Side view of a 16kg SBT
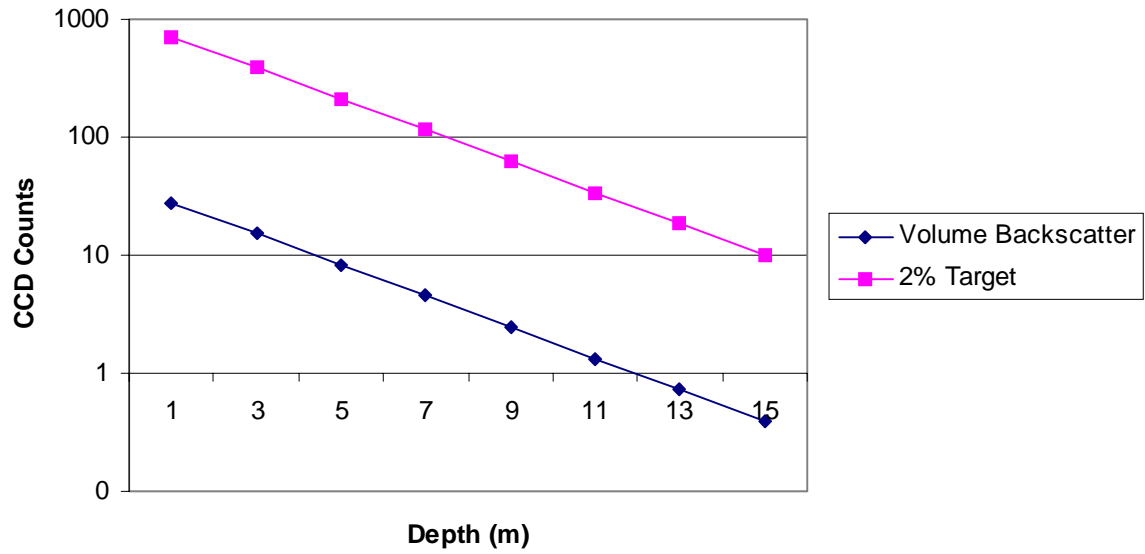
Figure 16. Example of radiometric calculation for ASTIL performance assuming a Lambertian reflector with 2% effective reflectivity. Aircraft is at 1000' and water is 0.15/m diffuse attenuation.

.
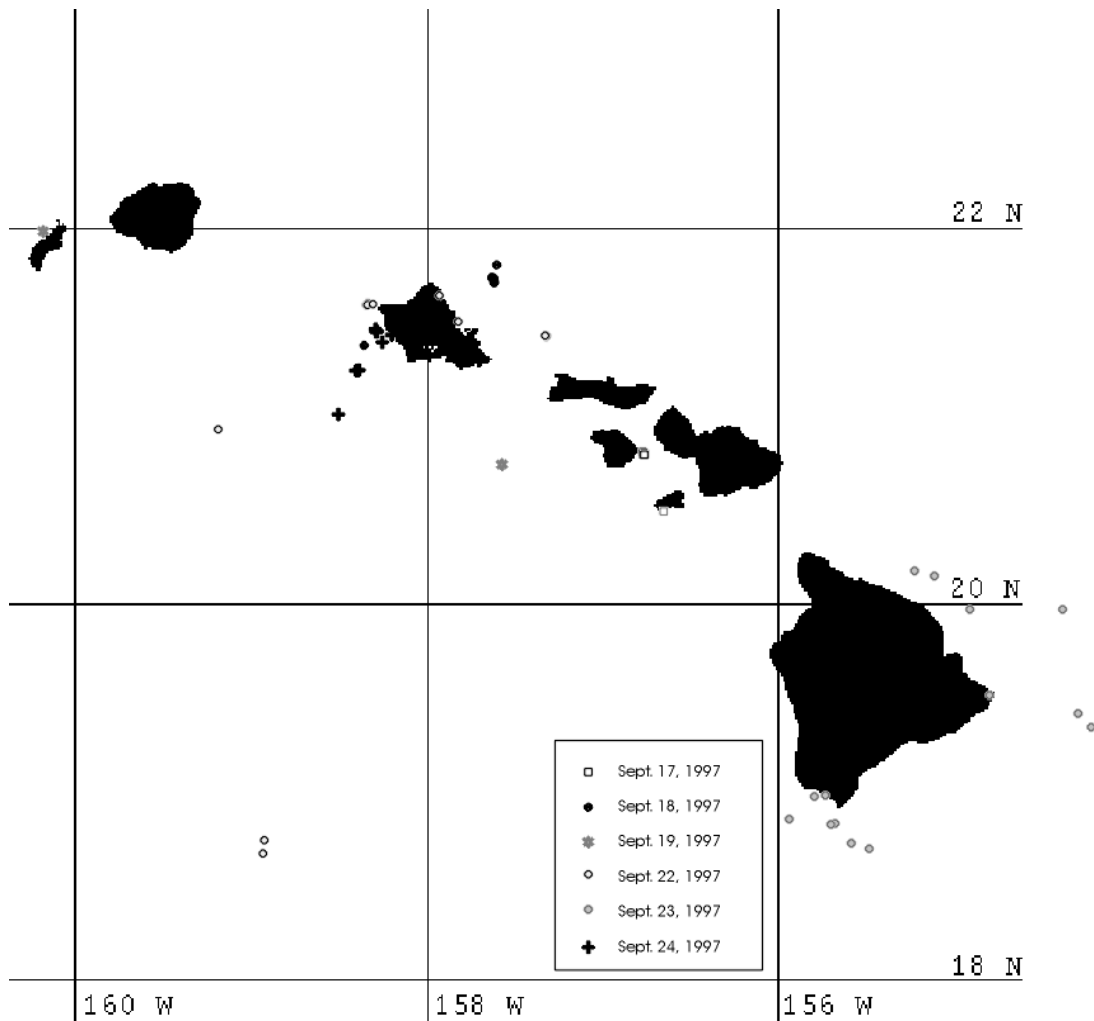
Figure 17. Regions flown in Hawaiian field tests.
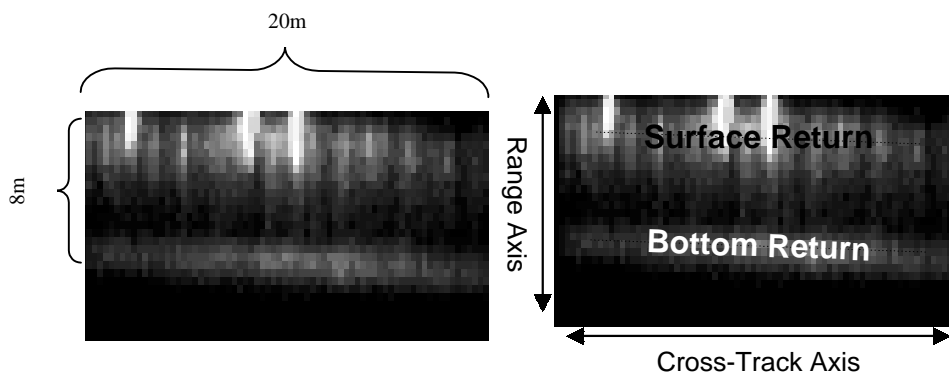
Figure 18. Example of ASTIL raw data showing the 2D nature of the data from each pulse of the laser. (a) Raw data from Boston Bay showing the return from both the surface and the bottom, (b) corresponding annotated image.

72
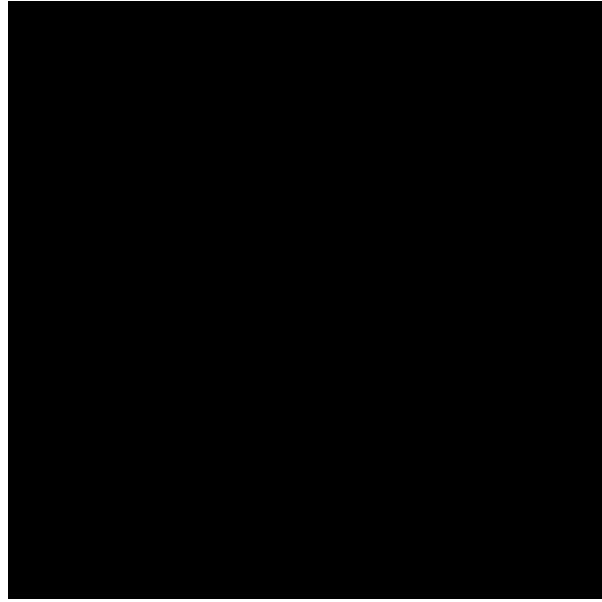
Figure 19. Average range-transect for raw data in Figure 18.
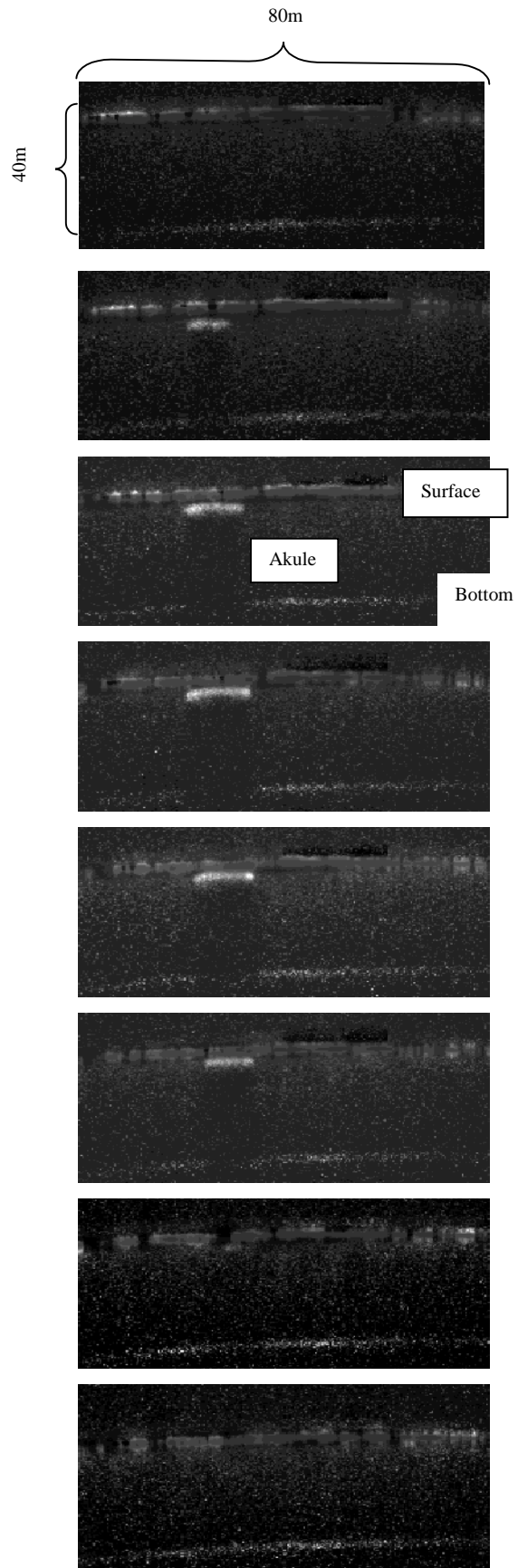
Figure 20. 2D Image sequence for an akule school (Hawaii, 1997)
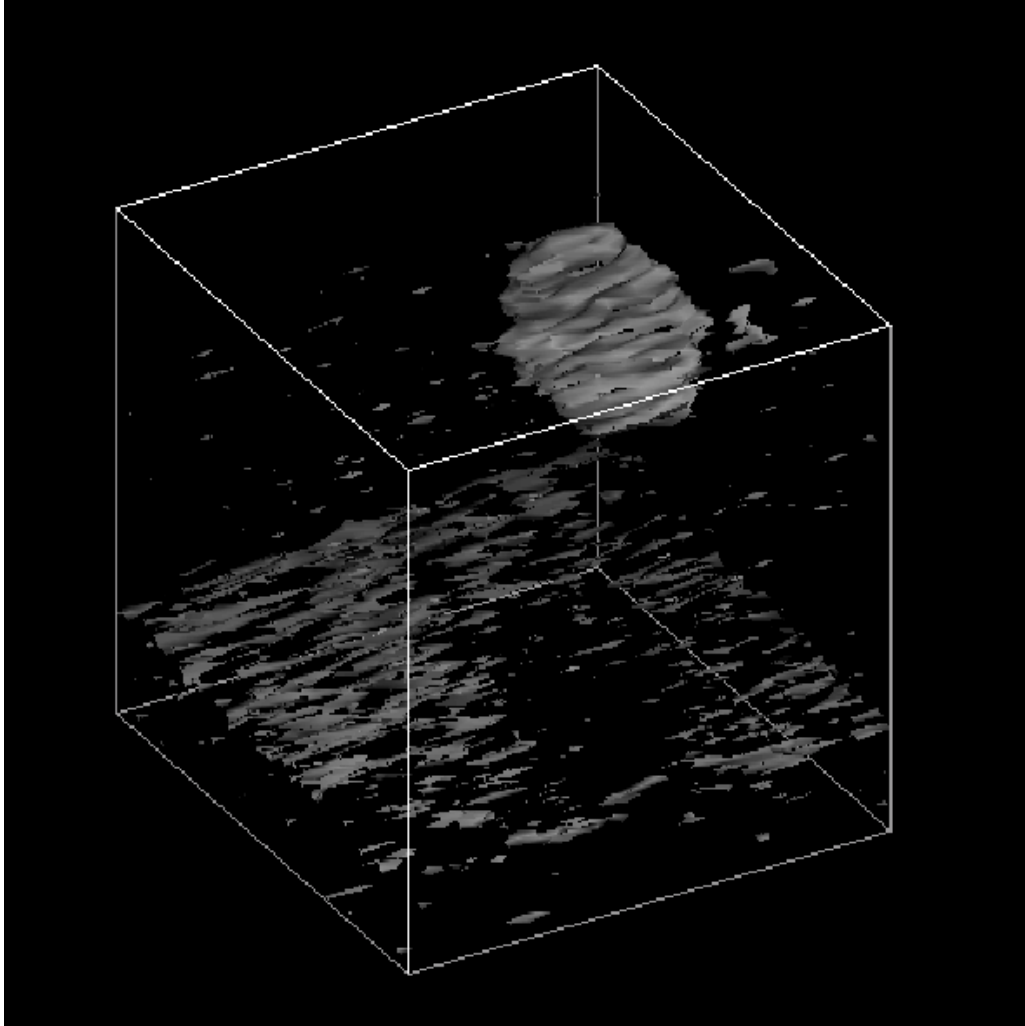
Figure 21. 3D Rendering of akule school from raw 2D data; surface is removed prior to rendering.
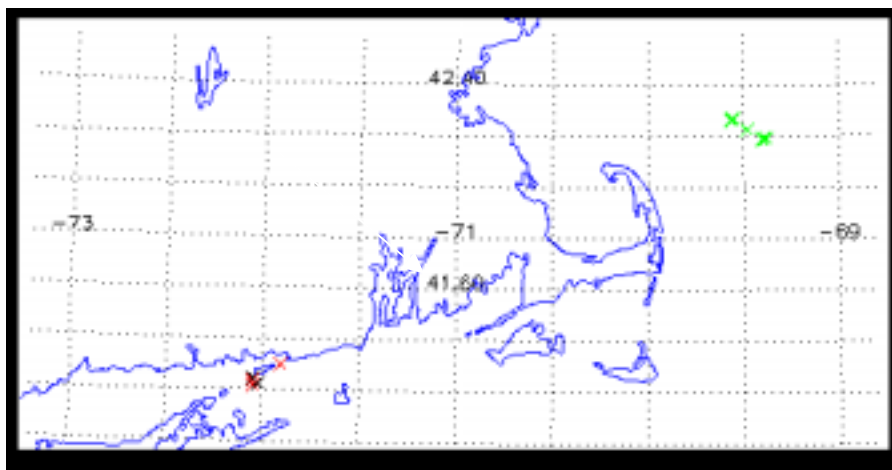
Figure 22. Location of experimental data collection for the GBFT experiments. The GBFT data presented in this report were gathered at the locations in the upper right hand region of the chart, off the northern tip of Cape Cod.

50m

2m
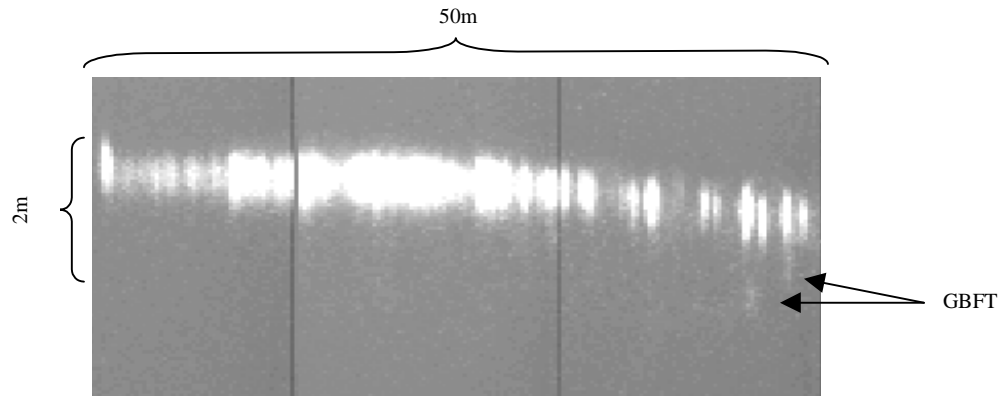
GBFT

Figure 23. Raw image of GBFT. The surface return dominates the image, however, small spots near the lower right hand side can be seen.

50m

2m
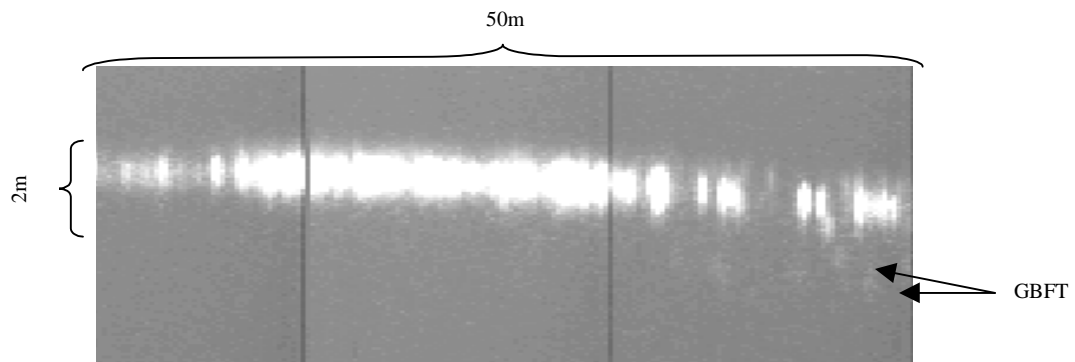
GBFT

Figure 24. Raw image of GBFT. Several faint signatures are visible on the right hand side of the image.

45m

3m
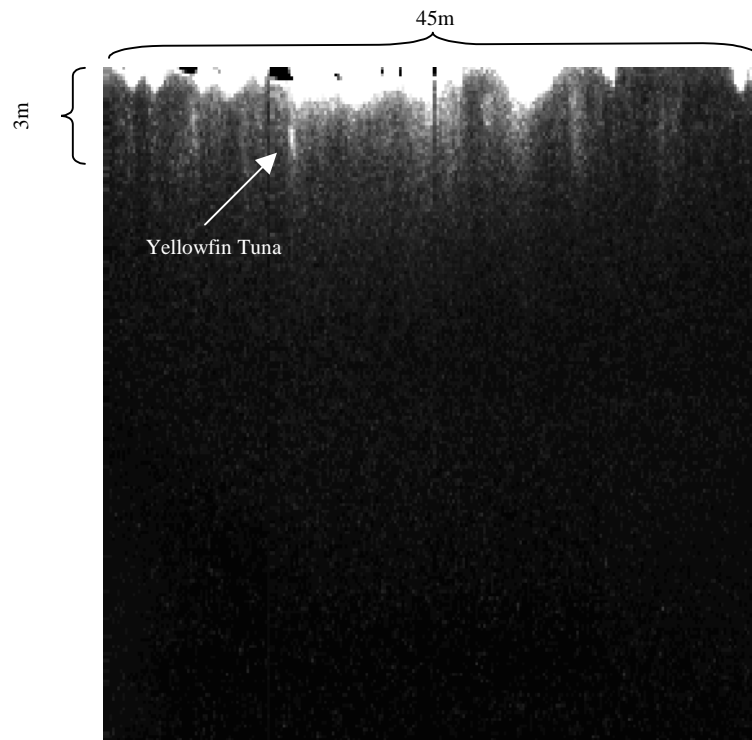
Yellowfin Tuna

Figure 25. ASTIL image of yellowfin tuna near Pearl Harbor, HI (September 1997). The tuna is the bright spot just beneath the surface in the left half of the image.
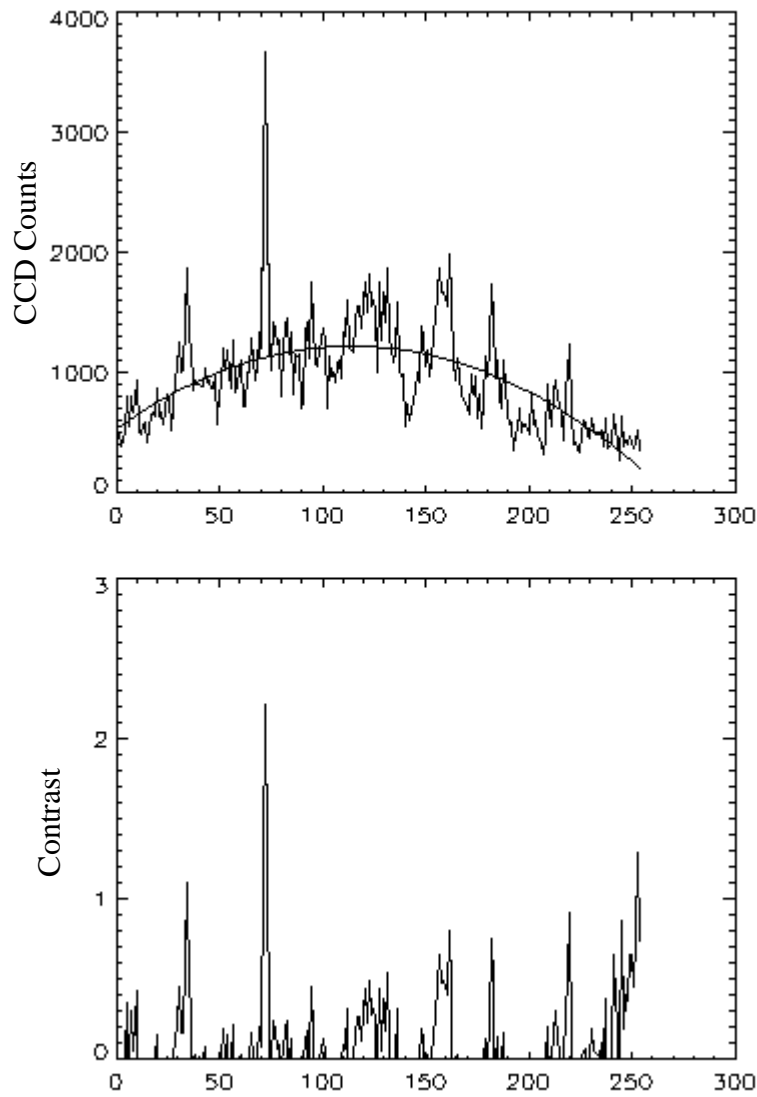
Figure 26. Cross-track (horizontal) slice through raw image of yellowfin tuna (upper) and its corresponding derived contrast. The tuna signature is at the 70th cross-track pixel and shows a contrast just above 2.   The possible under-resolved nature of the signature may have introduced a lower than usual contrast.
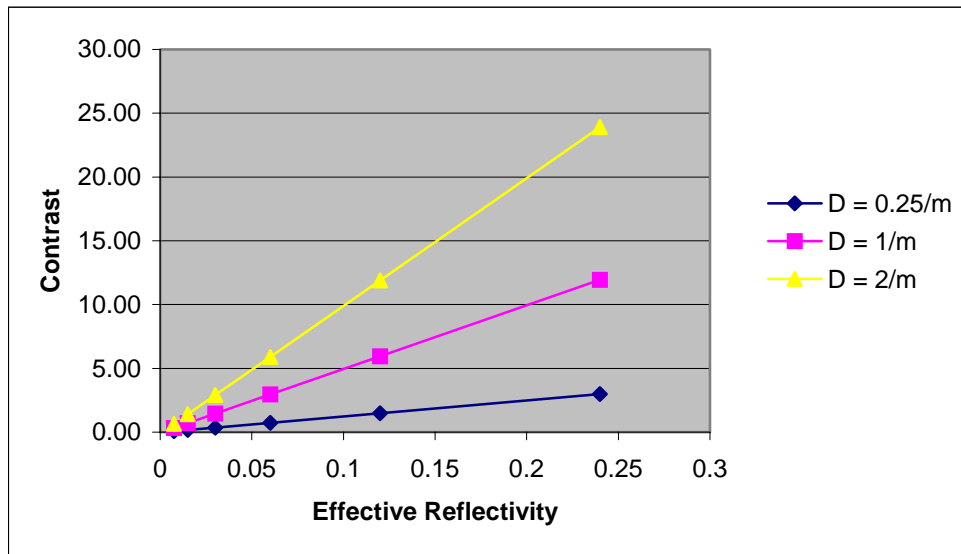
Figure 27. Contrast vs. effective reflectivity for several packing densities.
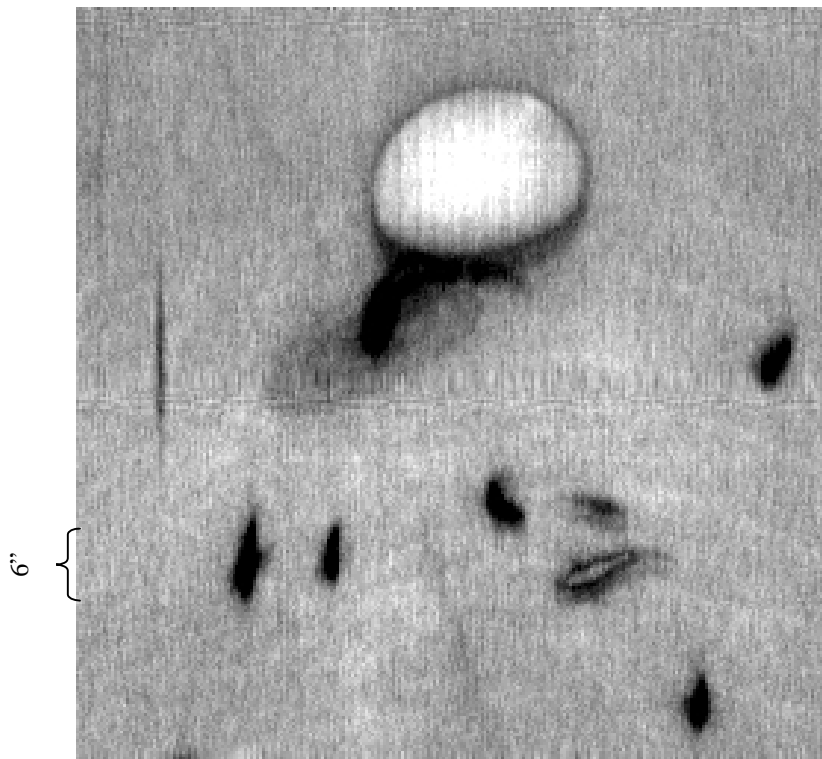
Figure 28. Shadow image of 6-inch fish collected from an underwater-class advanced technology STIL sensor.
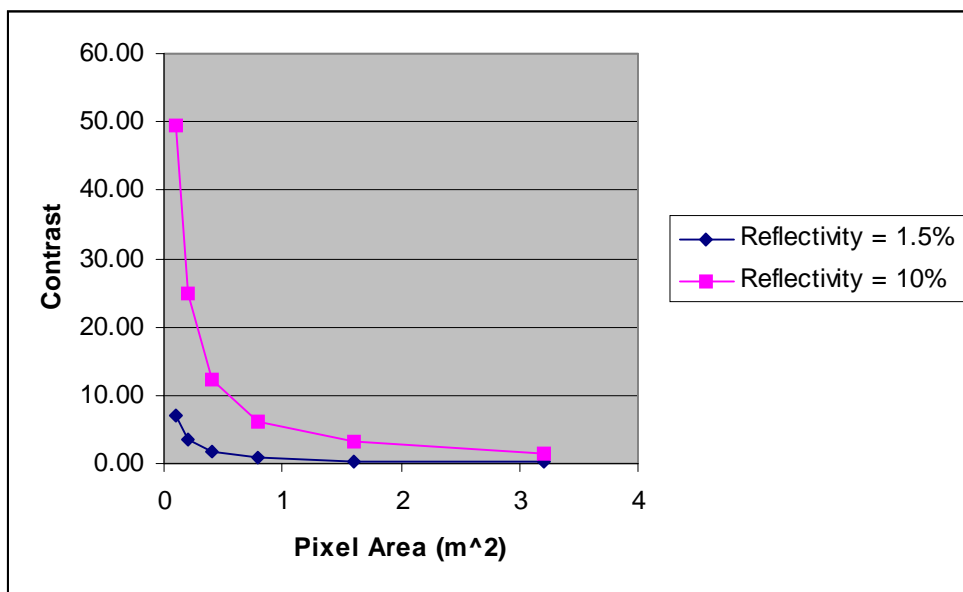
Figure 29. Contrast vs. pixel area (resolution element) for a 20kg tuna.
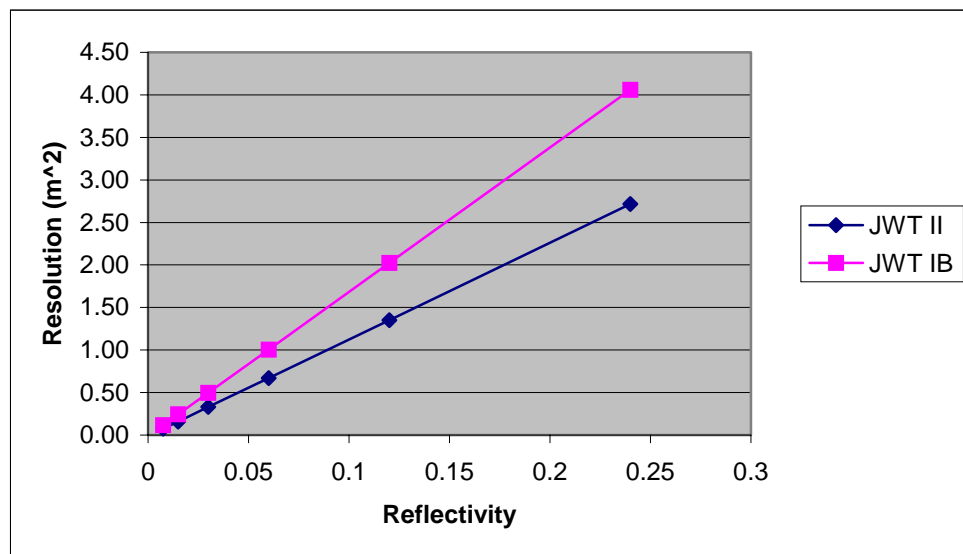
Figure 30. Required lateral resolution (m^2) to achieve contrast = 4.4 vs. tuna effective reflectivity, based on 20kg tuna. The packing density is 0.25/m^3
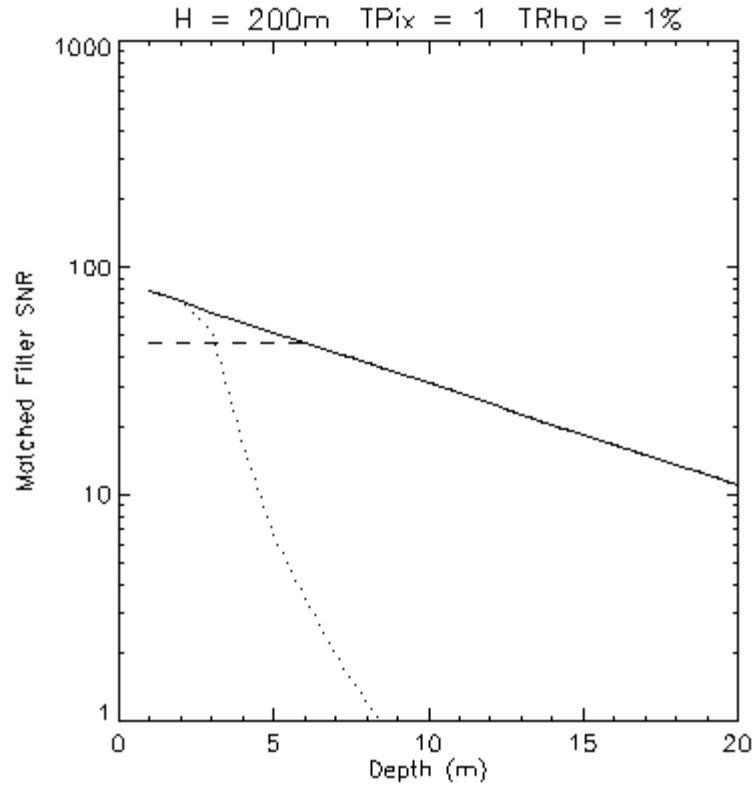
Figure 31. Pre-experimental signal-to-noise ratio calculations for GBFT; solid line is for non-scattering water media, dashed line is the theoretical maximum SNR for the camera system based on the available digitization, dotted line is the performance for scattering media.
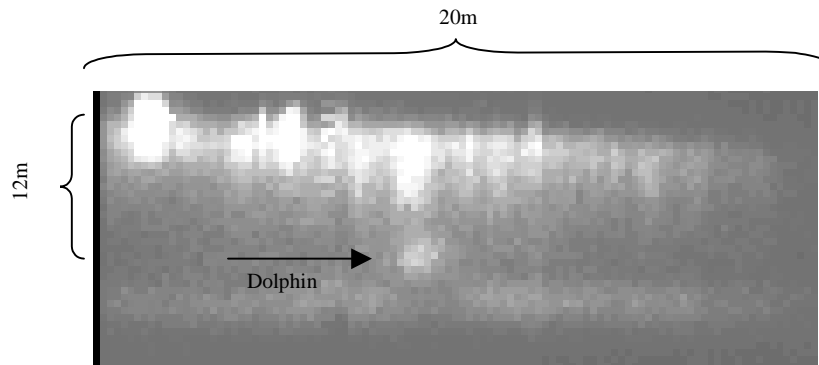
Figure 32. 2D ASTIL image of dolphin; water depth is 12m; dolphin is at 8m depth.

20m

12m
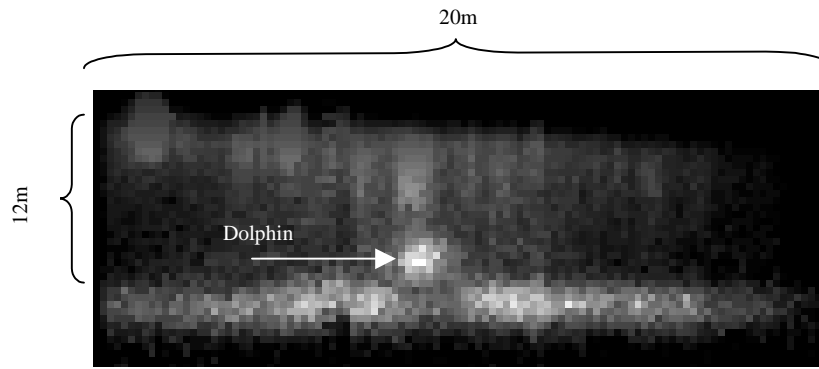
Dolphin

Figure 33. Image of dolphin in after range and exponential decay are corrected for.

50m

2m
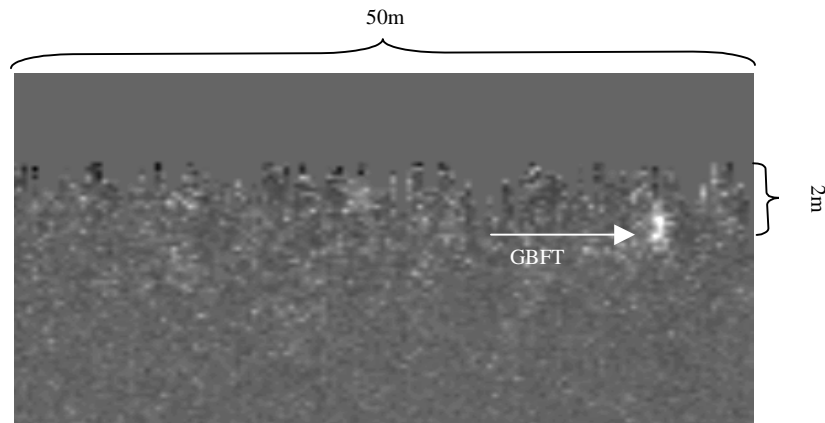
GBFT

Figure 34. Processed GBFT image corresponding to the raw data shown in Figure 23. A single GBFT dominates the data, seen near the middle right hand side of the image.

50m

2m
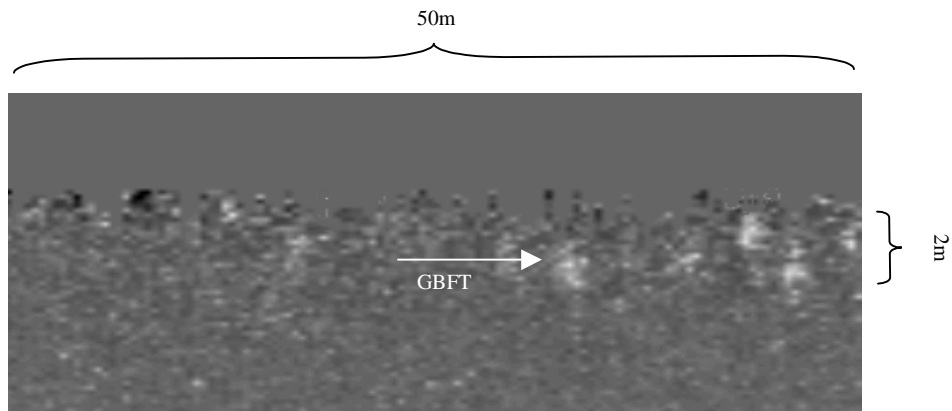
GBFT

Figure 35. Processed image of GBFT corresponding to the raw data in Figure 24. Six GBFT signatures are readily visible and one or two marginal instances are also present.
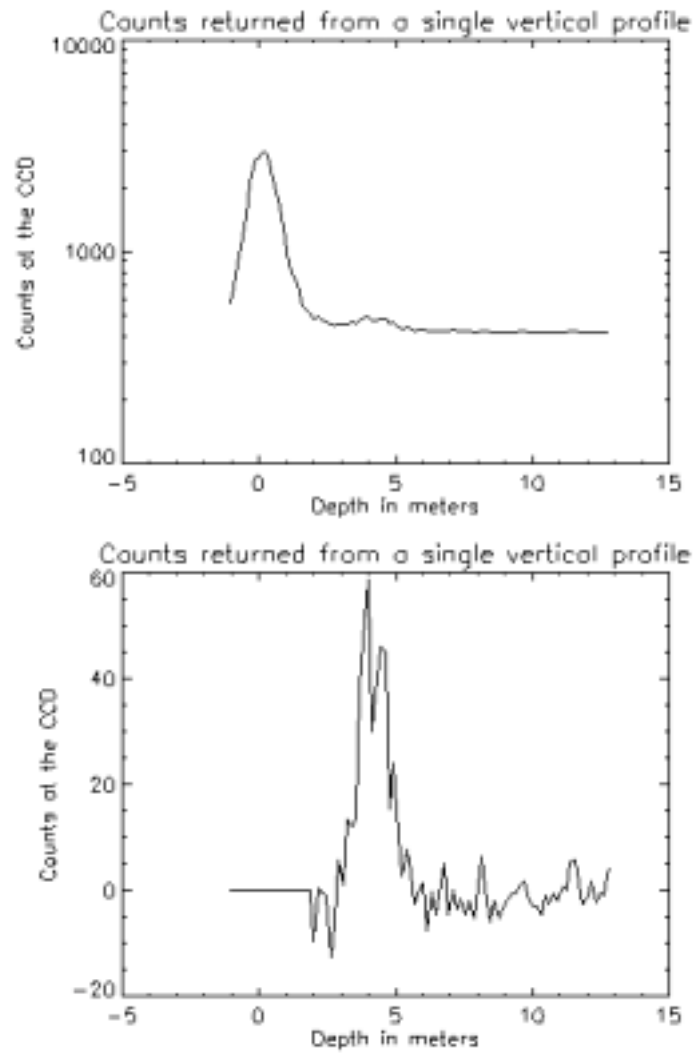
Figure 36. 1D profiles through the image of Figure 34. The upper profile shows the context of both surface and GBFT return on logarithmic scale; the lower profile focuses on the GBFT return and is plotted on a linear scale.
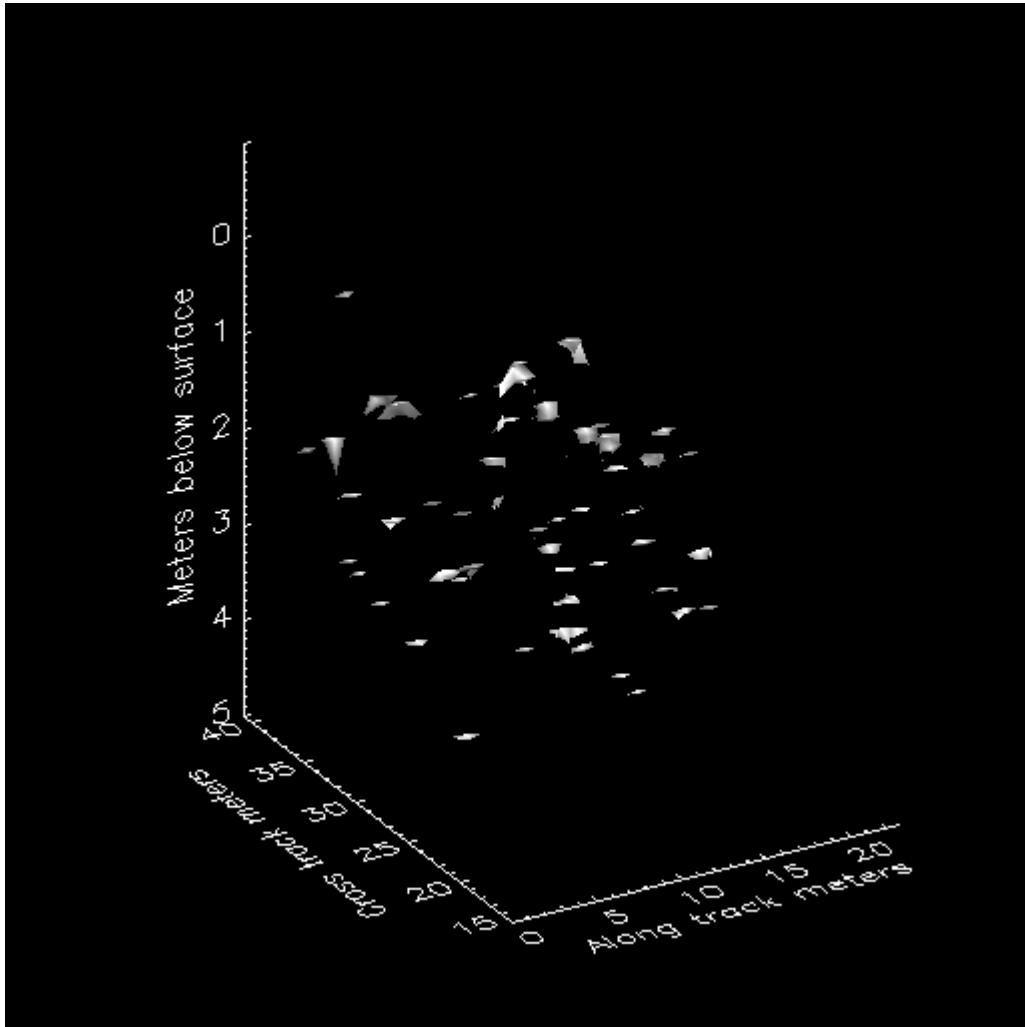
Figure 37. 3D image of a GBFT school near Cape Cod. The school spans an area roughly 20 x 40m laterally and extends from near the surface down to 5m in depth, as shown in the rendering.
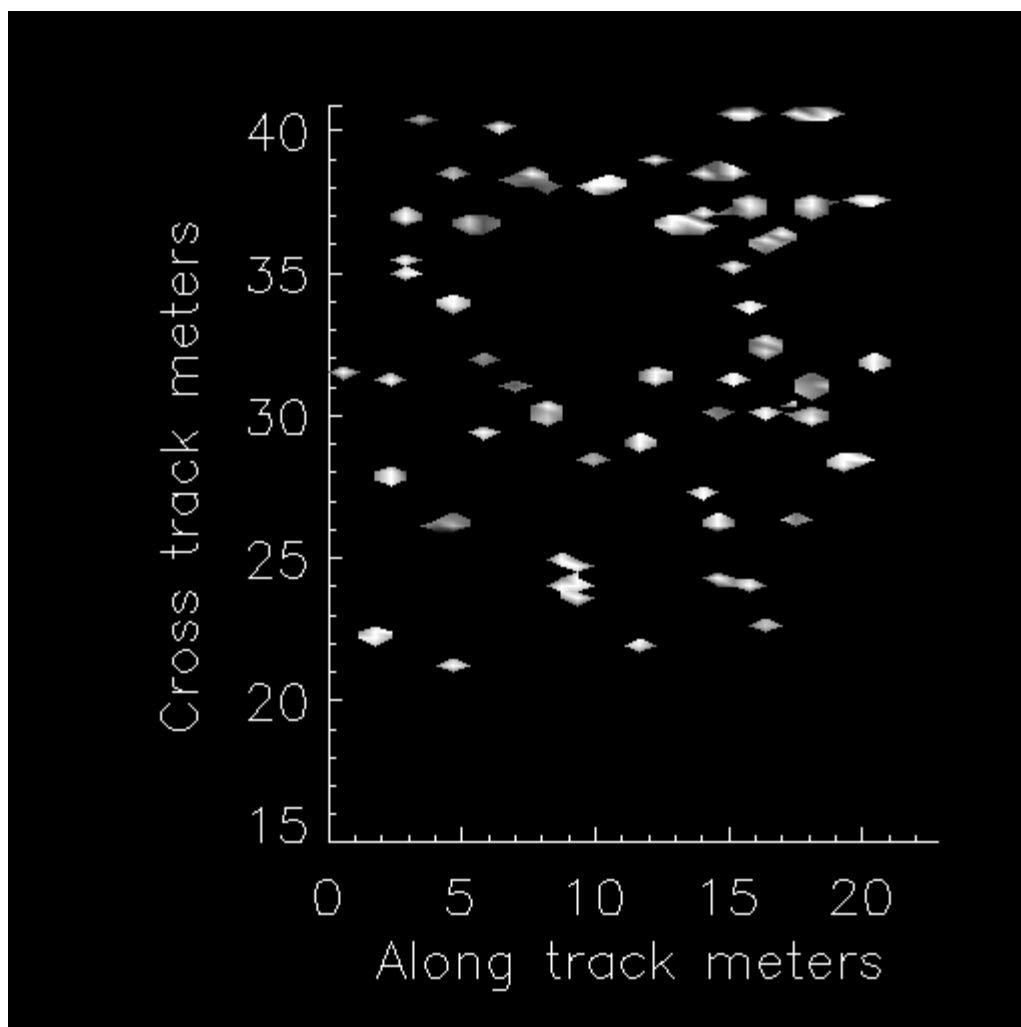
Figure 38. 2D topographical projection of the 3D data in Figure 37.
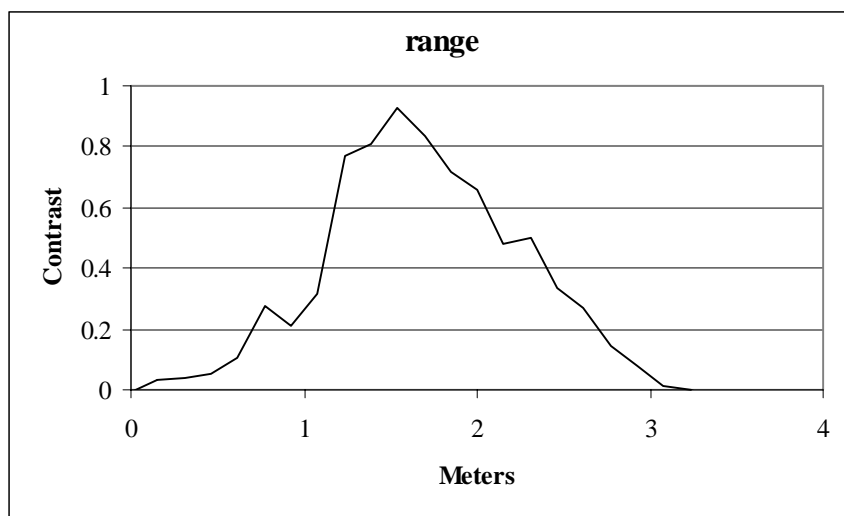
Figure 39. Average range profile of the GBFT data. The average is for range vectors aligned by matched filter peak location.
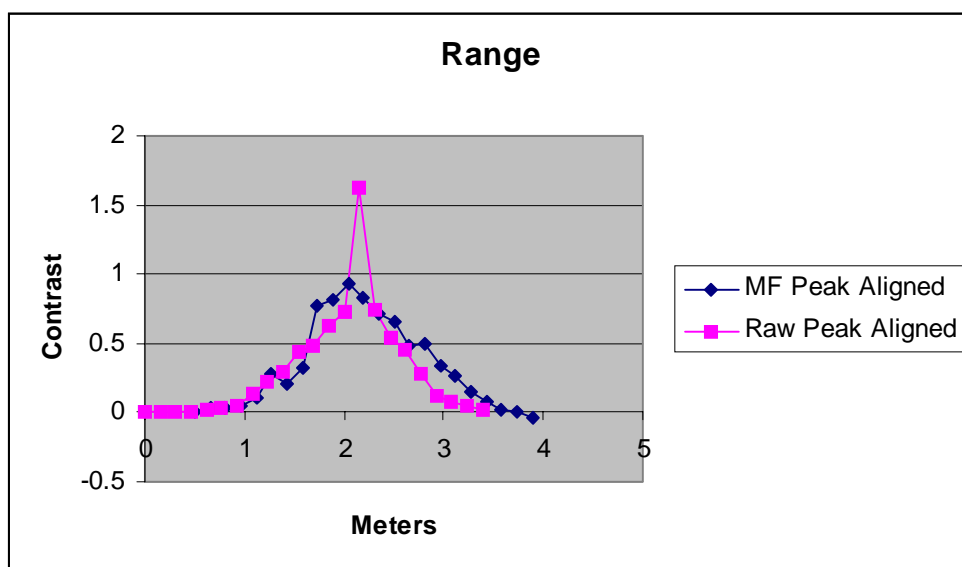
Figure 40. Average range profiles of GBFT. Average is formed by peak-alignment of the individual range vectors for rectangular data points and by peak-alignment via matched filtered peak.
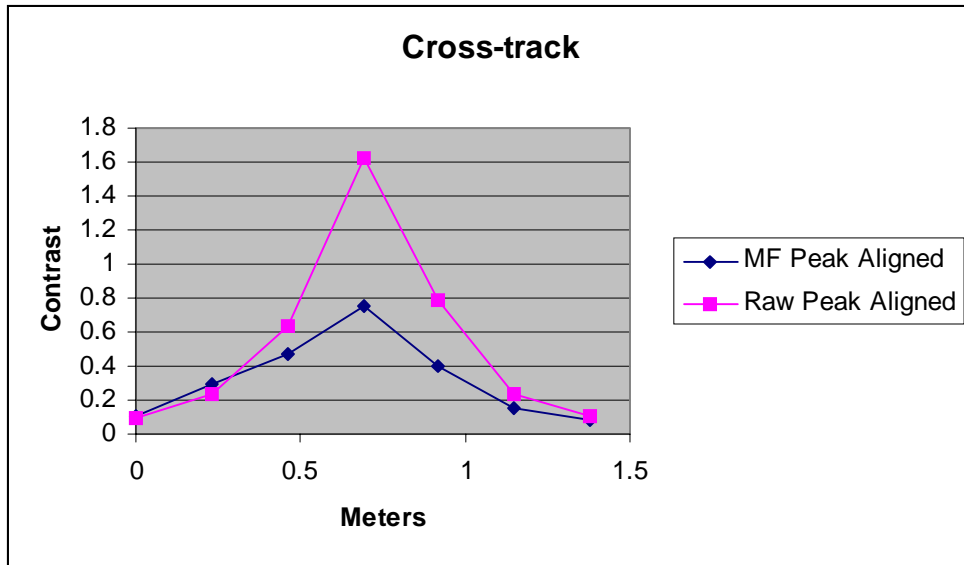
Figure 41. Average cross-track profiles of GBFT.
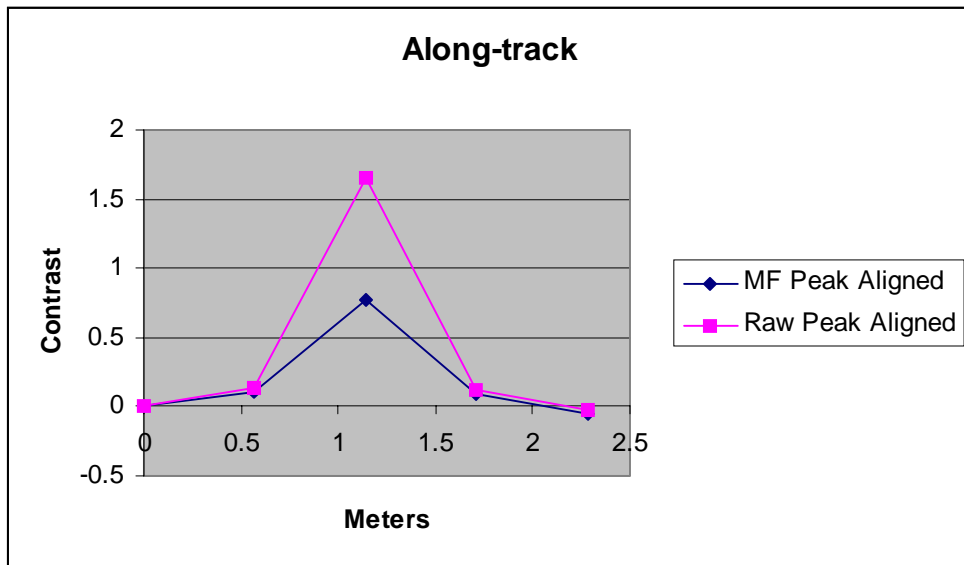
Figure 42. Average along-track profiles of GBFT.
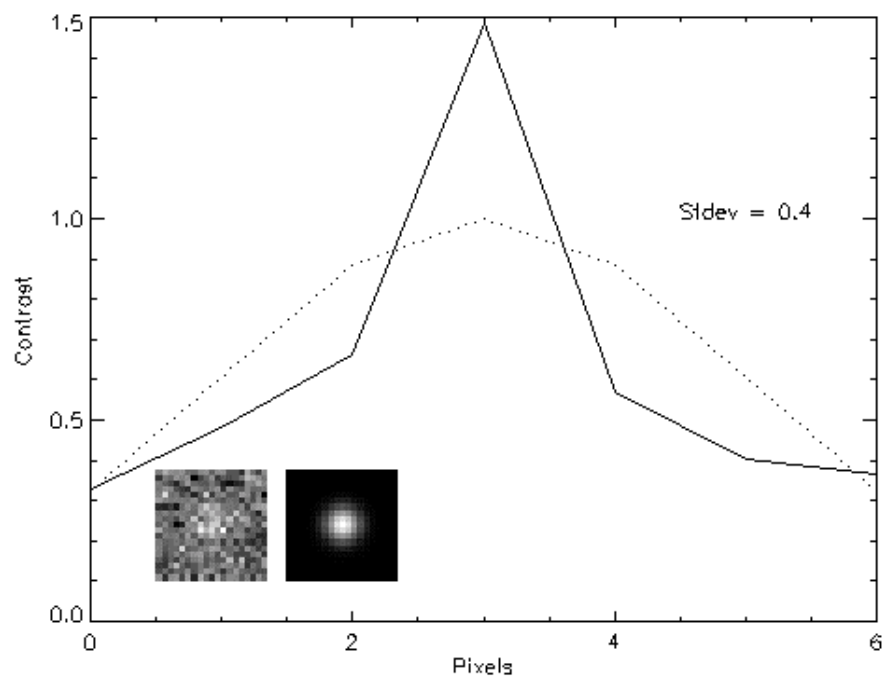
Figure 43. 1D profile for peaks with noisy raw-aligned computed data (solid line) and the original noiseless data (dotted line). A representative noisy image and the noiseless image are shown in the lower left hand corner. The noisy object has an SNR of 9.
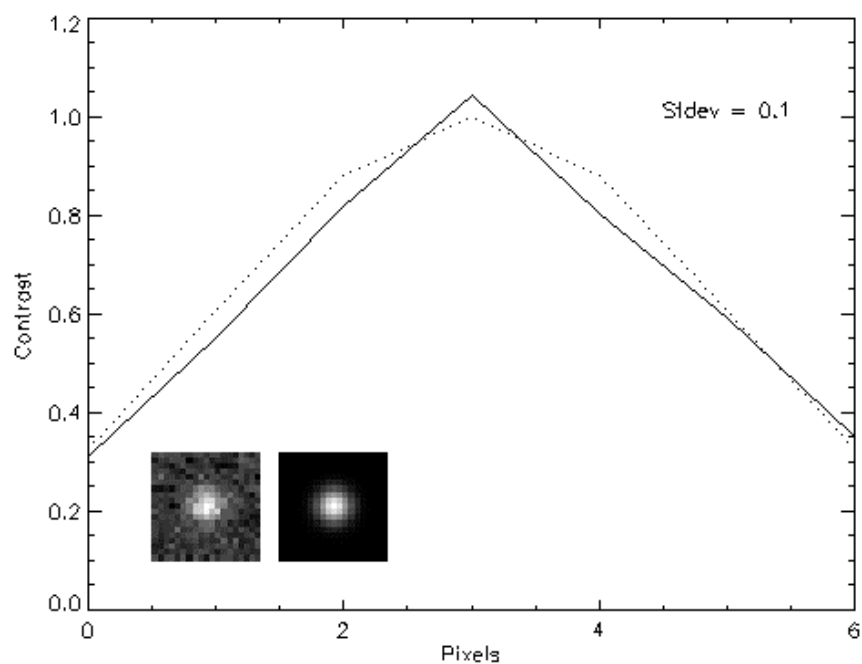
Figure 44. 1D profile for peaks with noisy raw-aligned computed data (solid line) and the original noiseless data (dotted line). A representative noisy image and the noiseless image are shown in the lower left hand corner. The noisy object has an SNR of 36.
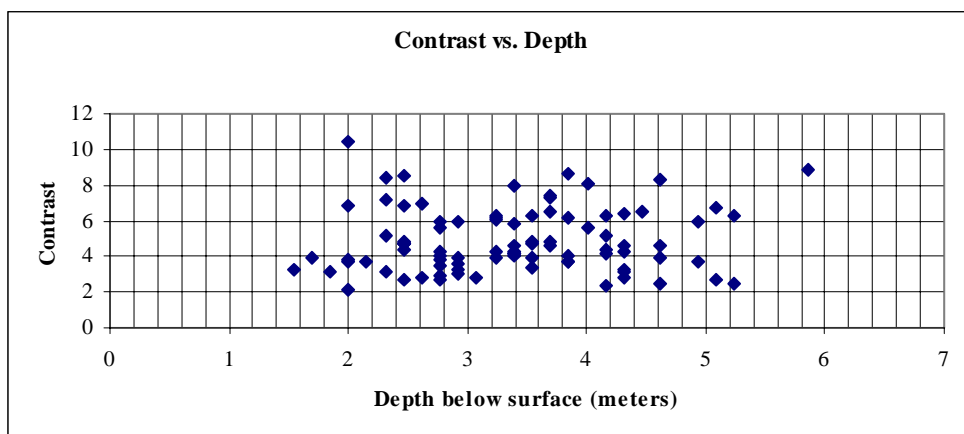
Contrast vs. Depth

Figure 45. Scatter plot of contrast versus GBFT depth. Median is 4.4; standard deviation is 1.8.

Depth Distribution
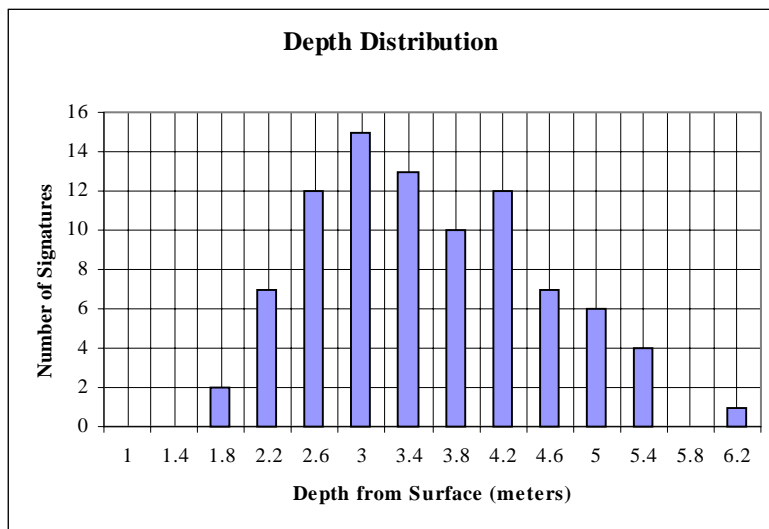
Figure 46. GBFT school depth distribution. Median depth is 3.4m; standard deviation is 0.94m.

Along Track Size Distribution
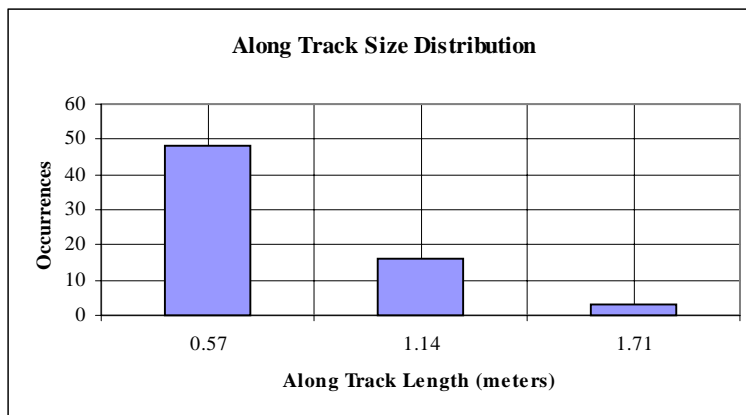
Figure 47. GBFT along-track size distribution. Median is 0.57m; standard deviation is 0.34m.
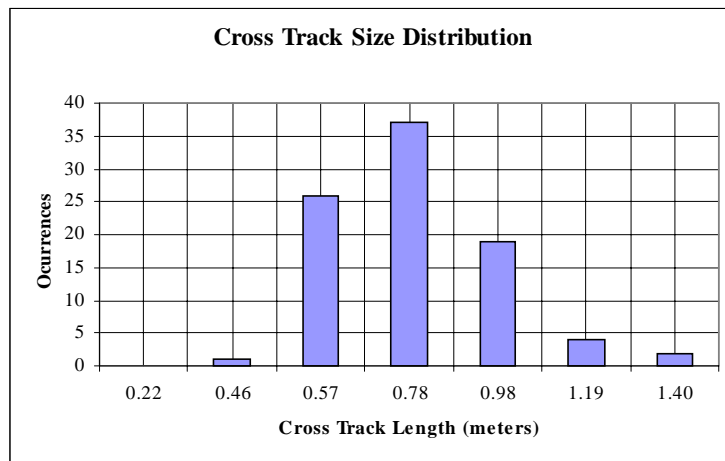
Figure 48. GBFT cross-track size distribution. Median is 0.55m; standard deviation is 0.14m.
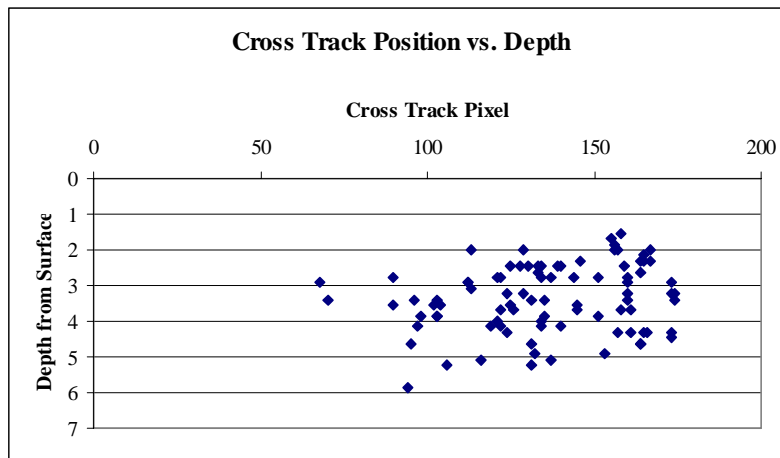
Figure 49. GBFT cross-track position as a function of depth (m) below the surface.
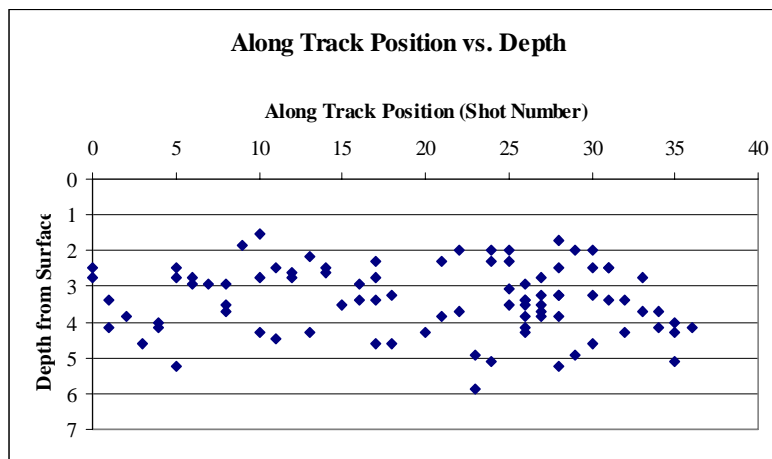
Figure 50. GBFT along-track position as a function of depth (m) below surface.
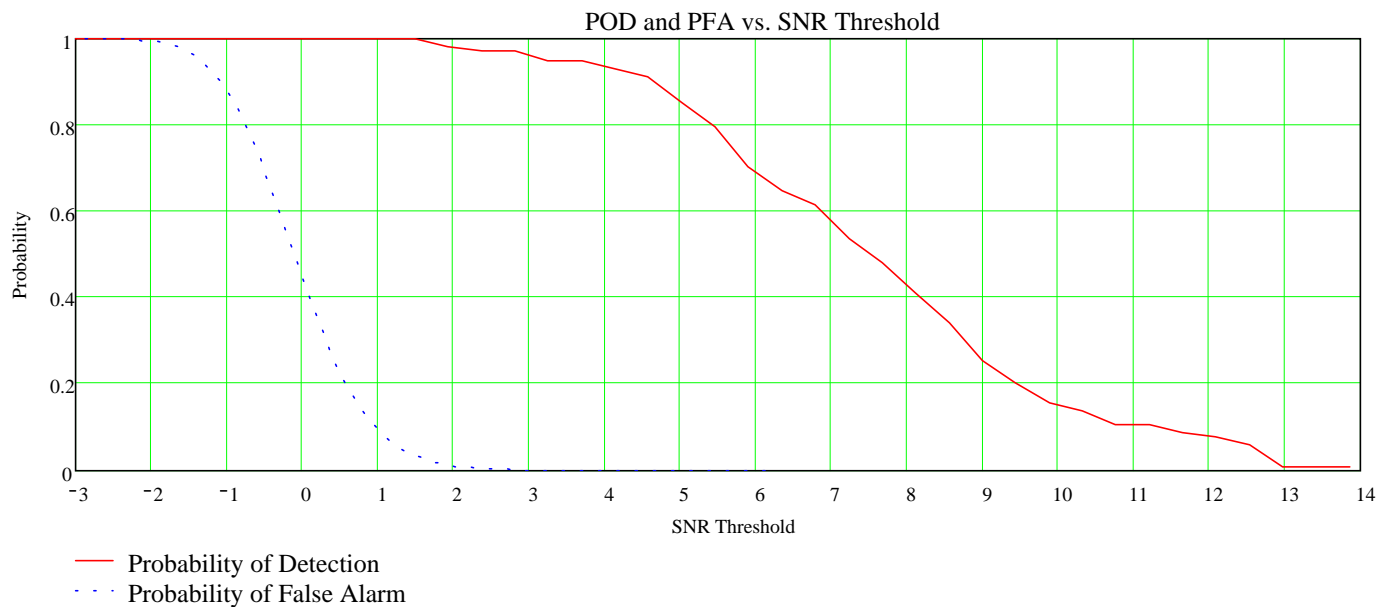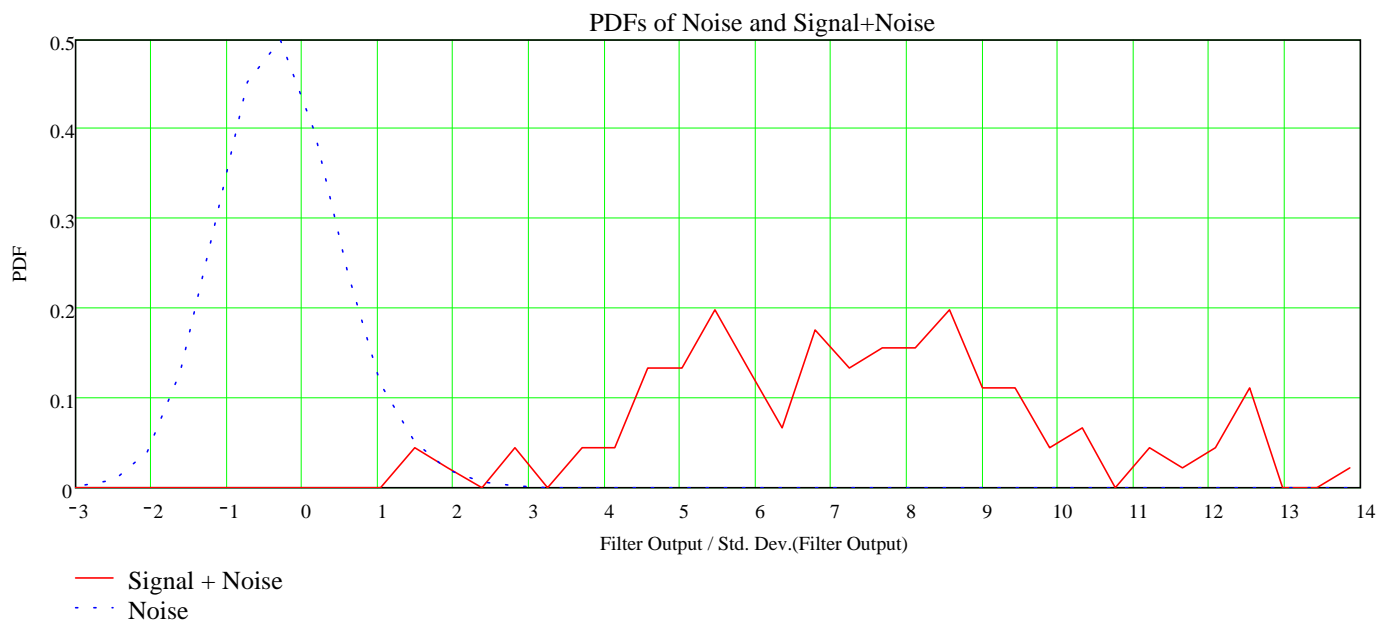
Figure 51. Histogram (top) and Cumulative distribution (bottom) graphs of the probability of detection (POD) and probability of false alarm (PFA) for GBFT with ASTIL.

RECEIVER OPERATING CHARACTERISTIC
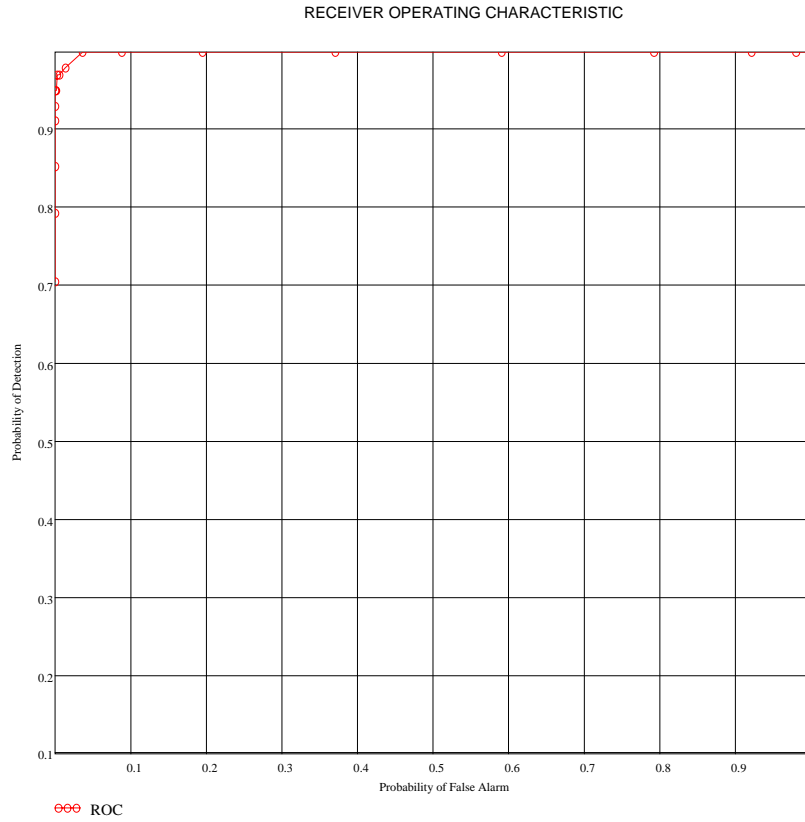
Figure 52. ASTIL receiver operating curve for GBFT; linear coordinates.

RECEIVER OPERATING CHARACTERISTIC
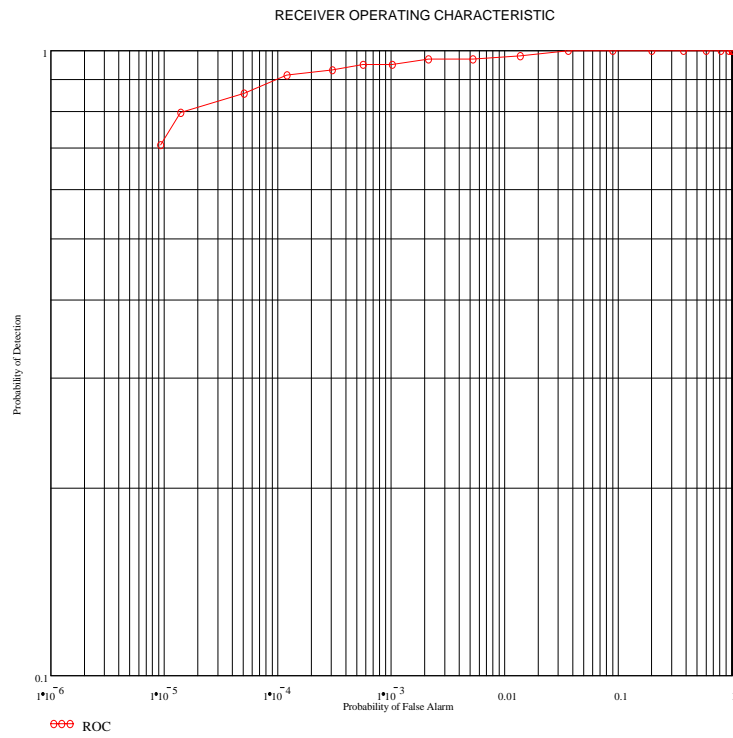
Figure 53. ASTIL receiver operating curve for GBFT; logarithmic coordinates.

(INTENTIONALLY LEFT BLANK)

LIDAR IMAGE SEGMENTATION ALGORITHM (LISA) RESULTS
FOR NEW ENGLAND DATA SETS
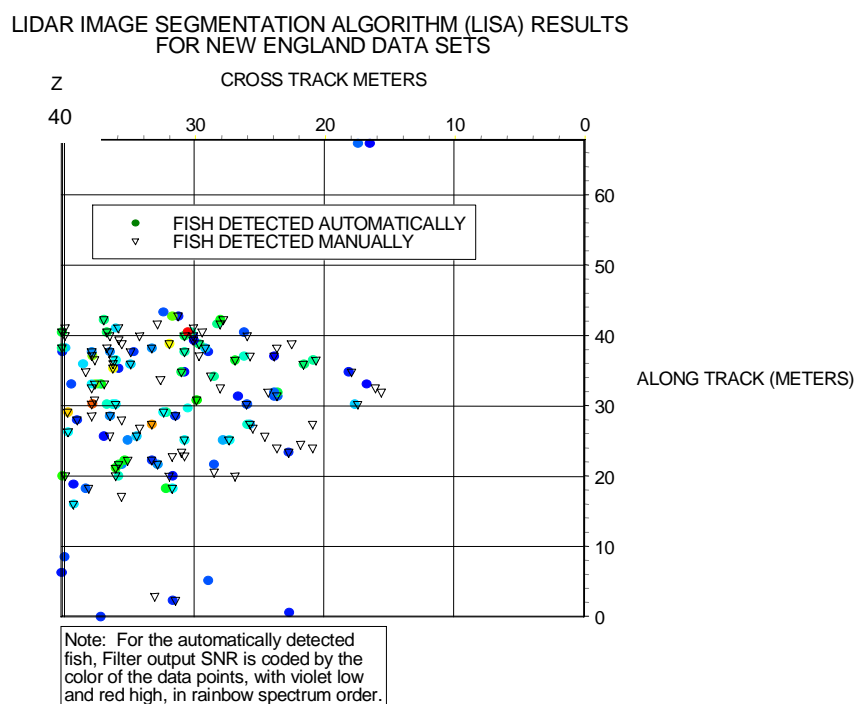
Figure 54. GBFT detection performance showing automatically detected tuna and the analyst-detected tuna for a region extending beyond the central school region by 50% in each direction.

LIDAR IMAGE SEGMENTATION ALGORITHM (LISA) RESULTS
FOR NEW ENGLAND DATA SETS
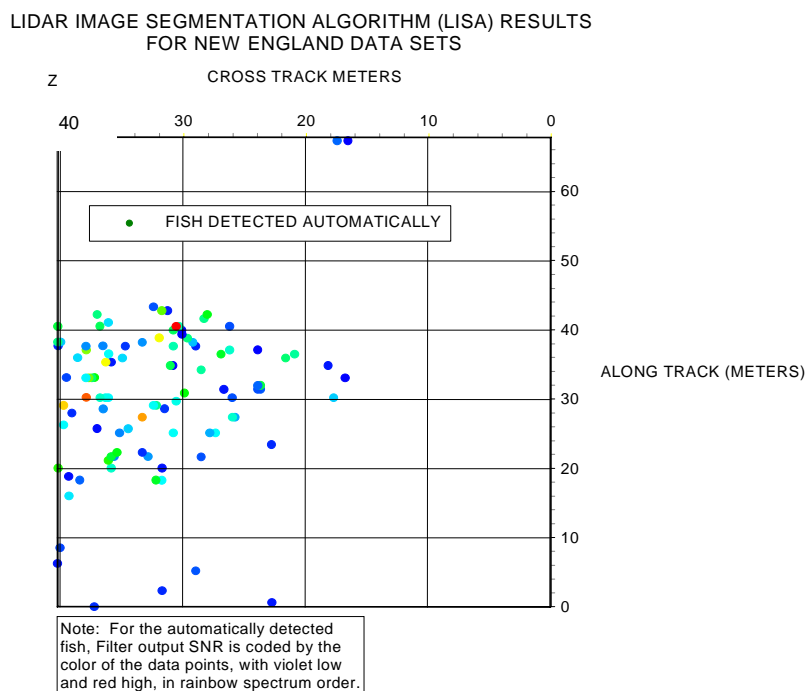
Figure 55. GBFT detection performance showing only automatically detected tuna for a region extending beyond the central school region by 50% in each direction.

(INTENTIONALLY LEFT BLANK)
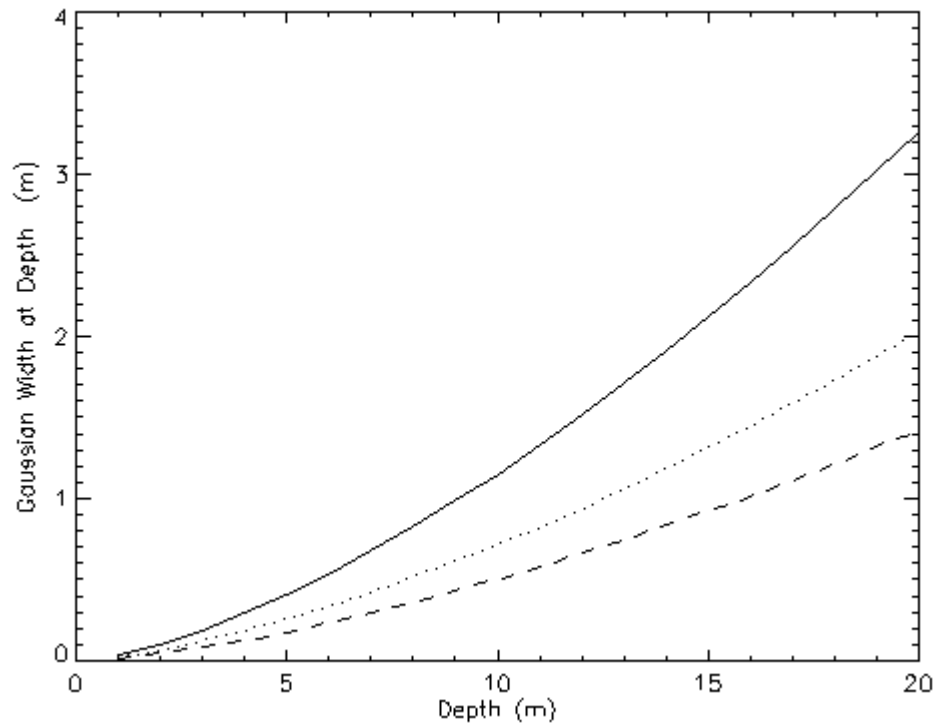
Figure 56. In-water spreading as a function of depth for 3 water types. Solid line is JWT-II; dotted is JWT-IB; dashed is JWT-IA.
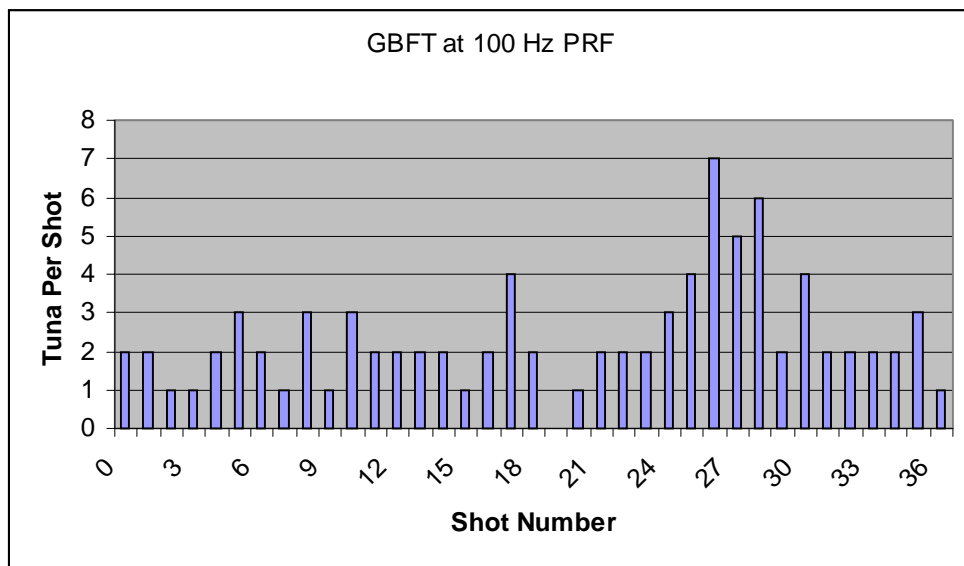
Figure 57. GBFT detected per shot for the central 40 shots over the GBFT school.

95
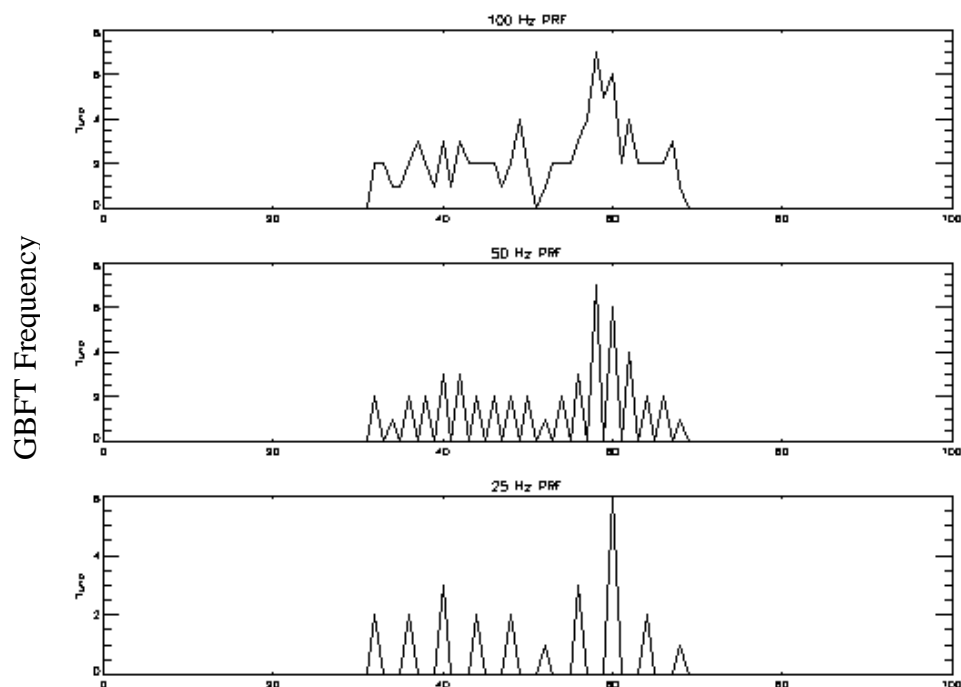
Figure 58. GBFT detected per shot for 3 different laser PRFs: 100 Hz (same as ASTIL configuration), 50 Hz, 25 Hz. Data are derived from the 100 Hz GBFT data already shown.
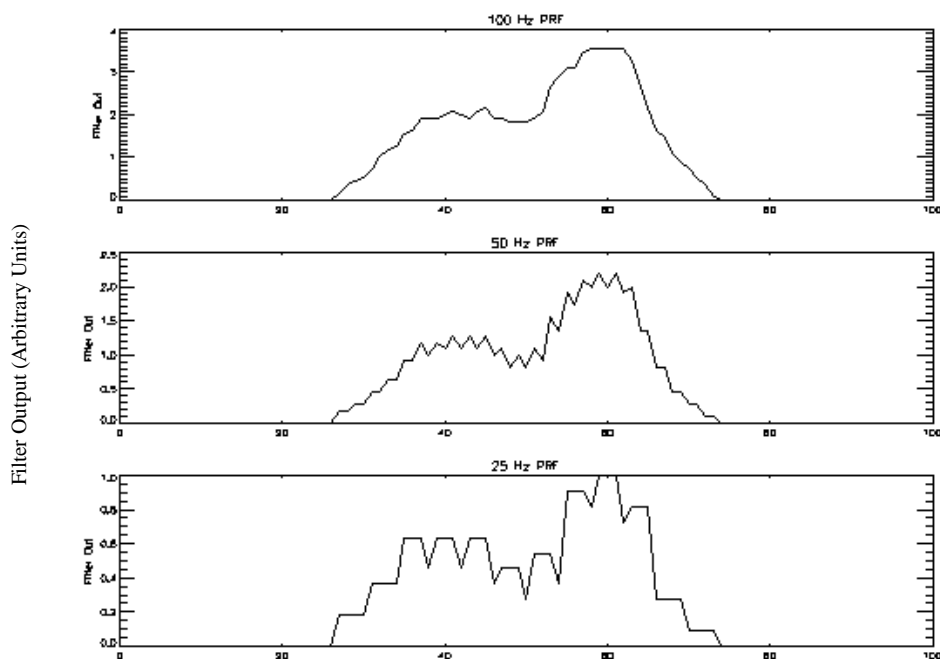
Figure 59. Filtered GBFT detected per shot for 3 different laser PRFs: 100 Hz (same as ASTIL configuration), 50 Hz, 25 Hz. Data are derived from the 100 Hz GBFT data already shown. An 11-point boxcar average has been applied to the data to produce the filtered output.
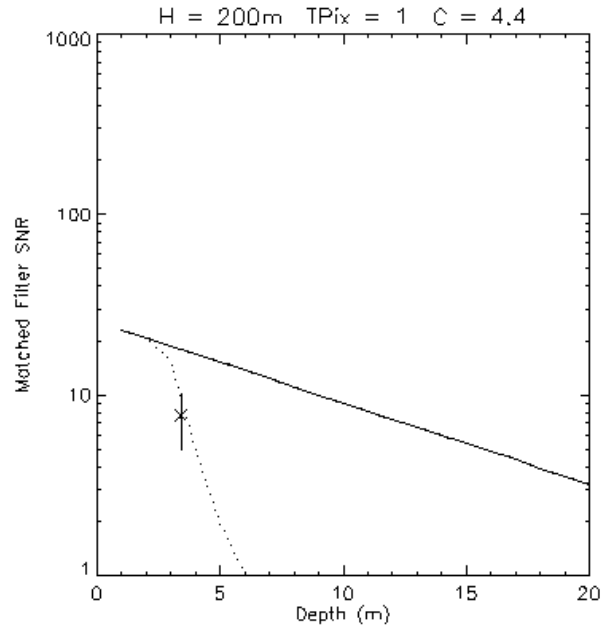
Figure 60. Comparison of measured SNR to theoretical SNR for both scattering and non-scattering media using a *measured target contrast*. Dotted line is SNR with scattering; solid line is SNR without scattering. GBFT SNR is shown as a single point with error bars, representing the measured GBFT statistics.
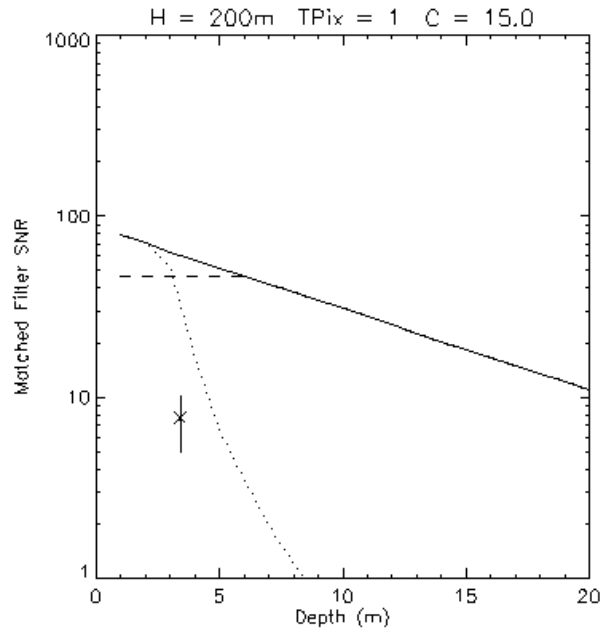
Figure 61. Comparison of measured GBFT SNR to theoretical SNR for both scattering and non-scattering media using a *derived target reflectivity*. Dotted line is SNR with scattering; solid line is SNR without scattering. GBFT SNR is shown as a single point with error bars, representing the measured GBFT statistics. The dashed line indicates the digitizer-limited maximum system SNR, to help distinguish the theoretical from the practical.
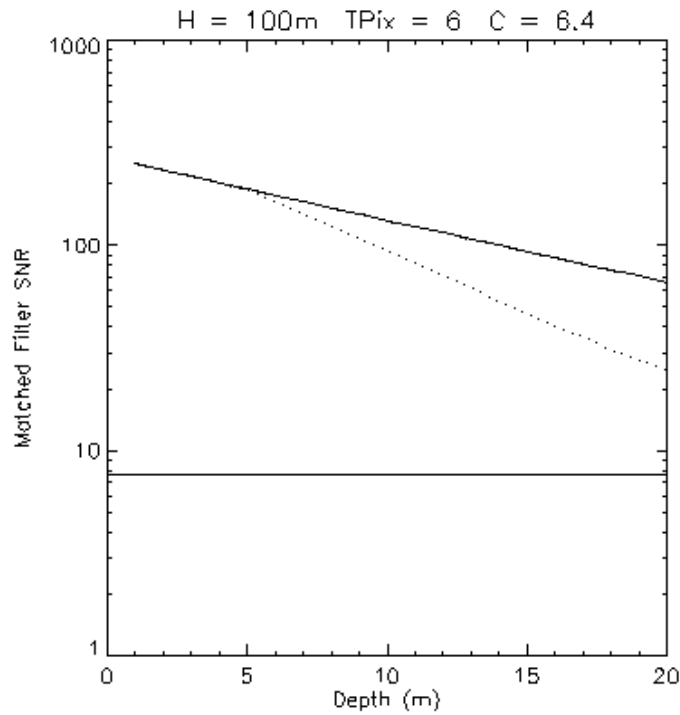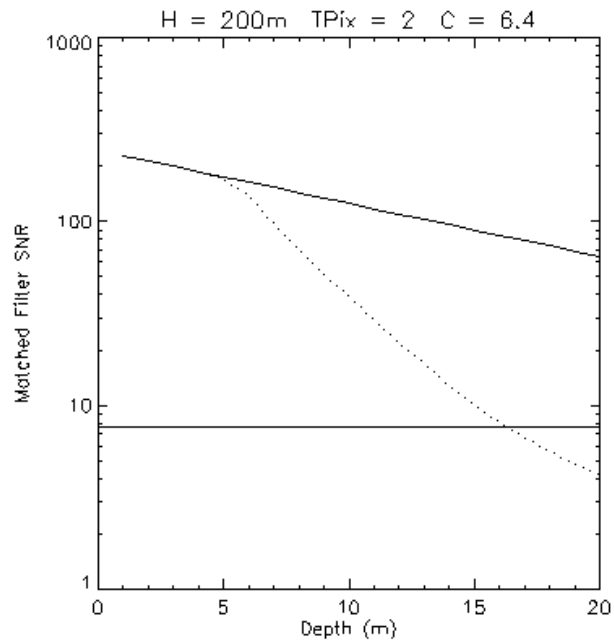
97
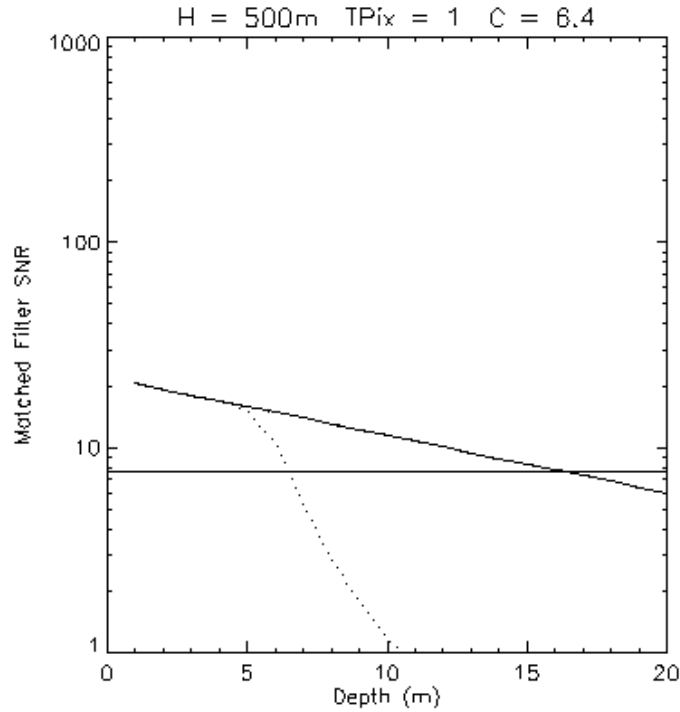
Figure 62. SNR performance estimate for 100cm yellowfin in the ETP; swath is 15 degrees, energy is 130 mJ/shot, resolution is 1024 pixels cross-track, water is JWT-IB, with mean square angle of 0.06 (estimated ETP value); altitude is 500m; contrast is 6.4.
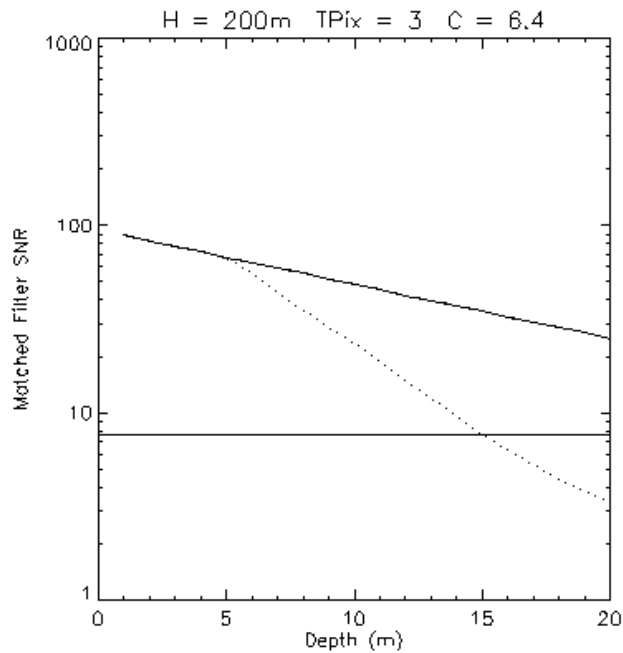
Figure 63. SNR performance estimate for 100cm yellowfin in the ETP; swath is 15 degrees, energy is 130 mJ/shot, resolution is 1024 pixels cross-track, water is JWT-IB, with mean square scattering angle of 0.06 (estimated ETP value); altitude is 200m; contrast is 6.4.
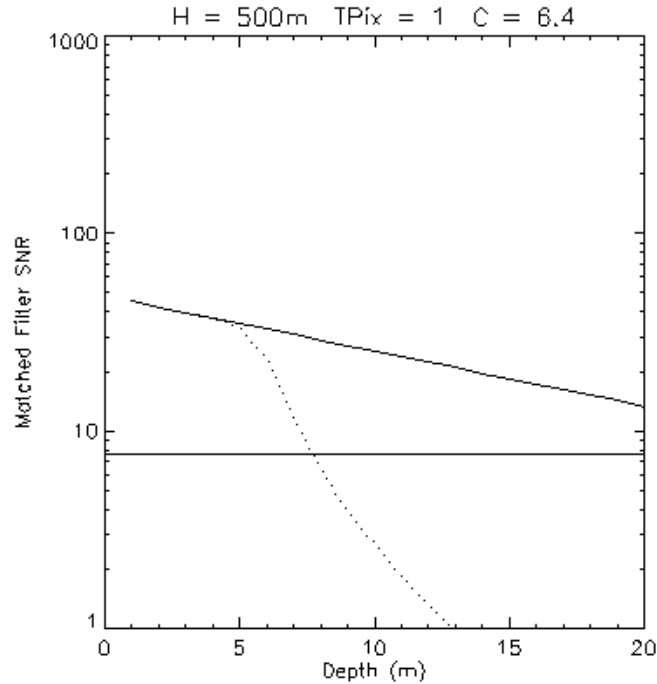
98

Figure 64. SNR performance estimate for 100cm yellowfin in the ETP; swath is 15 degrees, energy is 130 mJ/shot, resolution is 1024 pixels cross-track, water is JWT-IB, with mean square scattering angle of 0.06 (estimated ETP value); altitude is 100m; contrast is 6.4.
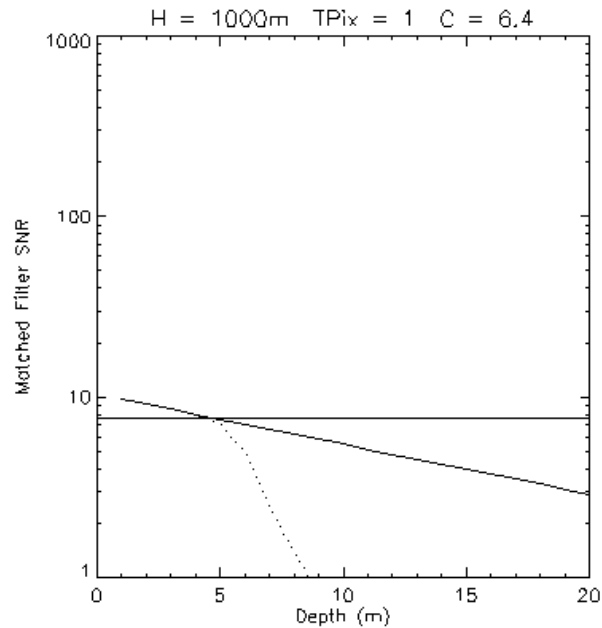

Figure 65. SNR performance estimate for 100cm yellowfin in the ETP; swath is 25 degrees, energy is 130 mJ/shot, resolution is 1024 pixels cross-track, water is JWT-IB, with mean square scattering angle of 0.06 (estimated ETP value); altitude is 200m; contrast is 6.4. Sensor has upgraded streak tube electronics, CCD camera, and principal lens assembly.

99

Figure 66. SNR performance estimate for 100cm yellowfin in the ETP; swath is 25 degrees, energy is 130 mJ/shot, resolution is 1024 pixels cross-track, water is JWT-IB, with mean square scattering angle of 0.06 (estimated ETP value); altitude is 500m; contrast is 6.4. Sensor has upgraded streak tube electronics, CCD camera, and principal lens assembly.

Figure 67. SNR performance estimate for 100cm yellowfin in the ETP; swath is 25 degrees, energy is 130 mJ/shot, resolution is 1024 pixels cross-track, water is JWT-IB, with mean square scattering angle of 0.06 (estimated ETP value); altitude is 1000m; contrast is 6.4. Sensor has upgraded streak tube electronics, CCD camera, and principal lens assembly.
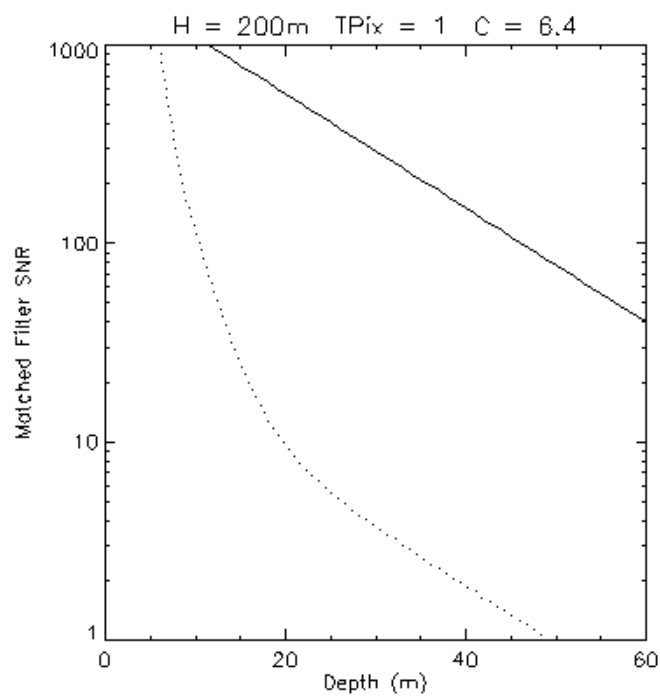
Figure 68. Multi-fish SNR performance estimated for single shot detection statistics at 1 body length packing within a 20000kg school at 200m altitude.
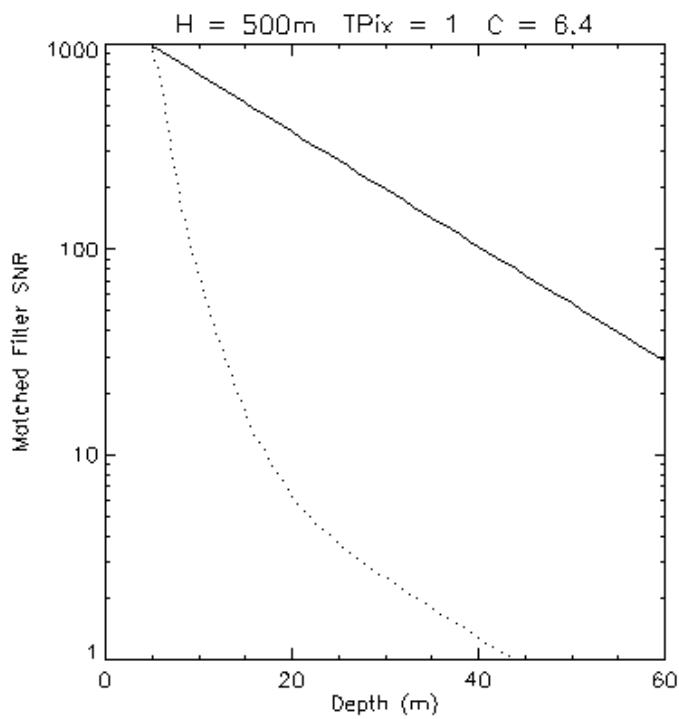

Figure 69. Multi-fish SNR performance estimated for single shot detection statistics at 1 body length packing within a 20000kg school at 500m altitude.
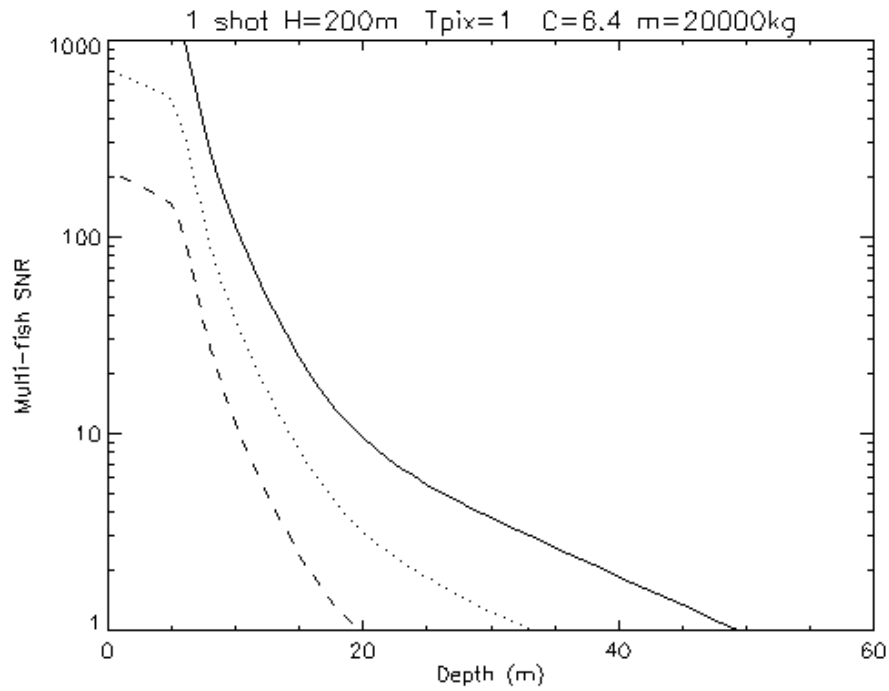
Figure 70. Multi-fish SNR performance estimated for single shot detection statistics at 3 different body lengths (solid = 1BL, dotted = 3BL, dashed = 10BL). Altitude is 200m.
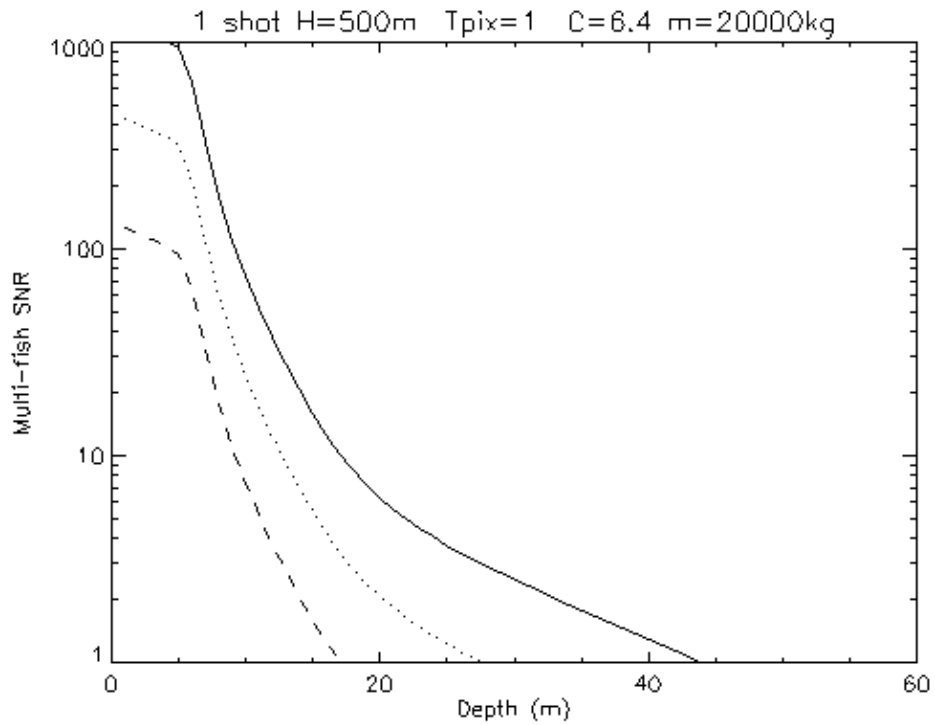

Figure 71. Multi-fish SNR performance estimated for single shot detection statistics at 3 different body lengths (solid = 1BL, dotted = 3BL, dashed = 10BL). Altitude is 500m.
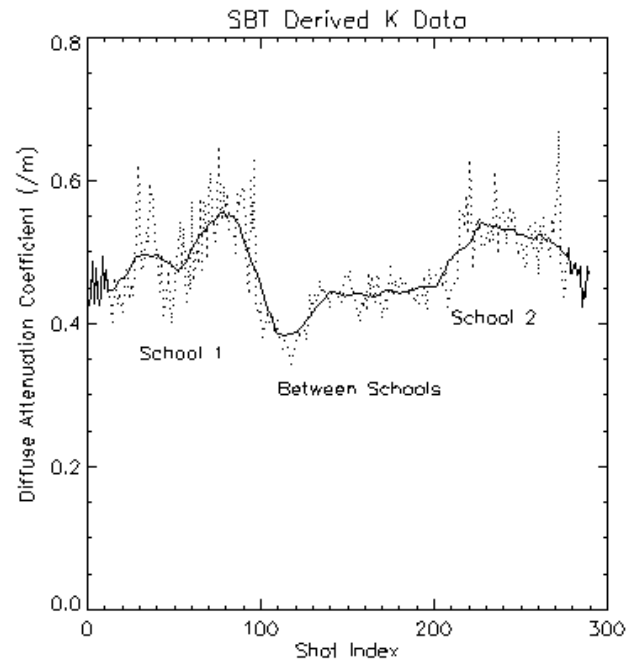
Figure 72. ASTIL-derived attenuation coefficient for SBT in Boston Bay (South Australia) and adjacent waters. Two captive schools were imaged, with approximately 50m of open water between them. Dotted line = raw K estimates per shot; solid line = smoothed version of raw K estimates.
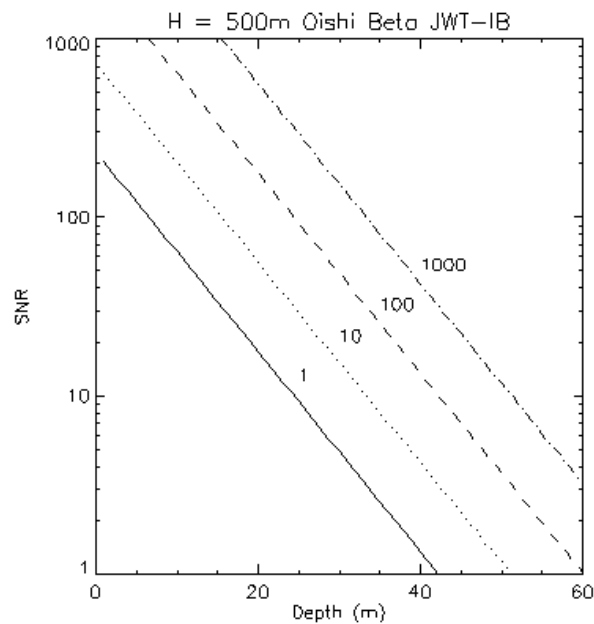

Figure 73. SNR associated with volume backscatter data for use in calculating apparent water attenuation. Shown are upgraded ASTIL performance data for 500m altitude, JWTII water, and range bins of 0.3m per range pixel. The individual curves are labeled for the number of cross-track pixels averaged to estimate the attenuation (1024 is the total cross-track pixels available).

103

(INTENTIONALLY LEFT BLANK)